ISSN 1980-9743

Soils and Rocks

An International Journal of Geotechnical and Geoenvironmental Engineering

Volume 31, N. 1
January-April 2008

Soils and Rocks
Volume 31, N. 1
2008

Soils and Rocks is an International Journal of Geotechnical and Geoenvironmental Engineering published by

ABMS - Brazilian Association for Soil Mechanics and Geotechnical Engineering
Av. Prof. Almeida Prado, 532, IPT/DEC-Prédio 54
05508-901 São Paulo, SP
Brazil

ABGE - Brazilian Association for Engineering Geology and the Environment
Av. Prof. Almeida Prado, 532, IPT/DIGEO- Prédio 59
05508-901 São Paulo, SP
Brazil

SPG – Portuguese Geotechnical Society
LNEC, Avenida do Brasil, 101
1700-066 Lisboa
Portugal

Issue Date: *April 2008*

Issue: *3,200 copies*

Manuscript Submission: *For review criteria and manuscript submission information, see Instructions for Authors at the end.*

SOILS and ROCKS

An International Journal of Geotechnical and Geoenvironmental Engineering

Editor Ennio Marques Palmeira - University of Brasília, Brazil

Co-editor Ricardo Oliveira - COBA, Portugal

Soils and Rocks publishes papers in English in the broad fields of Geotechnical Engineering, Engineering Geology and Geo-environmental Engineering. The Journal is published in April, August and December. Subscription price is US$ 90.00 per year. The journal, with the name "Solos e Rochas", was first published in 1978 by the Graduate School of Engineering-Federal University of Rio de Janeiro (COPPE-UFRJ). In 1980 it became the official magazine of the Brazilian Association for Soil Mechanics and Geotechnical Engineering (ABMS), acquiring the national character that had been the intention of its founders. In 1986 it also became the official Journal of the Brazilian Association for Engineering Geology and the Environment (ABGE) and in 1999 became the Latin American Geotechnical Journal, following the support of Latin-American representatives gathered for the Pan-American Conference of Guadalajara (1996). In 2007 the journal acquired the status of an international journal under the name of Soils and Rocks, published by the Brazilian Association for Soil Mechanics and Geotechnical Engineering (ABMS), Brazilian Association for Engineering Geology and the Environment (ABGE) and Portuguese Geotechnical Society (SPG).

Soils and Rocks

1978,	1 (1, 2)
1979,	1 (3), 2 (1,2)
1980-1983,	3-6 (1, 2, 3)
1984,	7 (single number)
1985-1987,	8-10 (1, 2, 3)
1988-1990,	11-13 (single number)
1991-1992,	14-15 (1, 2)
1993,	16 (1, 2, 3, 4)
1994-2007,	17-30 (1, 2, 3)
2008,	**31 (1,**

ISSN 1980-9743 CDU 624.131.1

ISSN 1980-9743

SOILS and ROCKS

An International Journal of Geotechnical and Geoenvironmental Engineering

Publication of

ABMS - Brazilian Association for Soil Mechanics and Geotechnical Engineering

ABGE - Brazilian Association for Engineering Geology and the Environment

SPG - Portuguese Geotechnical Society

Volume 31, N. 1, January-April 2008

Table of Contents

Articles

Soils and Rocks
v. 31, n. 1

Engineering Geological Properties of the Volcanic Rocks and Soils of the Canary Islands

Luis I. González de Vallejo, Teresa Hijazo, Mercedes Ferrer

Abstract. This paper analyses the engineering geological properties of the rocks and soils of the Canary Islands based on data from field studies, laboratory tests and extensive databases for volcanic materials. Geological properties and processes most relevant to geo-engineering are described. Geomechanical characterization of rock masses and soil deposits including rock mass classification, index and strength properties are presented. Some of the most relevant results show materials of low to very low density and low to very low values of strength and expansiveness. These materials, with an exceptional high anisotropy and irregular spatial distribution, are intensely affected by jointing of thermal origin and large discontinuities due to dykes; cavities and tubes can be also present. Landsliding and slope instability, collapse phenomena and other processes causing geotechnical problems are described. Discussion on the geomechanical properties and conditions that may help to identify and differentiate the geotechnical behaviour of the volcanic materials is included.

Key words: volcanic rocks, volcanic soils, Canary Islands, Tenerife, geomechanical properties.

1. Introduction

Geological materials in islands of volcanic origin show geomechanical properties and geotechnical behaviour completely different of materials with non-volcanic origin. This paper is focused on the geomechanical characterization of the volcanic rock masses and soil deposits of the Canary Islands and on the main geotechnical problems associated with these materials. Active geological processes such as landslides, collapse phenomena and expansiveness are also described. This study is based on field geomechanical surveys, laboratory tests and geotechnical data obtained from different sources including Regional Governmental agencies (Rodríguez-Losada *et al.*, 2007a) and geotechnical companies. From this information more than 400 data have been compiled (González de Vallejo *et al.*, 2006) which have been used for the purpose of this study. Geological and geotechnical maps (http://mapa.grafcan.com/Mapa) have been also used as basic information for field studies.

2. Geological Formations

The Canary Islands is a volcanic archipelago composed of seven islands (Fig. 1). Their volcanic activity, which spans from over 20 M.a. ago to the present, and their active geological processes, such as their great paleolandslides, have attracted the attention of scientists worldwide. The geology of Canary Islands has been extensively studied since the XIX Century. An update and comprehensive geological description can be found in Ancochea *et al.* (2004) and Carracedo *et al.* (2002).

The main geological formations of the Canaries relevant to engineering geology can be grouped in the following units: Basaltic, trachybasaltic and phonolitic lava flows; pyroclastic rocks, pyroclastic deposits and soil deposits of volcanic origin. A detailed geological and petrological description of these units is given by Rodríguez-Losada (2004).

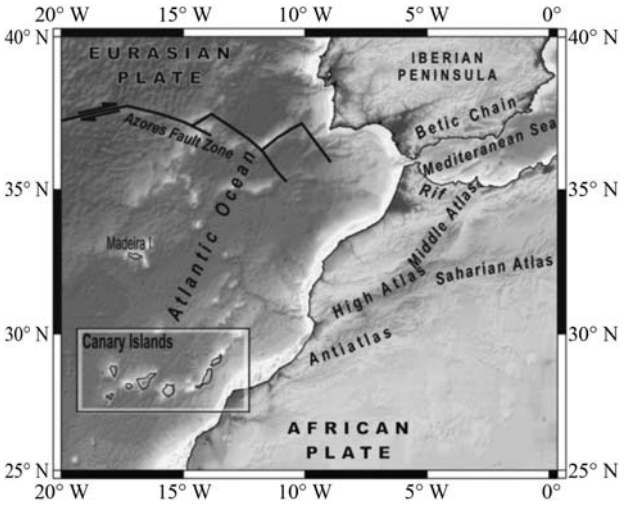

Figure 1 - Location of the Canary Islands (Spain).

The **basaltic, trachybasaltic and phonolitic lava flows** and also **dykes,** form the most abundant rock group in the Canary Islands. The typical structure of these rocks is a succession of basalt and scoria layers, with rough surfaces composed of broken lava blocks known as clinker. Among the basaltic materials, several types of basalts according to their texture, crystallinity and grain size, are distinguished. Basalts can also be characterized in terms of their vesicles, and are referred to as vesicular basalts when there is a high

Luis I. González de Vallejo, Professor of Geological Engineering, Universidad Complutense de Madrid, Spain. e-mail: vallejo@geo.ucm.es.
Teresa Hijazo, MSc. Engineering Geologist, Prospección y Geotecnia, Madrid, Spain.
Mercedes Ferrer, Associate Professor of Rock Mechanics, Instituto Geológico y Minero de España, Spain.
Submitted on May 24, 2007; Final Acceptance on January 18, 2008; Discussion open until August 29, 2008.

proportion of vesicles and as amygdaloidal basalts if the vesicles are infilled with minerals. Secondary clay minerals can occur as replacement of olivine, pyroxenes and interstitial glass materials in altered basalts forming smectites, chlorites, corrensites, etc. which can jeopardize the rock quality and its geomechanical behaviour.

Scoriaceous materials appear at the flow top or bottom, being often the result of lava flows of the "aa" type. Their thickness is variable, usually tens of centimetres, although it can exceed 1m. The appearance of the scoria is very irregular, being highly porous with many voids and cavities. Figure 2 shows a succession of basalt and scoria layers with a seam of red ochre paleosoil.

Discontinuities are the most outstanding features of the lava flows. Basalt layers are affected by vertical columnar joints, which are generally fairly open. Horizontal or spherical discontinuities may also appear. Apart from discontinuities, it can be found cavities, mostly no larger than half a meter in diameter. Occasional caves may appear, and less commonly lava tubes.

The **pyroclastic rocks** are divided in **tuffs, ignimbrites**, **agglomerates and agglomerate breccias** according to the compaction, welding, grain size and morphology of the rock fragments.

The **tuffs** generally appear in a massive state, with scarce discontinuities, appearing as a very homogenous deposit. Most tuff deposits are deposit of pyroclastic flow and pumiceous nature, with light-coloured or yellowish pumice clasts, although they may also be of basaltic composition. Their thickness varies from over one meter to dozens of meters depending on the zone. The size of grains or particles normally are between 2 and 64 mm, corresponding to lapilli.

The **ignimbrites** are comprised of welded pyroclastic deposits whose fragments are flattened and stretched to form so-called *fiammes*. These are generally hard, massive rocks although flow structures may also be observed, showing foliation, and cooling discontinuities.

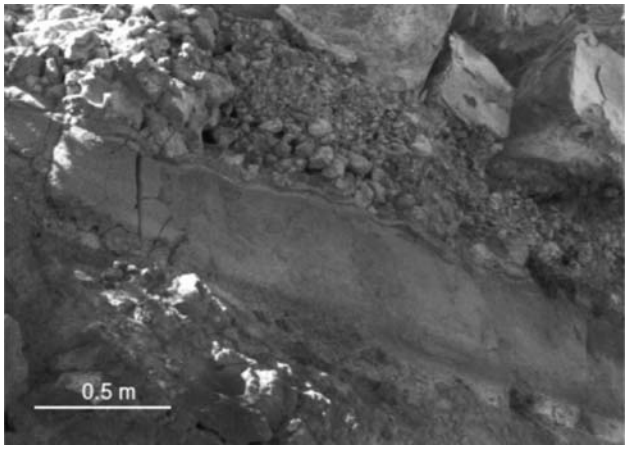

Figure 2 - Scoriaceous layer at the base of a lava flow on a well-developed reddish soil, northern Tenerife.

The **agglomerates** are compact rocks, which may display a high degree of consolidation, comprised of large uneven-sized heterogeneous clastic materials, often pyroclastic, within a finer matrix.

The **agglomerates breccias** are discerned owing to their angular fragments, being generally large with a matrix that can be sandy or clayey. These may form as the result of pyroclastic falls or may have an epiclastic mechanical-type origin related to landslides, avalanches and mudflows (debris avalanches, lahars, etc.). When their origin is epiclastic, the matrix is sandy or clayey since it is generated by the grinding of dragged materials. In this case, the fragments or clasts are generally angular and large and this agglomerate material is designated volcanic breccia (Fig. 3).

The **pyroclastic deposits** are comprised of fragments of glassy rock, generally loose or weakly compacted. They can be grouped as pyroclastic falls, with clean surfaces with no adhered particles, well-preserved crystal edges, with fragments without fractures and highly vesiculated glass with vesicles varying in shape (Fig. 4); pyroclastic surges,

Figure 3 - Volcanic breccia composed of large fragments embedded in a fine-grained matrix.

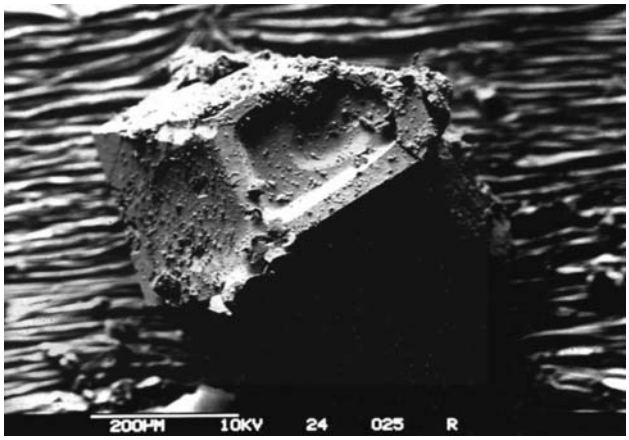

Figure 4 - Electron microscope image of pyroclastic fall from southern Tenerife showing a crystal with non-fractured edges. Approximate particle size 0.4 mm (Alonso, 1989).

with poorly vesiculated glass, highly modified by pyroclast abrasion (glass and crystals), equal-sized fragments with smooth concave-convex fracture surfaces and surfaces with cooling fissures; and pyroclastic flows with highly modified crystal edges, abundance of adhered ash, especially infilling vesicles and highly vesicular glass with a tendency towards elongated vesicles.

The **soil deposits** of the Canary Islands are mainly of coluvial origin, present in many areas particularly along the northern slopes of the western islands. Alluvial deposits are founded in gorges. River-lacustrine soils are also present in some valleys such as La Laguna Valley. Residual soils are the product of *in situ* weathering of pyroclastic materials, predominating silts and clays.

3. Geomechanical Properties of Volcanic Rocks

Basalt, trachybasalt and phonolite lava flows generally show high strength values, corresponding to geotechnical characteristics of hard or very hard rocks. Dykes with this composition can be also included in this geotechnical unit. The lithological heterogeneity determined by the alternating layers of basalts and scorias, the presence of discontinuities and cavities, the highly variable thicknesses of the lava layers and their irregular persistence are characteristical features of these materials that give rise to highly anisotropic and heterogeneous rock masses (Fig. 5).

The following types of rocks comprised of basalt lava flows have been distinguished (Table 1):

- Basalts with columnar jointing
- Basalts with spherical jointing
- Scoriaceous layers intercalated among the basalts
- Dykes

Rock masses formed by successions of basaltic lavas and associated scorias were classified according to their geomechanical indices RMR and Q. Table 1 shows the mean RMR and Q values obtained by analysing outcrops of fresh rocks or very scarcely weathered rocks with an extent of fracturing representative of the most common situations, excluding outcrops with extensive fractures or altered rocks.

From laboratory tests, the basalt lava flows show the following properties: dry densities range from 15 and 31 kN/m^3, being the most common values 23 to 28 kN/m^3; vesicular basalts can have densities of 15 to 23 kN/m^3, while massive basalts usually exceed 28 kN/m^3 (Fig. 6); uniaxial compressive strength values depends on mineral composition and volatile elements, giving rise to a wide range of strength values between 25 and 160 MPa, although the most common range is 40 to 80 Mpa; vesicular basalts can have strength under 40 MPa, while massive basalts may exceed 80 MPa (Fig. 7).

The main geotechnical problems related with the basaltic lava flow are as follows:

- Great spatial heterogeneity both in thickness and lateral and frontal extension.

Figure 5 - Cliffs showing basaltic lava flows successions and pyroclastic layers, dyke intrusions and different types of discontinuities, Anaga, Tenerife. Photograph window approximately 150 m wide.

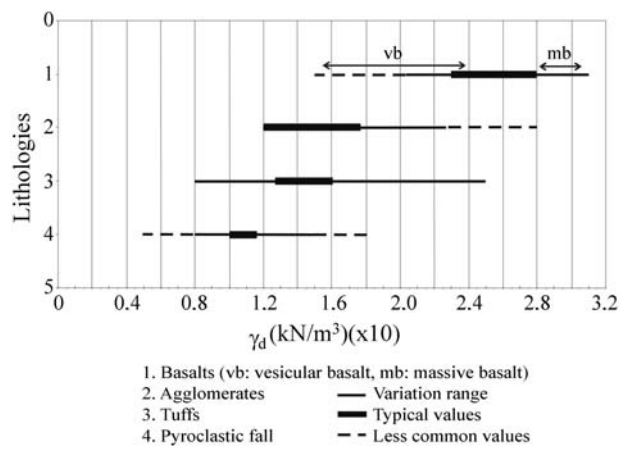

Figure 6 - Dry density values of the volcanic materials from the Canary Islands.

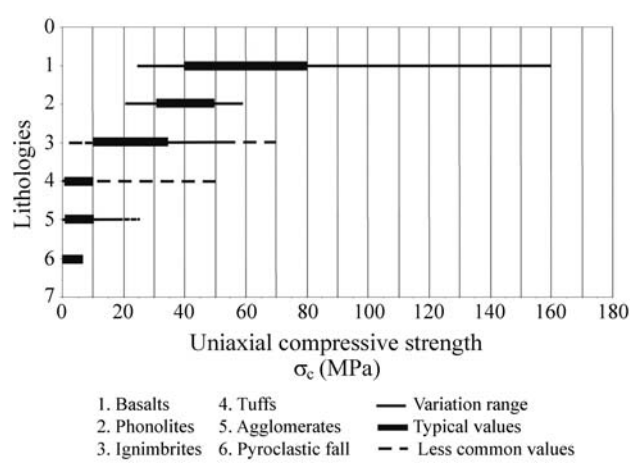

Figure 7 - Uniaxial compressive strength values according to the lithologies of the volcanic materials of the Canary Islands.

- Alternating layers of very hard material (basalts) with very porous and discontinuous levels (scorias).
- Soft materials underlying lava flows: lapillis, ashes and paleosoils.
- Vertical, open joints which can induce stability and water filtration problems, especially in tunnels and slopes.
- Cavities and volcanic tubes can lead to the collapse of basaltic scoriaceous cover lava materials.
- Overhangs may occur due to differential scoriaceous-basaltic layer erosion.
- Low strength surfaces between lava flows and pyroclastic layers favoring instabilities.
- Mechanical planes of discontinuities between dykes and wallrock that involve potential instability surfaces of great continuity.
- Slope instability mainly in cliff zones.
- Differential settlements in foundations when overlying different lithological formations.
- Alkaline reactions in concrete due to the glassy composition of volcanic materials with the possible formation of fissures and structural damage.
- Very hard and abrasive materials for excavations purposes.

Tuffs show the following representative properties: dry densities display a large range of values from below

Table 1 - Geomechanical characterization of basaltic and scoriaceous rock masses obtained from field surveys.

Characteristics		Columnar basalts		Spherical basalts	Scoriaceous layers
Lithology		Basalts, trachybasalts		Basalt	Basaltic with glassy texture
Thickness (m)		2-5		5-10	Several cm to 2 m
Structure		Vertical jointing		Spherical jointing	Non structured, abundant voids and welded
Intact rock	Texture	Aphanitic		Aphanitic	-
	Colour	Black, dark grey		Dark grey	-
	Weathering (ISRM, 1981)	Fresh- decoloured		Decoloured	-
	Strength (σ_c) (MPa) (Manual Test Hammer)	150-180 (Fig. 5 does not show these values)		Intermediate: 38	-
Discontinuities	Orientation	Vertical	Horizontal	Subvertical	-
	Dip	85º-90º	0º-5º (can reach 30º)	85º	-
	Spacing (mm)	200-600 (60-200)	200-600	60-200 to 200-600	-
	Continuity (m)	1-3	1	3-10	-
	Opening (mm)	0.25-2.5	0.2-0.5 to 0.5-2.5	-	-
	Roughness	Smooth, undulated	Rough	Smooth	-
	Infill	Uncommon but sandy if present	-	-	-
	Observations	-	Associated with massive basalts in thick layers	-	-
Rock mass	N. of sets of discontinuities	2 and 3		1	-
	Joints/m^3 (Jv)	4-8		< 1 (4-5)	-
	Block size (m^3)	< 0.5		Decimetric	Centimetric
	Block shape	Columnar, cubic & irregular		Irregular	Irregular fragments
	Weathering degree	II		III	II-VI
	Water	In general, there is no water		In general, there is no water	-
	Observations	-		-	Blocks welded but with granular appearance. Large cavities may form
Geomechanical classifications	RMR	70-75 Class II		60-65 Class II	Basalts and scorias 60-80 Class II
	Q	15 - 22 Good		30 - 180 Good to extremely good	Basalts and scorias 10-40 Intermediate to good

10 kN/m^3 to more than 25 kN/m^3, the range 8 to 18 kN/m^3 being typical for poorly-compacted tuffs and higher than 20 kN/m^3 for well-compacted tuffs; tuff composition affects their density, with higher densities shown by the basaltic tuffs and lower ones by acidic tuffs. The strength of the tuffs varies with the degree of compaction, grain size and composition, among other factors; uniaxial compressive strength ranged from 1 to 50 MPa for intact rock (Fig. 7); for saturated tuffs typical values are under 10 MPa. Angles of internal friction range from 30° to 50° for unweathered tuffs, although for a high degree of weathering these angles can be 12° to 30° (Fig. 8).

The use of geomechanical classifications based on discontinuity parameters that mainly affect the RMR and Q values is not recommended for massive tuffs due to their continuous and homogenous nature. Independently of this opinion, the results obtained were: RMR index ranged from 80-90, Class I; Q index ranged over 250 up until a value of 1000, classifying this rock as good to exceptionally good.

Ignimbrites have a uniaxial compressive strength ranging from 2 to 5 MPa for weathered ignimbrites and from 15 to 70 MPa for fresh ignimbrites (Fig. 7). Friction angles vary from 27° to 38°. RMR ratings assign these rocks to Class II, indicating good rock quality. Geotechnical properties of welded ignimbrites have been also described by Rodríguez-Losada *et al.* (2007b).

Volcanic agglomerates form a quite heterogeneous group. Dry densities depend on the nature of their clast components and the degree of compaction and porosity of the deposit. Agglomerates with a predominance of pumice clasts show low densities, even lower than 10 kN/m^3. In contrast, if the clasts are basaltic, densities are similar to those of basalt lavas. The most frequent dry density range for agglomerates is 12 to 18 kN/m^3, although there is a great scatter of values up to 28 kN/m^3 (Fig. 6). Uniaxial compressive strength is directly related to density and, therefore, to composition. Highest strength values were observed for agglomerates containing clasts of basic composition, and lowest values corresponded to those of felsic, or acidic, composition. The characteristic range is 0.5 to 25 MPa. Strength above 15 MPa were recorded for basaltic agglomerates; sometimes these were as high as 70 MPa (Fig. 7).

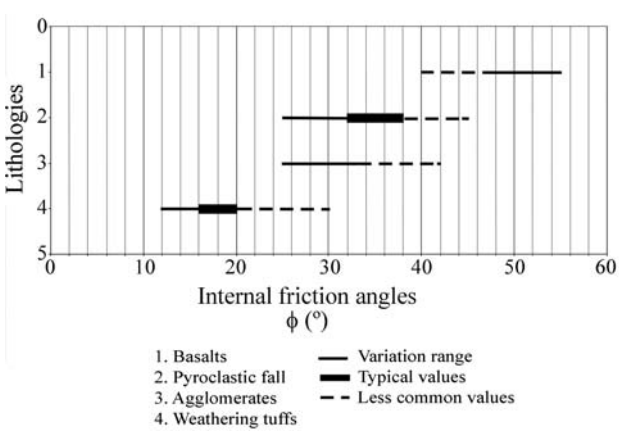

Figure 8 - Internal friction angles for different volcanic materials of the Canary Islands.

Tuffs, agglomerates, ignimbrites and pyroclastic flows can show the following geotechnical problems:

- Collapse of low-density tuffs or agglomerates.
- Weathering and devitrification processes producing expansive smectitic minerals (montmorillonites and nontronites).
- Open vertical fractures in ignimbrites may cause instability and water infiltration problems.
- Abrasive actions on machinery of the fine materials in these formations.
- Long-term plastic deformation.

The geomechanical properties of **pyroclastic deposits** depend on grain size, shape, porosity and petrologic composition, as well as the degree of packing between particles, the compaction state of the deposit and the strength of the particles. Dry densities of pyroclast falls range from 5 and 18 kN/m^3 (Fig.6). Density depends on the nature of the clasts and the extent of vesiculation, with basic pyroclasts being denser than felsic ones. The angle of internal friction ranges from 25° to 45° (Fig. 8). Uniaxial compressive strength varies from very low to 5 MPa (Fig. 7). Strength and deformability of low density pyroclasts has been described by Serrano *et al.* (2007a) and properties of lapilli for raw material uses has been also described by Lomoschitz *et al.* (2003).

The main geotechnical related problems of pyroclastics deposits are as follows:

- Very low density materials
- High deformation of lapilli and ashes in response to static or dynamic loads due to particle compaction and fracturing
- Collapsible ashes
- Low durability

4. Engineering Geological Properties of Soil Deposits

The properties of soils of volcanic origin in the Canary Islands are very dependent on the depositional environment and particle sizes. In coluvial materials the large grain sizes are predominant. Large boulders are very frequent in the alluvial deposits of the numerous gorges present in the islands. Alluvial and coluvial are very heterogeneous deposits with a wide range of particle sizes, but most of them are coarse materials. Fine soils are predominant in river-lacustrine deposits filling valleys or topographic depressions, with a range of granulometry from clays to sandy sizes.

Residual soils are the product of *in situ* weathering of pyroclastics materials with abundant silts to sandy soils and less frequently silty clays.

The lacustrine clays of La Laguna (Tenerife) have been studied by González de Vallejo *et al.* (1981). In some zones these clays have shown some degree of expansivity due to their montmorillonitic composition. However, their expansiveness is moderate due to the open structure of their microfabric, especially if this fabric is aggregated, which prevents volume changes. The swelling index for clay soils is 0.02 to 0.2 MPa, classifying these soils as non critical to critical. Clay soils of lacustrine origin show activity corresponding to inactive or normal clays. Atterberg limits range from 25% to 115% for the liquid limit and 15% to 95% for the plastic limit (Fig. 9). Specific weight of particles range from 22 to 30 kN/m^3 and dry density from 11 and 14 kN/m^3, although densities below 10 kN/m^3 may be found in other volcanic regions of the world.

The angle of friction varied from 23° to 40°, with the lower values corresponding to non-drained soils in non-consolidated conditions, whose pore pressure is very high. Friction angles above 35º were obtained for soils with a large proportion of sand-sized fractions and/or the presence of cementing agents. In clayey soils, residual friction angles were under 25°. In silty soils consolidated but not drained, the internal friction angle was generally low, less than 20°. Cohesion ranged from 0-0.2 MPa, the most common interval being 0-0.1 MPa. High cohesion values can be attributed to cementation processes between particles.

The compaction conditions of volcanic clayey soils improve when particles are more orientated such that the soil acquires an anisotropic structure. It has been demonstrated that compaction by kneading (Harvard miniature compaction test) is more efficient than by impact (standard Proctor test), (Lenz, 2004). The maximum density obtained here were between 12 and 15 kN/m^3 and optimum moisture values spanned a wide range, from 18 to 43%.

The properties of soils of volcanic origin and non-volcanic soils show a series of significant differences. Some of these differences determine that the usual correlations between properties and geotechnical behaviour used for non-volcanic soils are not directly applicable to volcanic soils (González de Vallejo, 1981). Among these differences next should be mentioned:

- In general, volcanic soils present high liquid limits and a much lower plasticity index than that of a non-volcanic clay-soil of similar liquid limit. The results of plasticity tests depend on the treatment applied to the sample; thus, usually the liquid limit increases with water content, dispersion and mixing time, while it decreases with drying.
- Granulometric fractions of less than two microns show large variation, from under 10% to over 80%, according to the treatment to which the sample was subjected before testing, and the way in which the granulometric analysis is conducted. Thus, the fraction under two microns increases depending on the energy of the dispersion agent used.
- Irreversible changes occur in properties as the moisture conditions are modified, particularly during the process of drying. This is among the most sensitive factors and the one that mostly affects the properties.
- Expansiveness is high to moderate for clays of montmorillonitic composition and high for halloysitic and allophanic clays, with abnormally low expansiveness observed in some montmorillonitic clays due to the effects of the microfabric.
- Shear strength is high despite the elevated liquid limits and very fine particle sizes. Similarly, unusual high internal friction angles are observed in relation to the index properties of the soils. The presence of cementing agents confers much higher shear strength than that expected for their composition.
- Compressibility index is lower than that corresponding to the soils' plasticity and granulometric properties.

The above mentioned differences between properties can be observed not only in the Canary Islands but in other volcanic regions, where it can be find slopes that are much steeper than would be expected according to the composition and granulometry of the soils. In addition, volcanic soils are highly sensitive to moisture conditions, which markedly affect their strength properties. Under intense rainfall, there is a rapid increase in pore pressures and a marked drop in strength, which may gives rise to slope instability problems. The presence of highly absorbent minerals and an open microfabric with weak particle junctions determines a highly unstable behaviour both in static and dynamic conditions (Konagai *et al.*, 2004).

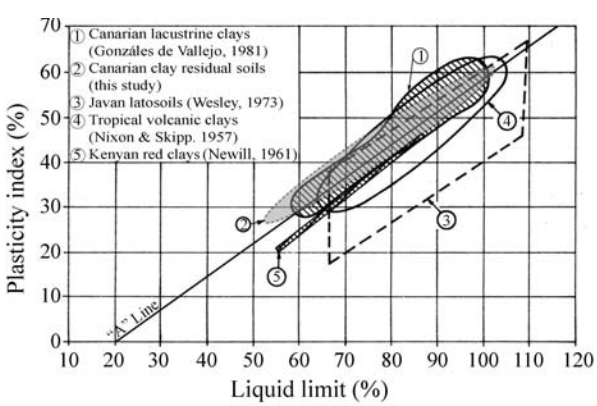

Figure 9 - Representation of volcanic soils on Casagrande's plasticity chart (modified from Gonzalez de Vallejo, 1981).

5. Discontinuities, Cavities and Tubes

Volcanic materials show an extensive sort of features comprising **joints, cavities and tubes**. Joins of thermal origin (cooling and retraction/contraction joints, with vertical, columnar, polygonal, radial, subhorizontal and spherical

jointing), of tectonic origin (faults, fractures and joints), discontinuities generated by intrusive structures (dykes, sills, plugs, etc.), discontinuities of gravitational origin (tension cracks, collapse fractures, slip surfaces, etc.), and discontinuities corresponding to contact surfaces between lava formations of depositional or erosive origin. The most common discontinuities found in the study areas are those of thermal origin, although all the discontinuities mentioned above may also be observed. Columnar joints are characteristic of basalt flows and often appear in massive lava materials, being generally polygonal or spherical in shape (Figs. 10 and 11). Spherical joints are the outcome of water infiltration towards inner zones of the flows. If the flow is very thick, retraction may also occur in horizontal planes creating bands that usually form at a distance of a third from the base (Fig. 12).

Discontinuities of tectonic origin are rarely observed in outcrops yet they can be easily recognized in caves and tunnels. Discontinuities produced by intrusion mechanisms (dykes) can be important for slope instability processes. In some cases, they constitute potential shear surfaces and hydrological barriers. Zones of mechanical contact between the wallrock rock and dyke exhibit series of open fractures parallel to the dyke; in some cases, relative displacements may be observed, behaving as normal faults.

Lava tubes and caves are the result of lava flow processes. When flows are very fluid, lavas continue to circulate beneath the already cooled outside crust to form so-called lava tubes. Since basalt rocks are very poor heat conductors, the surface of the flow solidifies and the molten lava continues flowing in its interior. This process ends with the material cooling down and subsequent formation of retraction fractures, which sometimes leads to the collapse of the tube roofs (Figs. 13 and 14).

6. Instability Processes

6.1. Collapse phenomena due to cavities

Collapse phenomena can occur as a consequence of the loss of strength of the materials that form the roof of lava tubes or cavities. These collapsing processes depend on the thickness of the lavas overlying the cavity and on their mechanical properties, as well as the size and depth of the cavities, although these are generally superficial. Figures 13 and 14 depict an example of collapsing lava tube roofs on the island of Lanzarote. Sometimes, these struc-

Figure 10 - Columnar jointing, Los Organos, La Gomera.

Figure 11 - Basaltic lava showing radial jointing, northern Tenerife. Photo window approxmate 4 x 3 m.

Figure 12 - Retraction band at a distance of a third from the base of the lava flow, northern Tenerife.

Figure 13 - Collapsed lava tube, Lanzarote.

Figure 14 - Cracking and collapsing of the roof of a lava tube, Lanzarote.

Figure 15 - Landslide on the cliffs of Famara, Lanzarote. Cliff height is 300 m.

tures appear as kilometres of sinuous troughs following the path of the flow that formed them.

The presence of cavities in lava-type volcanic materials is relatively frequent in the Canary Islands. Their origin could be the result of lava flows adapting to topographic irregularities, to spaces left by the fluids inside flows, to gasses associated with the flow or to differential cooling processes. The sizes of these cavities range from a few dm^3 to several m^3, forming caves. Their presence can give rise to geotechnical instability problems related to loads on foundations (Serrano *et al.*, 2007b).

6.2. Landslides and rockfalls

Instabilities associated with gravitational processes are relatively common in the Canary Islands and are usually induced by intense rainfall or linked to volcanic activity or even human actions. Some outstanding examples due to their magnitude and volume are found on the island of Gran Canaria, in the Tenteniguada basin (Quintana and Lomoschitz, 2001) and in the Tirajana depression (Lomoschitz, 1995). The latter are slow translational movements activated on repeated occasions, probably during rainy periods. In Lanzarote, ancient instabilities may be observed on the coastal cliffs of Famara, in the north of the island (Fig. 15). Of all the instability processes of the Canaries, the most common are those of rockfalls. Rockfall is provoked by intense rainfall and storms in coastal zones, and associated to high slopes in zones with escarpments and cliffs. Rockfall is particularly intense in high slope areas where lava and pyroclast layers alternate and in coluvial masses of low strength containing rocky blocks.

6.3. Paleolandslides

Massive large landslides have had a great influence on the evolution of volcanic islands and especially the Canary Islands. Thus, numerous large landslides have been described, mainly in the archipelago's western islands. Their impact in terms of risk is undeniable, although being linked to complex geological factors of extremely long return periods, their hazards are extremely low. The discovery and interpretation of the deposits of these gigantic landslides on marine bottoms has confirmed previous controversial hypotheses based on morphological features (Krastel *et al.*, 2001; Masson *et al.*, 2002; Acosta *et al.*, 2005). Deposits of the generally designated *debris avalanches* can cover areas of 200 to 2600 km^2 of the sea bottom, with calculated volumes between 25 and 650 km^3 and more than a hundred kilometers spanned from the island flank. On the Canaries, over 20 large landslides of this type have been described, 15 of which affected the western islands (Ferrer *et al.*, 2007).

7. Discussion and Conclusions

The main types of rock masses relevant to engineering geology in the Canary Islands are comprised of volcanic materials formed by basaltic, phonolitic and trachytic lava flows, along with materials of pyroclastic origin. The weatherings of pyroclastics products have developed surface formations of residual and transported soils. A summary of the properties of intact rocks, rock masses and soils are shown in Tables 2 and 3.

The effusive origin of these materials, their basic mineralogical composition, and the specific conditions of temperature, pressure, gasses, along with the environment and depositional setting, are the main geological influencing factors on geotechnical properties. The vitreous composition of pyroclastic products and their rapid decompression and cooling on expulsion causes rapid weathering, sometimes accompanied by hydrothermal alterations, with decisive effects on the geotechnical properties. The low density of many pyroclastic deposits, shape and size of their particles, degree of compaction and junctions between particles, can give rise to collapse phenomena.

The weathering of the rock minerals can generate soil deposits, which can sometimes show an expansive behaviour. Hygroscopic, mineralogic and microfabric properties, as well as moisture changes in volcanic soils, render differ-

Table 2 - Summary of geotechnical properties of the volcanic materials of Canary Islands.

Geotechnical properties / Material		G (kN/m^3)	γ_d (kN/m^3)	σ_c (MPa)	C (MPa)	ϕ (º)	E (GPa)	LL (%)	PL (%)	EI (MPa)	Other
Basalts		-	15-31 (23-28)	25-160 (40-80)	-	40-55	15-30	-	-	-	-
Tuffs		-	8-18 (poorly compacted) 18-25 (compacted)	1-50 < 10 (saturated)	0-1.45	12-30 (weathered tuffs)	0.1-22	-	-	-	-
Ignimbrites		13 to > 20	13 - > 20	2-5 (weak) 15-70 (hard)	0.1-2	27-38	30-50 (welded)	-	-	-	-
Agglomerates		-	12-28	0.5-25	≤ 0.4	25-42	0.1-3	-	-	-	-
Pyroclastic fall deposits		22-25	5-18	0-5	≤ 0.1	25-45 (32-38)	0.01-0.1	-	-	-	n(%): 45-65
Volcanic soils	Residual soils	22-30	12-13	-	≤ 0.1	23-40	0.510^{-3}-1110^{-3}	52-102	15-95	0.02-0.2	e: 1.6-2.88 W(%): 12-180 τ_u: 56-130 kPa $\gamma_{máx}$: 5-17.3 kN/m^3 Cc: 0.13-0.24
	Transported soils	27-29	11-14	-	-	-	-	35-90	25-45	0.02-0.15	

Indicated are maximum and minimum values. Most common values appear in brackets.
G: specific weight, γ_d: dry density, σ_c: uniaxial compressive strength, C: cohesion, ϕ: internal friction angle, E: elasticity modulus, LL: liquid limit, PL: plastic limit, EI: expansive index, n: porosity, e: pore index, W: moisture content, τ_u: shear strength, $\gamma_{máx}$: maximum Proctor density, C_c: compressibility coefficient.

Table 3 - Summary of engineering geological characteristics of pyroclastic materials.

Material	Composition	Granulometry-morphology	Structure	Origin	State*					Other geological features
					1	2	3	4	5	
Pyroclastic deposits	Acid (pumice) or basic	Ash < 2 mm Lapilli 2-64 mm Blocks, bombs & scorias > 64 mm	Bedded layers. Cinder cones	Pyroclastic fall	XXX	O or XX	O	O	X	Heterogeneous, discontinuous deposits
Tuffs	Pyroclastic generally of a pumitic nature	Lapilli & ash	Homogenous & continuous	Pyroclastic fall	O	XXX	XX	X	O	Massive, continuous deposits
				Pyroclastic flow	O	X	XXX	XX	O	
Ignimbrites	Pyroclastic major component: pumice	Lapilli & ash	Arranged as flow layers. Eutaxitic texture	Pyroclastic flow	O	O	XXX	XXX	O	Joints and fractures may develop as in flows
Agglomerates & agglomeratic breccias	Pyroclastic or polygenic. Large angular fragments in breccias	Unclassified thick, angular, heterometric fragments in fine matrix	Massive and lacking structure	Airfall	XX	XXX	XX	O	XX	Water transport
				Lahars	O	X	X	O	XX	
				Avalanches	O	X	X	O	XX	Gravitational sliding

(*)1: loose, 2: compact, 3: consolidated, 4: welded, 5: cemented ([1]), XXX: most common state, XX: Sometimes, X: scarcely, O: never, ([1]) Since cementation is a post-depositional process, its presence depends on the geochemical conditions of the environment.

ent geotechnical behaviour patterns to those expected for non-volcanic soils of similar granulometric characteristics. The low density of volcanic soils, their very open microstructure with weak junctions between particles and their mineralogic composition lead to unfavorable geotechnical behaviour patterns in terms of their strength, deformability, compactability and stability in response to static and dynamic loads.

Anisotropy and heterogeneity of the volcanic rock masses along with their irregular spatial organization determine abrupt changes in thickness and continuity. These circumstances markedly condition site investigations and consequently the geomechanical characterization of the rocks, which translates to further difficulties and uncertainties when trying to establish representative ground profiles. Dyke intrusion processes frequently observed on islands constitute very characteristic discontinuity structures that affect the strength of the rock masses and their hydrogeological conditions. Conditions of rapid cooling of lavas, flows and their build-up, render typologies of discontinuities specific to these materials as well as cavities and tubes.

Site investigation techniques in volcanic islands usually require larger number of boreholes and specific geophysical methods appropriated for volcanic materials. Some of the limitations on geophysical methods include the identification of low density materials, such as pyroclastics deposits underlying basaltic lava flows by using seismic refraction methods. The detection of cavities by geo-radar techniques is limited to 10 m depth; electric tomography is also limited to 50 m depth and gravimetric methods are not appropriate to identify small size cavities. Searching for cavities using geophysical methods should be complemented by rotary or percussion drilling and down-hole television cameras techniques. As a consequence of the particular geotechnical and geological characteristics of the volcanic materials a specific geotechnical group of materials should be established.

In spite of these unfavourable engineering geological conditions, most of the volcanic rocks show generally acceptable geomechanical behaviour for many conventional excavations and foundations, due to the high strength properties, roughness of their contact surfaces, irregular shape of their particles and excellent drainage conditions. Human actions such as deforestation, desertification, uncontrolled excavations, blocking the natural drainage network and inadequate site investigations, as well as environmental factors like intense rainfall or coastal erosion, can induce severe geotechnical problems, highlighting the importance of acquiring sound geomechanical knowledge and appropriated site investigation procedures.

Acknowledgments

The authors thank to Julia Seisdedos from Instituto Geológico y Minero de España (IGME) and Luis E. Hernández-Gutiérrez from the Geotechnical Laboratory of the

Regional Government of the Canary Islands. The authors acknowledge the support of IGME to this study carried out within the framework of the research project IGME-CYCIT (CGL 2004-00899).

References

Acosta, J.; Uchupi, E.; Muñoz, A.; Herranz, P.; Palomo, C.; Ballesteros, M. & ZEE Working Group (2005) Geologic evolution of the Older Canary Islands: Lanzarote, Fuerteventura, Gran Canaria and La Gomera with a brief description of the avalanches on the younger islands: Tenerife, La Palma and El Hierro. Mar. Geoph. Res., v. 24, p. 1-2.

Alonso, J.J. (1989) Estudio Volcanoestratigráfico y Volcanológico de los Piroclastos Sálicos del Sur de Tenerife. PhD. Thesis, Universidad de La Laguna, Tenerife, 257 pp.

Ancochea, E.; Hernán, F.; Bellido, F.; Muñoz, M.; Sagredo, J.; Brändle, J.L.; Huertas, M.J.; Barrera, J.L.; Cubas, C.R.; Herrera, R.; De la Nuez, J.; Coello, J. & Gómez, J.A. (2004) Canarias. Vera, J.A. (ed) Geología de España. Instituto Geológico y Minero de España, Madrid, pp. 637-671.

Carracedo, J.C.; Pérez Torrado, F.J.; Ancochea, E.; Meco, J.; Hernán, F.; Cubas, C.R.; Casillas, R.; Rodríguez Badiola, E. & Ahijado, A. (2002). Cenozoic volcanism II. The Canary Islands. Gibbson, W. & Moreno, T. (eds) Geology of Spain. The Geological Society, London, pp. 439-472.

Ferrer, M.; Seisdedos, J.; García, J.C.; González de Vallejo, L.I:; Coello, J.J.; Casillas, R.; Martín, C. & Navarro, J.M. (2007) Volcanic mega-landslides in Tenerife (Canary Islands, Spain). ISRM International Workshop on Volcanic Rocks, pp. 185-191. Ponta Delgada, Azores, 14 July.

González de Vallejo, L.I.; Hijazo, T.; Ferrer, M. & Seisdedos, J. (2006) Caracterización Geomecánica de los Materiales Volcánicos de Tenerife. Serie Medio Ambiente. Riesgos Geológicos, n. 8. Instituto Geológico y Minero de España, Madrid, 736 pp.

González de Vallejo, L.I.; Jiménez Salas, J.A. & Leguey Jiménez, S. (1981) Engineering geology of the tropical volcanic soils of La Laguna, Tenerife. Engineering Geology, v. 17, p. 1-17.

ISRM (1981) Suggested Methods for Rock Characterization, Testing and Monitoring. ISRM Suggested Methods. Pergamon Press, Oxford, 211 pp.

Konogai, K.; Johansson, J.; Mayorca, P.; Uzuoka, R.; Yamamoto, T.; Miyajima, M.; Pulido, N.; Sassa, K.; Fukuoka, H. & Duran, F. (2004). Las Colinas Landslide: Rapid and long-traveling soil flow caused by the January 13, 2001, El Salvador earthquake. Geological Society of America, Special Paper 375, pp. 39-53.

Krastel, S.; Schminke, H.U.; Jacobs, C.L.; Rihm, R.; Le Bas, T.P. & Alibés, B. (2001) Submarine landslides around the Canary Islands. J. Geoph. Res., v. 106, p. 3977-3997.

Lenz, O. (2004) Influencia de la fábrica de las arcillas volcánicas de la ciudad de Xapala en su comportamiento geotécnico. PhD. Thesis, Universidad Politécnica de Madrid, Madrid, 183 pp.

Lomoschitz, A.; Mangas, J. & Socorro, M. (2003) Geological characterization of lapilli in Gran Canaria Island, a raw material used as a gas granular filter. Macias, A. & Umbría, J. (eds) 4th European Meeting on Chemical Industry And Environment. Universidad de Las Palmas de Gran Canaria, v. 2, p. 21-32.

Lomoschitz, A. (1995) Análisis del origen y evolución de la depresión de Tirajana, Gran Canaria. PhD. Thesis, Universidad Politécnica de Cataluña, 203 pp.

Masson, D.G.; Watts, A.B.; Gee, M.J.R.; Urgeles, R.; Mitchell, N.C.; Le Bas, T.P. & Canals, M. (2002) Slope failures on the flanks of the western Canary Islands. Earth-Sci. Rev., v. 57, p. 1-35.

Quintana, P. y Lomoschitz, A. (2001) Caracterización de los depósitos de *debris avalanche* de la cuenca de Tenteniguada, Gran Canaria. Proceedings V Simp. Nac. Taludes y Laderas Inestables, p. 603-614.

Rodríguez-Losada, J.A. (2004) Las islas Canarias y el origen y clasificación de las rocas igneas. Iª Jornada Geotécnica para Edificación. Gobierno de Canarias, Consejeria Inf. Trans. y Viv, unpublished.

Rodríguez-Losada, J.A.; Hernández-Gutiérrez, L.E.; Olalla, C.; Perucho, A.; Serrano, A. & Del Potro, R. (2007a) The volcanic rocks of the Canary Islands. Geotechnical properties. ISRM International Workshop on Volcanic Rocks. Ponta Delgada, Azores. In Malheiro and Nunes (Eds). Taylor and Francis Group, pp. 53-57.

Rodríguez-Losada, J.A.; Hernández-Gutiérrez, L.E. & Mora-Figueroa, A.L. (2007b) Geotechnical features of the welded ignimbrites of the Canary Islands. ISRM International Workshop on Volcanic Rocks, pp. 29-34. Ponta Delgada, Azores. In Malheiro and Nunes (eds) Taylor and Francis Group.

Serrano, A.; Olalla, C.; Perucho, A. & Hernández-Gutiérrez, L.E. (2007a) Strength and deformability of low density pyroclasts. ISRM International Workshop on Volcanic Rocks, pp. 35-43. Ponta Delgada, Azores. In: Malheiro and Nunes (eds) Taylor and Francis Group.

Serrano, A.; Perucho, A.; Olalla, C. & Estaire, J. (2007b) Foundations in volcanic zones. 14th European Conference on Soils Mechanics and Geotechnical Eng. Millpress, Rotterdam, v. 4, pp. 1801-1815.

Some Applications of Linear Viscoelasticity to Problems of Consolidation under Variable Loading

Paulo Eduardo Lima de Santa Maria, Flávia Cristina Martins de Santa Maria,
Ian Schumann Marques Martins

Abstract. The main purpose of this paper is to present a general method to derive closed form solutions for one-dimensional consolidation problems under time dependent loading using the Linear Viscoelasticity theory. A review of the basic concepts of this theory is initially presented and, mainly for illustration purposes, the method is applied to three consolidation problems, leading to relevant solutions for Geotechnical Engineering. In the first application, considering Terzaghi's and Barron's solutions, creep functions are determined for vertical and radial drainage, allowing derivation of expressions for one-dimensional consolidation under a number of linear loads for these drainage conditions. Using Carrillo's equation, the creep function for combined vertical and radial drainage is obtained, leading to corresponding solution for linear variable loading. Partial submersion of embankments on soft soils is another consolidation problem under time dependent loading solved by means of Viscoelasticity. Classical approximate solutions are used in this second application to establish creep functions for vertical drainage and exact Barron's solution to establish creep function for radial drainage. An expression for late stages of consolidation is also derived for combined vertical and radial drainage condition. The third application considers the problem of load transfer from a consolidating deposit of soft clay to a pattern of drain columns of finite stiffness. Diagrams concerning a case of consolidation under linear variable three-step loading and consolidation with partial submersion of the fill are provided to illustrate the solutions obtained.

Key words: one-dimensional consolidation, viscoelasticity, variable loading, submersion of embankments, drain columns.

1. Introduction

The main purpose of this paper is to present a general and simple method to derive solutions for consolidation problems involving variable loading. The method consists in employing Linear Viscoelasticity to state constitutive equations and Laplace transforms to solve these equations. The corresponding creep function for each problem is obtained from existing solutions for constant loading.

Attention should be drawn to the words *viscoelasticity and creep function*, which might be misleading once there is no viscous phenomenon affecting primary consolidation. However, for total stress analysis, the method is perfectly applicable despite the hydrodynamic feature of the process once there is a time dependent strain for a constant total stress applied.

The method is illustrated through three applications involving practical problems of geotechnical engineering design, as explained below.

Construction of embankments on soft soils is usually performed in steps of loading. Owing to conditions such as construction timing and low strength of the underlying soil, these steps must be carefully planned as far as the rate of filling is concerned. Also, in order to abbreviate the time of construction, drain wells are often installed and therefore the analysis must contemplate consolidation with both vertical and radial drainage.

Conventional analyses of consolidation with variable loading usually lead to rather complex mathematical formulations. Nevertheless, a great deal of work has been accomplished in order to obtain solutions for one-dimensional consolidation with variable loading. Therefore, a number of approximate and exact solutions are now available (Terzaghi and Frölich, 1936; Taylor, 1942; Schiffman, 1958; Olson, 1977; Kurma Rao and Vijaya Rama Raju, 1990; Da Mota, 1996; Lekha *et al.*, 1998).

Using total stress linear viscoelastic approach, solutions to this first application may be obtained in an elegant and simple way, even for complex variable loading history and either for vertical, radial or combined drainage conditions. These solutions guarantee unquestionable benefits in accuracy when embankments construction conditions impose several steps of loading with different loading rates.

The second application regards the effect of the submersion of the fill, which is another important problem concerning one-dimensional consolidation with variable loading. Total stress viscoelastic analysis provides a closed form solution for vertical, radial or combined drainage conditions.

Paulo Eduardo Lima de Santa Maria, Ph.D., Associate Professor, COPPE, Universidade Federal do Rio de Janeiro, Rio de Janeiro, RJ, Brazil. e-mails: paulosm@coc.ufrj.br and pesantamaria@superig.com.br.
Flávia Cristina Martins de Santa Maria, D.Sc., Civil Engineer, Eletrobras Termonuclear S.A., Rio de Janeiro, RJ, Brazil. e-mails: fsmaria@eletronuclear.gov.br and fsantamaria@ superig.com.br.
Ian Schumann Marques Martins, D.Sc., Associate Professor, COPPE, Universidade Federal do Rio de Janeiro, Rio de Janeiro, RJ, Brazil. E-mail: ian@coc.ufrj.br.
Submitted on March 15, 2007; Final Acceptance on September 4, 2007; Discussion open until August 29, 2008.

The third application considers the problem of load transfer from a consolidating deposit of soft clay to a pattern of drain columns of finite stiffness.

The analyses presented in this paper consider linear behaviour of soils for small deformation problems. This is certainly an approximation and may introduce some inaccuracy in the results. However, this approximation is the same as that found in the Terzaghi's Theory of Consolidation, which produces reasonably accurate predictions for most of the practical situations. It is worth mentioning that despite Linear Viscoelasticity not applying to materials exhibiting nonlinear stress-strain behaviour, an extension to the linear superposition principle can be employed to derive nonlinear viscoelastic constitutive equations (Findley *et al.*, 1976).

2. Basic Concepts

2.1. Creep and relaxation functions

Many stress-strain-time relations existing in technical literature are basically empirical (Findley *et al.*, 1976; Bland, 1960). Most of them were established to fit experimental data obtained under constant stress and temperature. However, actual behaviour of materials has shown that the strain corresponding to a particular time depends on all the stress values to which the material has been submitted in the past and not on its final value. Therefore, the creep phenomenon is affected by the whole stress history. Considering this, several methods have been proposed to represent the viscoelastic behaviour of the materials. In general, however, there are two alternative mathematical procedures to represent the stress-strain-time behaviour of the materials: differential and integral forms.

The study carried out in this paper employed the integral form or, as frequently referred, hereditary integrals. The advantage of the hereditary integrals over the differential form consists of a higher flexibility of representation of the material properties inferred from laboratorial tests. Integral form can also be extended to describe the behaviour of aging materials and incorporate temperature effects. Besides, for problems involving rather complex time loading functions, the integral method leads to a simpler solution.

In a uniaxial creep test a step of constant stress $\sigma = \sigma_0 H(t)$, where $H(t)$ represents the unit step or Heaviside function, is applied to a viscoelastic material and the strain $\varepsilon(t)$ is measured. For materials exhibiting linear behaviour, the strain can be represented by

$$\varepsilon(t) = \sigma_0 J(t) \tag{1}$$

or

$$J(t) = \frac{\varepsilon(t)}{\sigma_0} \tag{2}$$

The function $J(t)$ is called creep function or creep compliance and is a material property.

In a relaxation test a step of constant strain $\varepsilon = \varepsilon_0 H(t)$ is prescribed to a viscoelastic material and the stress $\sigma(t)$ is measured. For linear materials the stress can be represented by

$$\sigma(t) = \varepsilon_0 R(t) \tag{3}$$

or

$$R(t) = \frac{\sigma(t)}{\varepsilon_0} \tag{4}$$

The function $R(t)$ is called relaxation function or relaxation modulus and, likewise the creep function, is a material property.

2.2. Integral representation of creep for uniaxial stress

If a viscoelastic body with linear behaviour is subjected to a continuous stress function $\sigma(t)$ with finite derivative within the concerned time interval, representing the stress history, the corresponding strain function $\varepsilon(t)$ can be obtained from the equation

$$\varepsilon(t) = \int_0^t J(t-\tau)\frac{\partial\sigma(\tau)}{\partial\tau}\,d\tau \tag{5}$$

where τ is an auxiliary variable and $J(t - \tau)$ the creep function. Expression (5) may also be alternatively represented by

$$\varepsilon(t) = \sigma(t)J(0) - \int_0^t \frac{\partial J(t-\tau)}{\partial\tau}\sigma(\tau)\,d\tau \tag{6}$$

if $J(t - \tau)$ is continuous and differentiable.

Expressions (5) and (6) apply to the particular case where the process begins at time $t = 0$ and the initial value of the stress is zero, *i.e.*, $\sigma(0) = 0$. For the general case, with the process beginning at time τ_0 and the initial value of the stress being different from zero, the following equations hold

$$\varepsilon(t) = \sigma(\tau_0)J(t-\tau_0) + \int_{\tau_0}^t J(t-\tau)\frac{\partial\sigma(\tau)}{\partial\tau}\,d\tau \tag{7}$$

$$\varepsilon(t) = \sigma(t)J(0) - \int_{\tau_0}^t \frac{\partial J(t-\tau)}{\partial\tau}\sigma(\tau)\,d\tau \tag{8}$$

Once the creep function $J(t)$ is identified, one of the Eqs. (5), (6), (7) and (8) can be employed to predict the stress function $\sigma(t)$ given a prescribed strain history $\varepsilon(t)$. However, resolving $\sigma(t)$ using one of the above equations involves the solution of an integral equation, which is mathematically much more complicated than a direct integration. Otherwise, the following equations can be written

$$\sigma(t)=\varepsilon(\tau_0)R(t-\tau_0)+\int_{\tau_0}^{t}R(t-\tau)\frac{\partial\varepsilon(\tau)}{\partial\tau}d\tau \quad (9)$$

$$\sigma(t)=\varepsilon(t)R(0)-\int_{\tau_0}^{t}\frac{\partial R(t-\tau)}{\partial\tau}\varepsilon(\tau)d\tau \quad (10)$$

Therefore, to determine $\sigma(t)$ from a prescribed strain history $\varepsilon(t)$, the relaxation function $R(t)$ must be known.

2.3. The method proposed

The proposed method consists of three steps:

(1) Using Eq. (2) and the relevant consolidation solution for *constant total stress*, define the creep function;

(2) Taking into account the creep function defined in (1) and the total stress history of the problem, the Laplace transform one of the Eqs. (5), (6), (7) and (8) leads to the solution or to an algebraic equation that can be easily solved;

(3) Find the inverse Laplace transform of the solution obtained in (2).

The last step is often the most difficult one, presenting in some cases no closed form solution.

3. First Application: Analysis of One-Dimensional Consolidation under a Number of Linear Variable Loads

The analysis presented in this paper establishes creep functions derived from Terzaghi's and equal strain Barron's equations for vertical and radial drainage respectively. Therefore, the same assumptions made to obtain those equations are also considered here, as follows:

(1) The soil is considered homogeneous and fully saturated;

(2) The compressibility of the soil particles and the water are negligible in comparison with that of the soil structure;

(3) There is only vertical displacement of the soil particles and vertical water flow for Terzaghi's equation and radial water flow for Barron's equation;

(4) Darcy's law is strictly valid;

(5) The stress-strain relationship of the soil structure is linear.

3.1. First case: vertical drainage

Suppose a homogeneous deposit of soft clay (Fig. 1) subjected to a loading constituted by a set of linear variable loads (Fig. 2). According to Terzaghi and Frölich (1936), the average degree of consolidation U_v for one-dimensional consolidation with vertical drainage and constant loading is

$$U_v=1-\sum_{0}^{\infty}\frac{2}{M^2}e^{-M^2T_v} \quad (11)$$

where

$$M=(2m+1)\frac{\pi}{2} \quad (12)$$

$$T_v=\frac{c_v t}{H^2} \quad (13)$$

where c_v = coefficient of consolidation for vertical flow, t = time and H = maximum drainage distance.

It may also be written

$$U_v=\frac{s(t)}{s(\infty)}=\frac{\bar{\varepsilon}(t)}{\bar{\varepsilon}(\infty)} \quad (14)$$

where $s(t)$ = settlement of the top of the layer at time t, $s(\infty)$ = final settlement of the top of the layer, at infinite time, $\bar{\varepsilon}(t)$ = average vertical strain at time t and $\bar{\varepsilon}(\infty)$ = final average vertical strain, at infinite time.

For a homogeneous deposit of soft soil, the average strain at infinite time may be written as

$$\bar{\varepsilon}(\infty)=m_v\sigma_0 \quad (15)$$

where m_v = coefficient of volume compressibility and σ_0 = total stress applied.

Therefore

$$\bar{\varepsilon}(t)=m_v\sigma_0\left(1-\sum_{0}^{\infty}\frac{2}{M^2}e^{-M^2\frac{c_v t}{H^2}}\right) \quad (16)$$

Taking into account expression (16) and recalling that

$$J(t)=\frac{\varepsilon(t)}{\sigma_0} \quad (2)$$

follows

$$\bar{J}_v(t)=m_v\left(1-\sum_{0}^{\infty}\frac{2}{M^2}e^{-M^2\frac{c_v t}{H^2}}\right) \quad (17)$$

Let $q(t)$ be the loading acting on the surface of the clay deposit, as illustrated in Fig. 2. For $t \le t_n$, this loading may be represented by

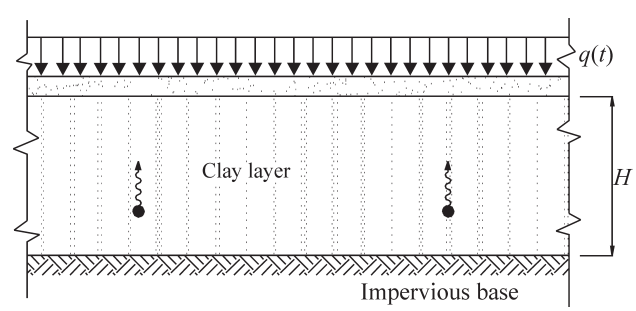

Figure 1 - Representation of a clay layer subjected to one-dimensional consolidation with vertical drainage under variable loading.

$$q(t)=\sum_{1}^{n}\{q_i(t-t_{i-1})[H(t-t_{i-1})-H(t-t_i)]\} \tag{18}$$

where $t_0 = 0$ and $H(t)$ is the Heaviside function, as previously mentioned.

Equation (6) may be written as

$$\bar{\varepsilon}(t)=q(t)\bar{J}_v(0)-\int_0^t q(\tau)\frac{\partial \bar{J}_v(t-\tau)}{\partial \tau}d\tau \tag{19}$$

or

$$\bar{\varepsilon}(t)=q(t)\bar{J}_v(0)-\sum_{1}^{n}\left\{\int_0^t q_i(\tau-t_{i-1})[H(\tau-t_{i-1})-H(\tau-t_i)]\frac{\partial \bar{J}_v(t-\tau)}{\partial \tau}d\tau\right\} \tag{20}$$

Considering Eq. (17) and bearing in mind that

$$\bar{J}_v(0)=m_v\left(1-\sum_{0}^{\infty}\frac{2}{M^2}\right)=0 \tag{21}$$

$$q_k(\tau-t_{k-1})=\sum_{1}^{k-1}\Delta q_i+\frac{\Delta q_k}{t_k-t_{k-1}}(\tau-t_{k-1}) \tag{22}$$

the integral of Eq. (20) may be evaluated, giving

$$\bar{\varepsilon}(T_v)=m_v\sum_{1}^{k-1}\left\{\Delta q_i\left[1-\frac{2}{T_{v_i}-T_{v_{(i-1)}}}\times\sum_{0}^{\infty}\frac{1}{M^4}(1-e^{-M^2(T_{v_i}-T_{v_{(i-1)}})})\times e^{-M^2(T_v-T_{v_i})}\right]\right\}+m_v\Delta q_k\times\left[\frac{T_v-T_{v_{(k-1)}}}{T_{v_k}-T_{v_{(k-1)}}}-\frac{2}{T_{v_k}-T_{v_{(k-1)}}}\sum_{0}^{\infty}\frac{1}{M^4}\left(1-e^{-M^2(T_v-T_{v_{(k-1)}})}\right)\right] \tag{23}$$

and

$$U_v(T_v)=\sum_{1}^{k-1}\left\{\rho_i\left[1-\frac{2}{T_{v_i}-T_{v_{(i-1)}}}\sum_{0}^{\infty}\frac{1}{M^4}\times\left(1-e^{-M^2(T_{v_i}-T_{v_{(i-1)}})}\right)\times e^{-M^2(T_v-T_{v_i})}\right]\right\}+\rho_k\left[\frac{T_v-T_{v_{(k-1)}}}{T_{v_k}-T_{v_{(k-1)}}}-\frac{2}{T_{v_k}-T_{v_{(k-1)}}}\sum_{0}^{\infty}\frac{1}{M^4}\left(1-e^{-M^2(T_v-T_{v_{(k-1)}})}\right)\right] \tag{24}$$

where

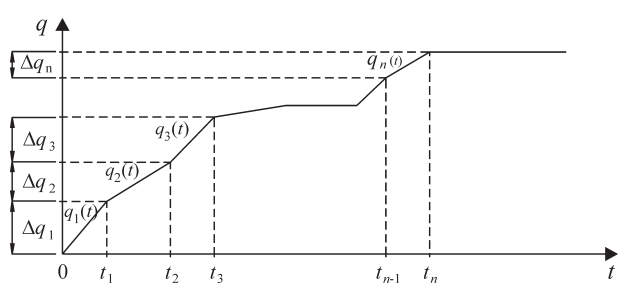

Figure 2 - General loading history considered in the analysis.

$$\rho_i=\frac{\Delta q_i}{\sum_{i}^{n}\Delta q_i} \tag{25}$$

T_{v_i} = time factor for vertical drainage relative to time t_i.

Expressions (23) and (24) are valid for $t_{k-1} \le t \le t_k$ ($k \le n$). For $t > t_n$ the loading history is represented by

$$q(t)=\sum_{1}^{n}\{q_i(t-t_{i-1})[H(t-t_{i-1})-H(t-t_i)]\}+q_n(t_n)H(t-t_n) \tag{26}$$

where

$$q_n(t_n)=\sum_{1}^{n}\Delta q_i \tag{27}$$

Substituting Eq. (26) into Eq. (19) and integrating, yields

$$\bar{\varepsilon}(T_v)=m_v\sum_{1}^{n}\left\{\Delta q_i\left[1-\frac{2}{T_{v_i}-T_{v_{(i-1)}}}\times\sum_{0}^{\infty}\frac{1}{M^4}(1-e^{-M^2(T_{v_i}-T_{v_{(i-1)}})})\times e^{-M^2(T_v-T_{v_i})}\right]\right\} \tag{28}$$

and

$$U_v(T_v)=\sum_{1}^{n}\left\{\rho_i\left[1-\frac{2}{T_{v_i}-T_{v_{(i-1)}}}\sum_{0}^{\infty}\frac{1}{M^4}\times\left(1-e^{-M^2(T_{v_i}-T_{v_{(i-1)}})}\right)\times e^{-M^2(T_v-T_{v_i})}\right]\right\} \tag{29}$$

Expressions (28) and (29) are therefore valid for $t \ge t_n$.

3.2. Second case: radial drainage

This case considers a homogeneous deposit of soft clay with vertical drains (Fig. 3) subjected to the same general loading scheme admitted in the first case (Fig. 2). It is assumed that no vertical drainage occurs in the clay.

The degree of consolidation U_r for one-dimensional consolidation with radial drainage, constant loading and equal strain (Barron, 1948) is

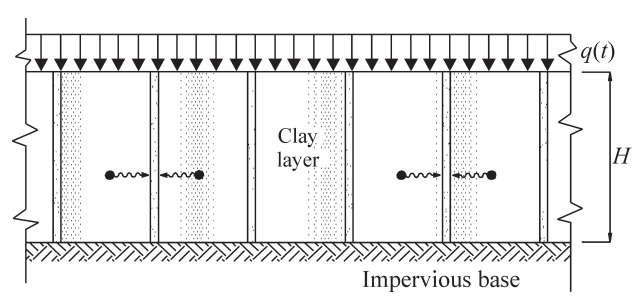

Figure 3 - Representation of a clay layer subjected to one-dimensional consolidation with radial drainage under variable loading.

$$U_r = 1 - e^{-\frac{8T_r}{f(n)}} \tag{30}$$

where

$$T_r = \frac{c_r t}{4r_e^2} \tag{31}$$

$$f(n) = \left[\frac{n^2}{n^2-1}\ln(n) - \frac{3n^2-1}{4n^2}\right] \tag{32}$$

$$n = \frac{r_e}{r_d} \tag{33}$$

where c_r = coefficient of consolidation for radial flow, t = time, r_e = radius of the zone of influence of the drain and r_d = radius (or equivalent radius) of the drain.

Taking into account that $\varepsilon(z, t)$ in this case is constant along the depth z, the following equation may be written

$$U_r = \frac{s(t)}{s(\infty)} = \frac{\varepsilon(t)}{\varepsilon(\infty)} \tag{34}$$

and so

$$\varepsilon(t) = m_v \sigma_0 \left(1 - e^{-\frac{2c_r t}{f(n) r_e^2}}\right) \tag{35}$$

Therefore, the creep function for radial drainage is

$$J_r(t) = m_v \left(1 - e^{-\frac{2c_r t}{f(n) r_e^2}}\right) \tag{36}$$

In this case, Eq. (6) may be written as

$$\varepsilon(t) = q(t) J_r(0) - \int_0^t q(\tau) \frac{\partial J_r(t-\tau)}{\partial \tau} d\tau \tag{37}$$

For $t \le t_n$, the vertical strain $\varepsilon(t)$ due to the loading history $q(t)$ represented by Eq. (18) is

$$\varepsilon(t) = q(t) J_r(0) - \sum_1^n \left\{ \int_0^t q_i(\tau - t_{i-1})[H(\tau - t_{i-1}) - H(\tau - t_i)] \frac{\partial J_r(t-\tau)}{\partial \tau} d\tau \right\} \tag{38}$$

Inserting Eq. (36) into the right-hand side of Eq. (38), recalling that

$$J_r(0) = 0 \tag{39}$$

$$q_k(\tau - t_{k-1}) = \sum_1^{k-1} \Delta q_i + \frac{\Delta q_k}{t_k - t_{k-1}}(\tau - t_{k-1}) \tag{22}$$

and evaluating Eq. (38), yields

$$\varepsilon(T_r) = m_v \sum_1^{k-1} \left\{ \Delta q_i \left[1 - \frac{f(n)}{8(T_{r_i} - T_{r_{(i-1)}})} \left(1 - e^{-\frac{8}{f(n)}(T_{r_i} - T_{r_{(i-1)}})} \right) \times e^{-\frac{8}{f(n)}(T_r - T_{r_i})} \right] \right\} + m_v \Delta q_k \left[\frac{T_r - T_{r_{(k-1)}}}{T_{r_k} - T_{r_{(k-1)}}} - \frac{f(n)}{8(T_{r_k} - T_{r_{(k-1)}})} \times \left(1 - e^{-\frac{8}{f(n)}(T_r - T_{r_{(k-1)}})} \right) \right] \tag{40}$$

and

$$U_r(T_r) = \sum_1^{k-1} \rho_i \left[1 - \frac{f(n)}{8(T_{r_i} - T_{r_{(i-1)}})} \left(1 - e^{-\frac{8}{f(n)}(T_{r_i} - T_{r_{(i-1)}})} \right) \times e^{-\frac{8}{f(n)}(T_r - T_{r_i})} \right] + \rho_k \left[\frac{T_r - T_{r_{(k-1)}}}{T_{r_k} - T_{r_{(k-1)}}} - \frac{f(n)}{8(T_{r_k} - T_{r_{(k-1)}})} \times \left(1 - e^{-\frac{8}{f(n)}(T_r - T_{r_{(k-1)}})} \right) \right] \tag{41}$$

where

$$\rho_i = \frac{\Delta q_i}{\sum_i^n \Delta q_i} \tag{25}$$

T_{r_i} = time factor for radial drainage relative to time t_i.

Expressions (40) and (41) hold for $t_{k-1} \le t \le t_k$ ($k \le n$). For $t > t_n$, using the loading history represented by Eq. (26), $\varepsilon(t)$ may be expressed by

$$\varepsilon(T_r) = m_v \sum_1^n \left\{ \Delta q_i \left[1 - \frac{f(n)}{8(T_{r_i} - T_{r_{(i-1)}})} \left(1 - e^{-\frac{8}{f(n)}(T_{r_i} - T_{r_{(i-1)}})} \right) \times e^{-\frac{8}{f(n)}(T_r - T_{r_i})} \right] \right\} \tag{42}$$

and

$$U_r(T_r) = \sum_1^n \rho_i \left[1 - \frac{f(n)}{8(T_{r_i} - T_{r_{(i-1)}})} \left(1 - e^{-\frac{8}{f(n)}(T_{r_i} - T_{r_{(i-1)}})} \right) \times e^{-\frac{8}{f(n)}(T_r - T_{r_i})} \right] \tag{43}$$

Expressions (42) and (43) must be applied when $t > t_n$.

3.3. Third case: combined vertical and radial drainage

For combined vertical and radial drainage and constant loading Carrillo (1942) has proved that

$$(1 - U_{vr}) = (1 - U_v) \times (1 - U_r)^1 \tag{44}$$

1 For the sake of simplicity the representation U and J is employed instead of $U(t)$ and $J(t)$.

where U_{vr} = average degree of consolidation for combined vertical and radial drainage, U_v = average degree of consolidation for vertical drainage and U_r = degree of consolidation for radial drainage.

Recalling that

$$\bar{J}_v = m_v U_v \tag{45}$$

$$J_r = m_v U_r \tag{46}$$

$$\bar{J}_{vr} = m_v U_{vr} \tag{47}$$

and considering Eq. (44), the following expression may be written

$$\bar{J}_{vr} = \bar{J}_v + J_r - \frac{\bar{J}_v J_r}{m_v} \tag{48}$$

or, taking into account Eqs. (17) and (36), then

$$\bar{J}_{vr}(t) = m_v \left[1 - \sum_0^\infty \frac{2}{M^2} e^{-\left(M^2 + \frac{2c_r H^2}{c_v f(n) r_e^2}\right)\frac{c_v t}{H^2}} \right] \tag{49}$$

Making

$$\theta = \frac{2c_r H^2}{c_v f(n) r_e^2} \tag{50}$$

and comparing Eqs. (49) and (17), it is apparent that the solution for combined drainage may be easily obtained from substituting $M^2 T_v$ by $(M^2 + \theta)T_v$ in the expressions derived for vertical drainage. Therefore, the following equations apply to combined vertical and radial drainage.

For $t_{k-1} \le t \le t_k$ $(k \le n)$

$$\begin{aligned}\bar{\varepsilon}(T_v) = m_v \sum_1^{k-1} \Bigg\{ \Delta q_i \Bigg[1 - \frac{2}{T_{v_i} - T_{v(i-1)}} \sum_0^\infty \frac{1}{M^2(M^2+\theta)} \times \\ \left(1 - e^{-(M^2+\theta)(T_{v_i} - T_{v(i-1)})}\right) \times e^{-(M^2+\theta)(T_v - T_{v_i})} \Bigg] \Bigg\} + \\ m_v \Delta q_k \Bigg[\frac{T_v - T_{v(k-1)}}{T_{v_k} - T_{v(k-1)}} - \frac{2}{(T_{v_k} - T_{v(k-1)})} \sum_0^\infty \frac{1}{M^2(M^2+\theta)} \times \\ \left(1 - e^{-(M^2+\theta)(T_v - T_{v(k-1)})}\right) \Bigg]\end{aligned} \tag{51}$$

and

$$\begin{aligned}U_{vr}(T_v) = \sum_1^{k-1} \Bigg\{ \rho_i \Bigg[1 - \frac{2}{T_{v_i} - T_{v(i-1)}} \sum_0^\infty \frac{1}{M^2(M^2+\theta)} \times \\ \left(1 - e^{-(M^2+\theta)(T_{v_i} - T_{v(i-1)})}\right) \times e^{-(M^2+\theta)(T_v - T_{v_i})} \Bigg] \Bigg\} + \\ \rho_k \Bigg[\frac{T_v - T_{v(k-1)}}{T_{v_k} - T_{v(k-1)}} - \frac{2}{T_{v_k} - T_{v(k-1)}} \sum_0^\infty \frac{1}{M^2(M^2+\theta)} \times \\ \left(1 - e^{-(M^2+\theta)(T_v - T_{v(k-1)})}\right) \Bigg]\end{aligned} \tag{52}$$

where

$$\rho_i = \frac{\Delta q_i}{\sum_i^n \Delta q_i} \tag{25}$$

For $t > t_n$

$$\begin{aligned}\bar{\varepsilon}(T_v) = m_v \sum_1^n \Bigg\{ \Delta q_i \Bigg[1 - \frac{2}{T_{v_i} - T_{v(i-1)}} \sum_0^\infty \frac{1}{M^2(M^2+\theta)} \times \\ \left(1 - e^{-(M^2+\theta)(T_{v_i} - T_{v(i-1)})}\right) \times e^{-(M^2+\theta)(T_v - T_{v_i})} \Bigg] \Bigg\}\end{aligned} \tag{53}$$

and

$$\begin{aligned}U_{vr}(T_v) = \sum_1^n \Bigg\{ \rho_i \Bigg[1 - \frac{2}{T_{v_i} - T_{v(i-1)}} \sum_0^\infty \frac{1}{M^2(M^2+\theta)} \times \\ \left(1 - e^{-(M^2+\theta)(T_{v_i} - T_{v(i-1)})}\right) \times e^{-(M^2+\theta)(T_v - T_{v_i})} \Bigg] \Bigg\}\end{aligned} \tag{54}$$

Equations (23), (24), (28), (29), (40), (41), (42) and (43) are consistent with corresponding solutions presented in technical literature (Terzaghi and Frölich, 1936; Taylor, 1942; Schiffman, 1958; Olson, 1977; Kurma Rao and Vijaya Rama Raju, 1990; Da Mota, 1996; Lekha *et al.*, 1998), for one linear variable loading, since one makes $k = 1$ in Eqs. (23), (24), (40) and (41), vanishing the first term, and $n = 1$ in Eqs. (28) (29), (42) and (43).3.4.

A case solution

In order to present an application to the equations derived in this section, a consolidation analysis of a clay layer submitted to the loading history shown in Fig. 4 has been performed.

The loading features are

- 3 equal steps of loading with constant rate $\Delta q/\Delta t$
- 2 equal resting intervals of time between loadings with length $k\Delta t$

The analysis considers the three cases studied

- Only vertical drainage for $T_{v_1} = 0.1$; k = 5, 10 and 20

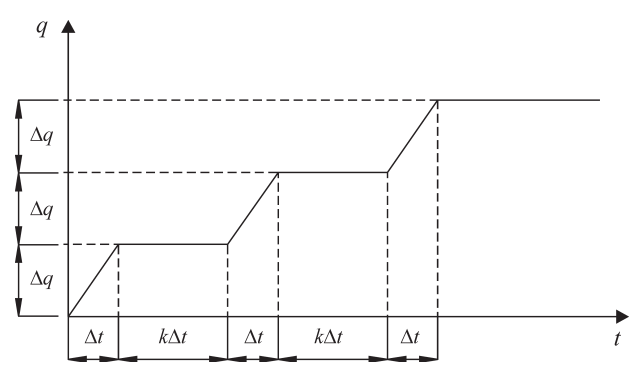

Figure 4 - Particular loading history considered in the application studied (linear variable three-step loading).

- Only radial drainage for $T_{r_1} = 0.1$; $k = 5$, 10 and 20; $n = 10$ and 30
- Combined vertical and radial drainage for $T_{v_1} = 0.1$; $k = 5$, 10 and 20; $\theta = 10$ and 100

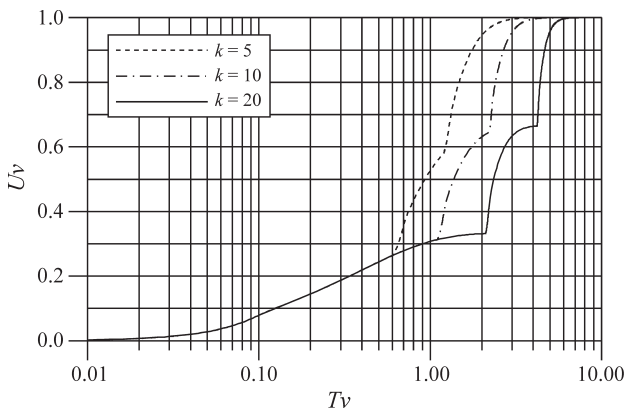

Figure 5 - Curves U_v x T_v for one-dimensional consolidation with vertical drainage under linear variable three-step loading and $T_{v_1} = 0.1$.

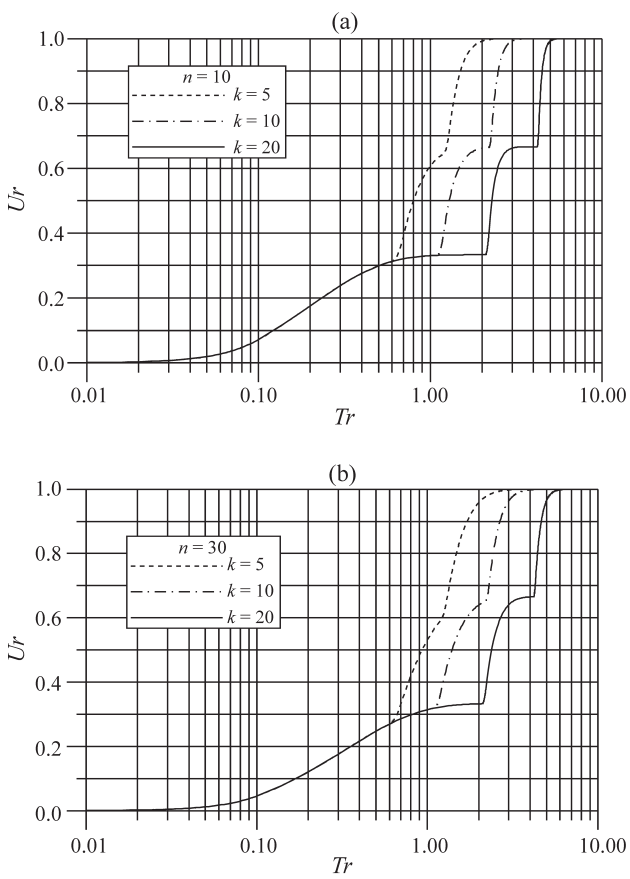

Figure 6 - Curves U_r x T_r for one-dimensional consolidation with radial drainage under linear variable three-step loading, $T_{r_1} = 0.1$, (a) $n = 10$ and (b) $n = 30$.

Figures 5 to Fig. 7 illustrate the results obtained. Consolidation for the second and third increments of load exhibits a steeper slope in the curves owing to the logarithmic scale. Values of U_r for $n = 10$ (Fig. 6a) increases faster than for $n = 30$ (Fig. 6b) because of the higher density of vertical drains in the former case. It can also be noticed that the progress of consolidation illustrated in Fig. 7(b) is faster than in Fig. 7(a). This behaviour can be explained by the magnitude of the parameter θ, representing the relative importance between vertical and radial drainage in combined conditions. Low values of θ indicate that vertical drainage plays a major role in consolidation. On the other hand, high values of θ mean that radial drainage is prevailing.

4. Second Application: Analysis of One-Dimensional Consolidation of Soft Soils under Embankment Loading With Partial Submersion of the Fill

When an embankment is constructed on the surface of a clay deposit with high water table level, its self-weight decreases with time owing to the partial submersion of the fill caused by the settlements. Therefore, consolidation analysis in this case must take into account the resulting variable de-

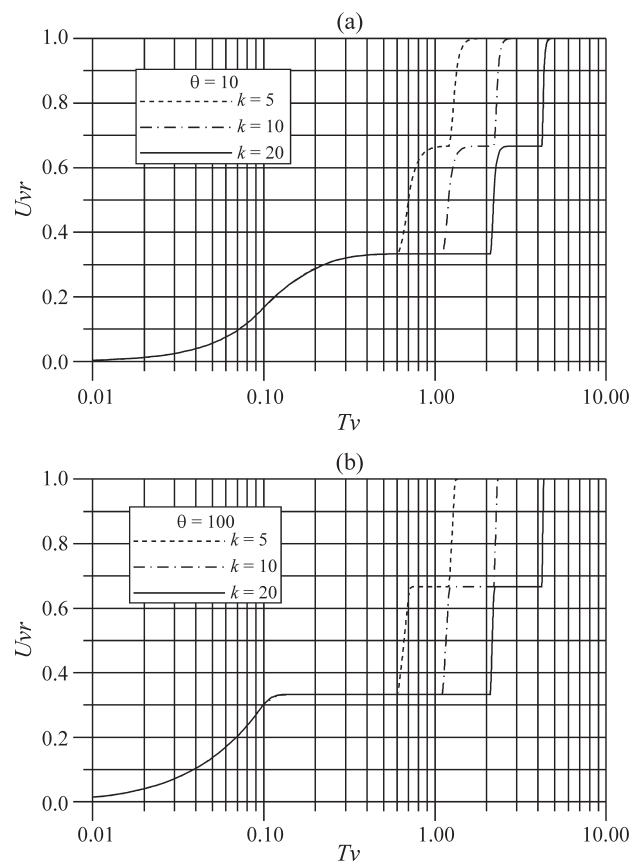

Figure 7 - Curves U_{vr} x T_v for one-dimensional consolidation with combined vertical and radial drainage under linear variable three-step loading, $T_{v_1} = 0.1$, (a) $\theta = 10$ and (b) $\theta = 100$.

creasing loading. Linear Viscoelasticity theory provides the necessary background for this analysis regarding the same basic assumptions considered in the previous application.

4.1. First case: vertical drainage

If a fill of height h and unit weight γ_t is placed onto a homogeneous deposit of soft clay of thickness H, the initial loading on the clay layer is (Fig. 8a)

$$q_0 = \gamma_t \times h \tag{55}$$

After an interval of time t, supposing for simplicity the water table located at the surface of the clay layer[2], the loading is (Fig. 8b).

$$q(t) = q_0 - \Delta\gamma H \bar{\varepsilon}(t) \tag{56}$$

where

$$\Delta\gamma = \gamma_t - \gamma_b, \tag{57}$$

γ_b = submerged (buoyant) unit weight of the fill.

Recalling that

$$\bar{\varepsilon}(t) = q(t)\bar{J}_v(0) - \int_0^t q(\tau)\frac{\partial \bar{J}_v(t-\tau)}{\partial \tau}d\tau \tag{19}$$

and substituting Eq. (56) into Eq. (19), yields

$$\bar{\varepsilon}(t) = \left[q_0 - \Delta\gamma H\bar{\varepsilon}(t)\right]\bar{J}_v(0) - \int_0^t \left[q_0 H(\tau) - \Delta\gamma H\bar{\varepsilon}(\tau)\right]\frac{\partial \bar{J}_v(t-\tau)}{\partial \tau}d\tau \tag{58}$$

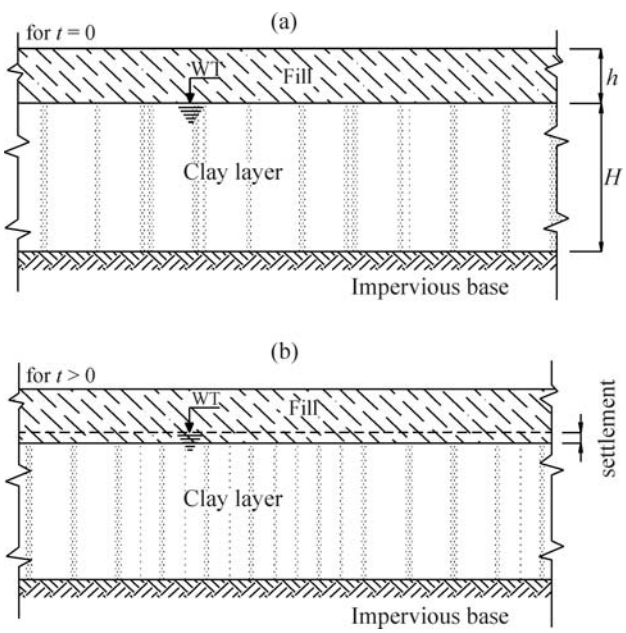

Figure 8 - Representation of partial submersion of an embankment constructed on the surface of a clay layer due to one-dimensional consolidation with vertical drainage.

An easier solution to Eq. (58) can be obtained if the approximate expressions for $U(T_v)$ are employed instead of the rigorous Terzaghi's solution, as follows

• early stages of consolidation $U_v = \left(\frac{4}{\pi}T_v\right)^{\frac{1}{2}}$ (59)

• late stages of consolidation $U_v = 1 - \frac{8}{\pi^2}e^{-\frac{\pi^2 T_v}{4}}$ (60)

4.1.1. Early stages of consolidation

From Eq. (59), it may be written

$$\bar{\varepsilon}(t) = m_v q_0 \left(\frac{4c_v t}{\pi H^2}\right)^{\frac{1}{2}} \tag{61}$$

and, therefore

$$\bar{J}_v(t) = m_v \left(\frac{4c_v t}{\pi H^2}\right)^{\frac{1}{2}} \tag{62}$$

Substituting Eq. (62) into Eq. (58), yields

$$\bar{\varepsilon}(t) = \frac{m_v}{H}\left(\frac{c_v}{\pi}\right)^{\frac{1}{2}}\left[q_0\int_0^t H(\tau)\times(t-\tau)^{-\frac{1}{2}}d\tau - \Delta\gamma H\int_0^t \bar{\varepsilon}(\tau)\times(t-\tau)^{-\frac{1}{2}}d\tau\right] \tag{63}$$

Applying Laplace transform to Eq. (63), resolving for $\hat{\bar{\varepsilon}}(s)$ and applying the inverse transform, results

$$\bar{\varepsilon}(T_v) = \frac{q_0 m_v}{\alpha}\left[1 - e^{\alpha^2 T_v} \times erfc\left(\alpha T_v^{\frac{1}{2}}\right)\right] \tag{64}$$

and

$$U_v(T_v) = \frac{1+\alpha}{\alpha}\left[1 - e^{\alpha^2 T_v} \times erfc\left(\alpha T_v^{\frac{1}{2}}\right)\right] \tag{65}$$

where

$$\alpha = m_v \Delta\gamma H \tag{66}$$

erfc ( ) = complementary error function

4.1.2. Late stages of consolidation

It may be inferred from Eq. (60) that

$$\bar{\varepsilon}(t) = m_v q_0 \left(1 - \frac{8}{\pi^2}e^{-\frac{\pi^2 c_v}{4H^2}t}\right) \tag{67}$$

and, therefore

2 Actually, the water table can be at any location. If, for instance, it is above the clay surface, q_0 should be conveniently calculated considering its initial partial submersion. On the other hand, if it is below the clay surface, $\Delta\gamma$ should take into account what soil is going to be submerged (clay only or clay and fill).

$$\bar{J}_v(t) = m_v\left(1-\frac{8}{\pi^2}e^{-\frac{\pi^2 c_v}{4H^2}t}\right) \tag{68}$$

Substituting Eq. (68) into Eq. (58), yields

$$\bar{\varepsilon}(t) = [q_0 - \Delta\gamma H\bar{\varepsilon}(t)]\times\left[m_v\left(1-\frac{8}{\pi^2}\right)\right] + \frac{2m_v c_v}{H^2}\times \left[q_0\int_0 H(\tau)e^{-\frac{\pi^2 c_v}{4H^2}(t-\tau)}d\tau - \int_0 \bar{\varepsilon}(\tau)e^{-\frac{\pi^2 c_v}{4H^2}(t-\tau)}d\tau\right] \tag{69}$$

Applying Laplace transform to Eq. (69), resolving for $\hat{\bar{\varepsilon}}(s)$ and finding the inverse transform, yields

$$\bar{\varepsilon}(T_v) = \frac{q_0 m_v}{(1+\alpha)}\left[1-\frac{8}{\pi^2}\frac{1}{1+\alpha\left(1-\frac{8}{\pi^2}\right)}e^{-\frac{1+\alpha}{1+\alpha\left(1-\frac{8}{\pi^2}\right)}\frac{\pi^2}{4}T_v}\right] \tag{70}$$

and the average degree of consolidation

$$U_v(T_v) = 1-\frac{8}{\pi^2}\frac{1}{1+\alpha\left(1-\frac{8}{\pi^2}\right)}e^{-\frac{1+\alpha}{1+\alpha\left(1-\frac{8}{\pi^2}\right)}\frac{\pi^2}{4}T_v} \tag{71}$$

For $T_v \to \infty$, Eq. (70) becomes

$$\bar{\varepsilon}(\infty) = \frac{q_0 m_v}{(1+\alpha)} = \frac{\bar{\varepsilon}(T_v \to \infty, \text{without submersion})}{1+\alpha} \tag{72}$$

Considering the logarithmic relationship between void ratio and vertical effective stress,

$$m_v = \frac{C_c}{q_0(1+e_0)}\log\left(\frac{p_0'+q_0}{p_0'}\right) \tag{73}$$

where e_0 = initial void ratio, p_0' = initial effective stress and C_c = compression index, the parameter α may be evaluated from

$$\alpha = \frac{\Delta\gamma H}{q_0}\times\frac{C_c}{1+e_0}\times\log\left(\frac{p_0'+q_0}{p_0'}\right) \tag{74}$$

It can be observed that Eqs. (65) and (71), for situations (4.1.1) and (4.1.2) respectively, assume the same value for T_v approximately equal to $\frac{0.213}{1+3\alpha/2}$. Therefore, the following may be stated:

For $T_v \le \frac{0.213}{1+3\alpha/2}$, use equations

$$\bar{\varepsilon}(T_v) = \frac{q_0 m_v}{\alpha}\left[1-e^{\alpha^2 T_v}\times erfc\left(\alpha T_v^{\frac{1}{2}}\right)\right] \tag{64}$$

$$U_v T_v = \frac{1+\alpha}{\alpha}\left[1-e^{\alpha^2 T_v}\times erfc\left(\alpha T_v^{\frac{1}{2}}\right)\right] \tag{65}$$

For $T_v \ge \frac{0.213}{1+3\alpha/2}$ use equations

$$\bar{\varepsilon}(T_v) = \frac{q_0 m_v}{(1+\alpha)}\left[1-\frac{8}{\pi^2}\frac{1}{1+\alpha\left(1-\frac{8}{\pi^2}\right)}e^{-\frac{1+\alpha}{1+\alpha\left(1-\frac{8}{\pi^2}\right)}\frac{\pi^2}{4}T_v}\right] \tag{70}$$

$$U_v(T_v) = 1-\frac{8}{\pi^2}\frac{1}{1+\alpha\left(1-\frac{8}{\pi^2}\right)}e^{-\frac{1+\alpha}{1+\alpha\left(1-\frac{8}{\pi^2}\right)}\frac{\pi^2}{4}T_v} \tag{71}$$

Curves U_v x T_v for α = 0.20, 0.50 and 0.80 and T_v x α for U_v = 50%, 70% and 90% are shown in Figs. 9 and 10.

4.2. Second case: radial drainage

Now suppose a fill of height h and unit weight γ_t placed onto the surface of a homogeneous deposit of soft

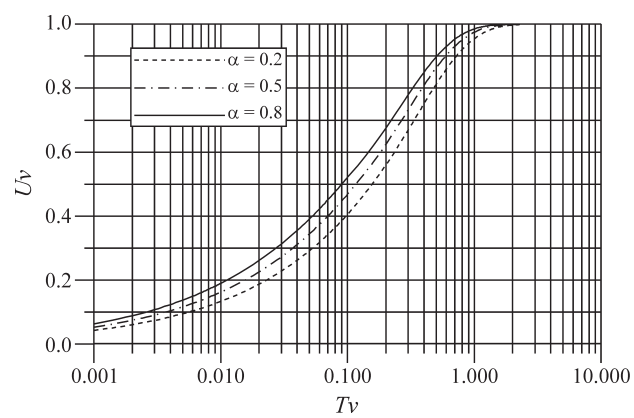

Figure 9 - Curves U_v x T_v for vertical drainage with partial submersion of the fill.

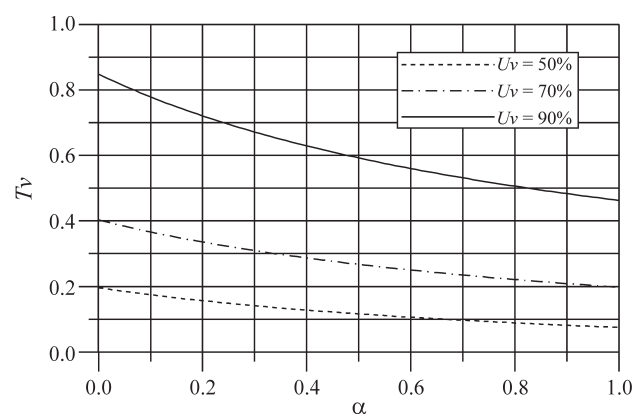

Figure 10 - Curves T_v x α for vertical drainage and partial submersion of the fill.

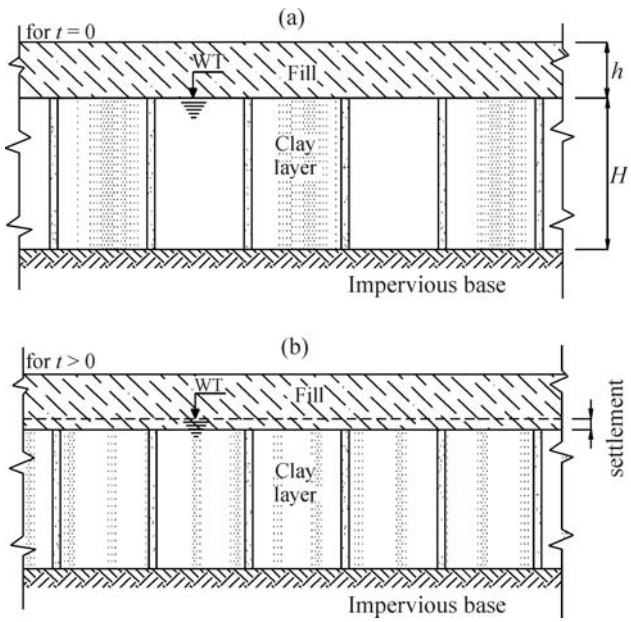

Figure 11 - Representation of partial submersion of an embankment constructed on the surface of a clay layer due to one-dimensional consolidation with radial drainage.

clay of thickness H, where vertical drains have been installed, assuming no vertical drainage occurring (Fig. 11). As in the first case (vertical drainage), the initial loading is

$$q_0 = \gamma_t \times h \tag{55}$$

and the loading after an interval of time t is

$$q(t) = q_0 - \Delta\gamma H \varepsilon(t) \tag{56a}$$

where $\Delta\gamma$ has the same meaning as in the first case.

Recalling that

$$\varepsilon(t) = q(t) J_r(0) - \int_0^t q(\tau) \frac{\partial J_r(t-\tau)}{\partial \tau} d\tau \tag{37}$$

and inserting Eq. (56a) into Eq. (37), results

$$\varepsilon(t) = \left[q_0 - \Delta\gamma H \varepsilon(t)\right] J_r(0) - \int_0^t \left[q_0 H(\tau) - \Delta\gamma H \varepsilon(\tau)\right] \frac{\partial J_r(t-\tau)}{\partial \tau} d\tau \tag{75}$$

Substituting Eq. (36) (creep function for radial drainage) into Eq. (75), applying Laplace transform, resolving for $\hat{\varepsilon}(s)$ and finding the inverse transform, yields

$$\varepsilon(T_r) = \frac{q_0 m_v}{(1+\alpha)} \left[1 - e^{-\frac{8T_r(1+\alpha)}{f(n)}}\right] \tag{76}$$

and the degree of consolidation is

$$U_r(T_r) = 1 - e^{-\frac{8T_r(1+\alpha)}{f(n)}} \tag{77}$$

Similarly to the vertical drainage case, the final strain is

$$\varepsilon(\infty) = \frac{q_0 m_v}{(1+\alpha)} = \frac{\varepsilon(T_r \to \infty, \text{without submersion})}{1+\alpha} \tag{78}$$

Figures 12 and 13 present respectively the curves U_r x T_r for n = 10 and 30 and α = 0.20, 0.50 and 0.80, and T_r x α for n = 10 and 30 and U_r = 50%, 70% and 90%.

4.3. Third case: combined vertical and radial drainage

Solution for combined vertical and radial drainage regarding the early stages of consolidation cannot be easily derived. However, a straightforward approximate solution can be obtained for the late stages, as follows.

Using Carrillo's expression (44), it has been shown that

$$\bar{J}_{vr} = \bar{J}_v + J_r - \frac{\bar{J}_v J_r}{m_v} \tag{48}$$

Substituting Eqs. (68) and (36) into Eq. (48), results

$$\bar{J}_{vr}(t) = m_v \left(1 - \frac{8}{\pi^2} e^{-\left(\frac{\pi^2}{4}+\theta\right)\frac{c_v t}{H^2}}\right) \tag{79}$$

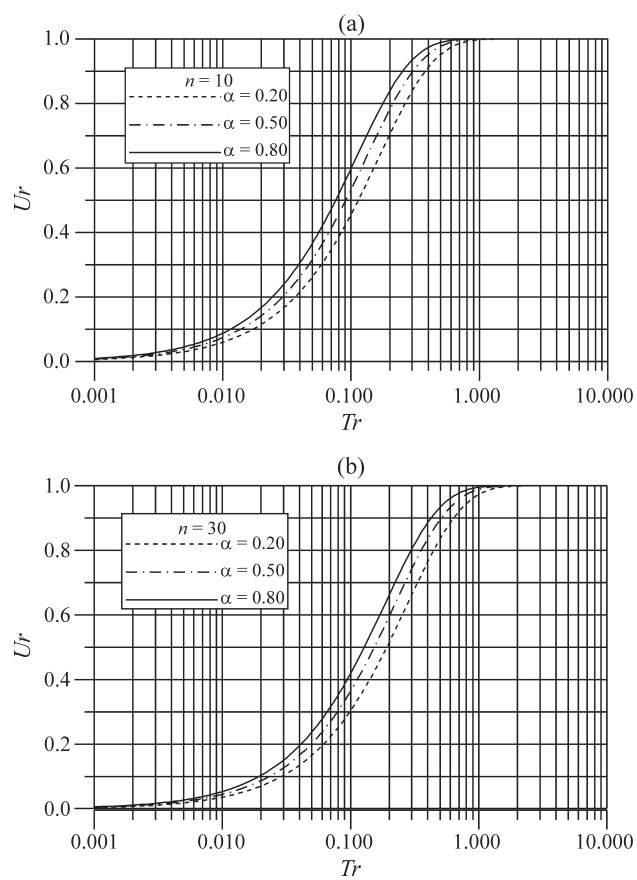

Figure 12 - Curves U_r x T_r for radial drainage with partial submersion of the fill, (a) n = 10 and (b) n = 30.

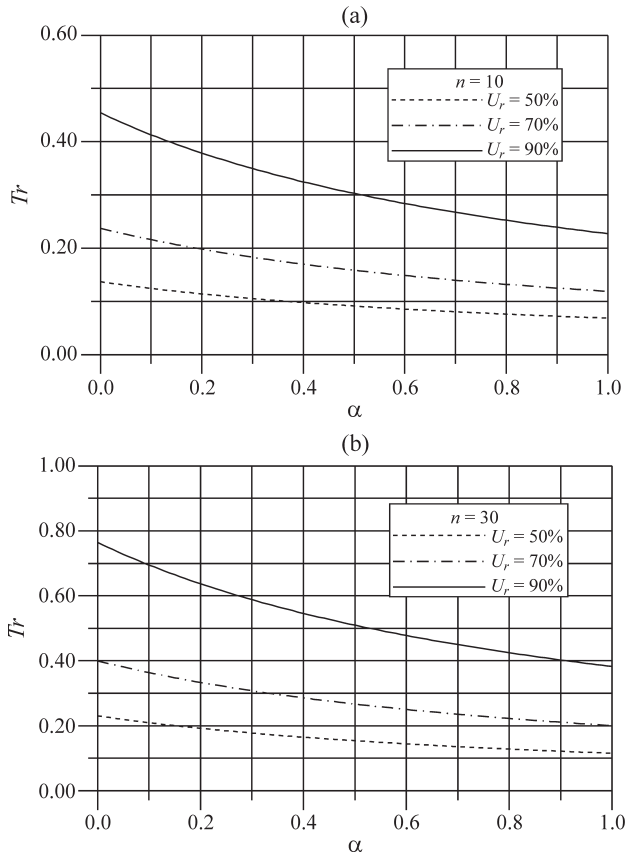

Figure 13 - Curves T_r x α for radial drainage and partial submersion of the fill, (a) n = 10 and (b) n = 30.

It can be written

$$\bar{\varepsilon}(t)=\left[q_0-\Delta\gamma H\bar{\varepsilon}(t)\right]\bar{J}_{vr}(0)-\int_0^t\left[q_0H(\tau)-\Delta\gamma H\bar{\varepsilon}(\tau)\right]\frac{\partial\bar{J}_{vr}(t-\tau)}{\partial\tau}d\tau \tag{80}$$

Substituting Eq. (79) into Eq. (80), applying Laplace transformation, resolving for $\hat{\bar{\varepsilon}}(s)$ and finding the inverse transform, yields

$$\bar{\varepsilon}(T_v)=\frac{q_0m_v}{(1+\alpha)}\left[1-\frac{8}{\pi^2}\frac{1}{1+\alpha\left(1-\frac{8}{\pi^2}\right)}\times e^{-\frac{1+\alpha}{1+\alpha\left(1-\frac{8}{\pi^2}\right)}\left(\frac{\pi^2}{4}+\theta\right)T_v}\right] \tag{81}$$

and

$$U_{vr}(T_v)=1-\frac{8}{\pi^2}\frac{1}{1+\alpha\left(1-\frac{8}{\pi^2}\right)}\times e^{-\frac{1+\alpha}{1+\alpha\left(1-\frac{8}{\pi^2}\right)}\left(\frac{\pi^2}{4}+\theta\right)T_v} \tag{82}$$

which hold for

$$T_v\geq\frac{0.213}{1+\frac{3\alpha}{2}} \tag{83}$$

Naturally, for $T_v\to\infty$, Eq. (81) gives

$$\bar{\varepsilon}(\infty)=\frac{q_0m_v}{(1+\alpha)}=\frac{\bar{\varepsilon}(T_v\to\infty,\text{ without submersion})}{1+\alpha} \tag{72}$$

Figure 14 illustrates the results of combined drainage through the curves U_{vr} x T_v for α = 0.20, 0.50 and 0.80 and θ = 10.

4.4. Final remark on the second application

The non-dimensional parameter α varies mainly between 0 and 1 and affects both the amount of settlement and the consolidation rate, as can be seen from Eqs. (64), (70), (76) and (81). Diagrams of Figs. 9-10 and Figs. 12-14 show how α affects the progress of consolidation. However, although larger α implies faster consolidation in terms of time factor, when vertical drainage takes place this conclusion may not hold for real time if one compares deposits of different thicknesses.

5. Third application: Analysis of One-Dimensional Consolidation of Soft Soils by Drain Columns of Finite Stiffness

Installation of drain wells in soft clay deposits aiming the acceleration of the consolidation process is a technique ordinarily employed in design of embankments on soft soils. Although the use of flexible pre-fabricated drain poses generally economic advantages, there are particular situations where the availability of low cost sand or stone nearby the work site allows the utilization of these materials as drain columns. Besides, drain columns of finite vertical stiffness also reduce the final settlement, becoming thus an economically attractive solution in some cases.

The purpose of this application is to solve the problem of the one-dimensional consolidation of a cell comprised by a cylinder of soil having a diameter d_e surround-

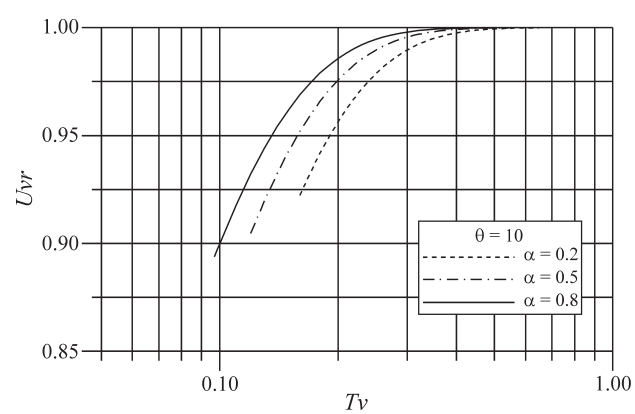

Figure 14 - Curves U_{vr} x T_v for combined vertical and radial drainage with partial submersion of the fill and θ = 10.

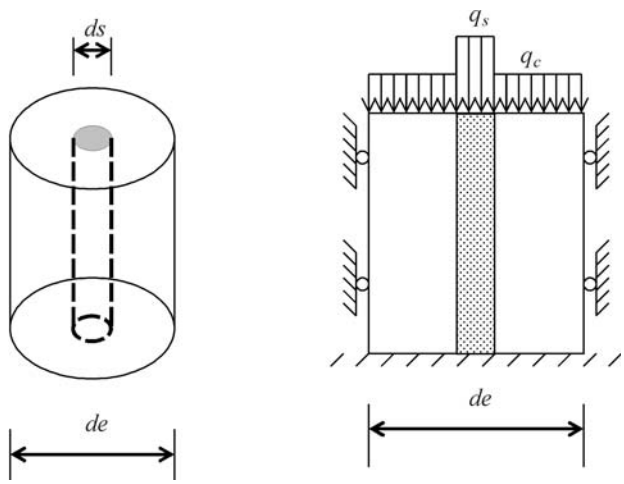

Figure 15 - Representation of a cylinder of soil surrounding a stiff drain column (after Barksdale and Bachus, 1983, modified).

ing a stiff drain column having a diameter d_s (Fig. 15). In most of the practical problems the influence of the vertical drainage may be neglected when compared to the radial drainage and, therefore, only this latter condition is considered herein.

Besides the assumptions regarding the behaviour of the clay considered in the first application presented, the following assumptions are also assumed:

(6) the drain column material has finite stiffness with linear stress-strain relationship;

(7) the lateral displacements of the drain column are very small, not affecting therefore the consolidation of the clay;

(8) the clay layer and the drain column have the same strain at any time after loading (equal strain).

Taking into account the high values of vertical strains normally associated with problems of embankments on soft soils, one can assume that the drain column is under failure condition in most of its length. However, as the radial compressive stresses acting on the column also increase with the strain, owing to the increase in the effective stresses in the clay layer, it is reasonable to admit, as an approximation, the linear stress-strain behaviour stated in the assumption (6).

According to Barksdale and Bachus (1983), area replacement ratio, a_s, is defined as

$$a_s = \frac{A_s}{A} \tag{84}$$

where A_s is the area of the drain column and A is the total area within the cell. The ratio of the area of the soil remaining, A_c, to the total area A is then

$$a_c = 1 - a_s \tag{85}$$

The area replacement ratio, a_s, may also be expressed as a function of the diameter and spacing of the drain columns by the following equation

$$a_s = C_1 \left(\frac{d_s}{s} \right)^2 \tag{86}$$

where d_s = diameter of the drain column, s = centre-to-centre spacing of the drain columns and C_1 = constant dependent upon the pattern of drain columns used; for a square pattern $C_1 = \pi/4$; for equilateral triangular pattern $C_1 = \pi/(2\sqrt{3})$, or

$$a_s = \frac{1}{n^2} \tag{87}$$

Stress concentration factor, ν, is defined as

$$\nu = \frac{q_s}{q_c} \tag{88}$$

where q_s = vertical loading stress acting on the top of the drain column and q_c = vertical loading stress acting on the surface of the clay layer.

The mean vertical loading stress q on the top of the cell can be obtained by equilibrium condition, as follows

$$q = q_s \times a_s + q_c (1 - a_s) \tag{89}$$

Denoting K_s the modulus of deformation of the drain column, one may write for any time t

$$\varepsilon(t) = \frac{q_s(t)}{K_s} \tag{90}$$

Equating the strain in the clay layer (Eq. (37)) to the strain in the column (Eq. (90)) and applying Laplace transform to the resulting expression and also to Eq. (89), yields

$$\begin{cases} \dfrac{\hat{q}_s(s)}{K_s} = \dfrac{2c_r}{r_e^2 f(n)} \times \dfrac{1}{s + \dfrac{2c_r}{r_e^2 f(n)}} \times \hat{q}_c(s) \\ \dfrac{q}{s} = \hat{q}_s(s) \times a_s + \hat{q}_c(s) \times (1 - a_s) \end{cases} \tag{91}$$

Resolving the system of Eqs. (91) and finding the inverse transform, yields

$$\frac{q_c(T_r)}{q} = \frac{1}{1 - a_s} \left[\frac{1 - a_s + \beta \times e^{-8 \frac{(1 - a_s + \beta)}{(1 - a_s) f(n)} T_r}}{1 - a_s + \beta} \right] \tag{92}$$

$$\frac{q_s(T_r)}{q} = \frac{1}{a_s} \left[1 - \frac{1 - a_s + \beta \times e^{-8 \frac{(1 - a_s + \beta)}{(1 - a_s) f(n)} T_r}}{1 - a_s + \beta} \right] \tag{93}$$

where

$$\beta = a_s K_s m_v \tag{94}$$

The stress concentration factor, ν, can be obtained from Eqs. (88), (92) and (93).

The vertical strain in the soil layer can be obtained substituting Eqs. (36) and (92) into Eq. (37), which may be solved using Laplace transforms, giving

$$\varepsilon(T_r) = q\frac{m_v}{1-a_s+\beta}\left(1-e^{-8\frac{(1-a_s+\beta)}{(1-a_s)f(n)}T_r}\right) \tag{95}$$

The average degree of consolidation is, then

$$U(T_r) = 1-e^{-8\frac{(1-a_s+\beta)}{(1-a_s)f(n)}T_r} \tag{96}$$

The parameter β represents the relative stiffness between the drain column and a fictitious column of soil having the diameter d_e, previously defined. The progress of the concentration factor with time can be seen in Fig. 16 for a particular case of $a_s = 0.02$ and $\beta = 0.2$, evidencing the gradual and partial unloading of the soil, shifting the embankment weight from the clay layer to the drain columns.

The parameter β varies in the range 0-∞. It is worth discussing the above equations for two particular values of β, corresponding to $K_s = 0$ and $K_s = 1/m_v$.

(1) $\beta = 0$ (for $K_s = 0$)

In this case, $\frac{q_c}{q} = \frac{1}{1-a_s}$ and $\frac{q_s}{q} = 0$, representing the consolidation of a clay layer under a constant loading $\frac{q}{1-a_s}$.

(2) $\beta = a_s$ (for $K_s = 1/m_v$)

In this case, clay and drain have the same compressibility. Since the drain behaves as an elastic-instantaneous material (*i.e.*, it has no time-dependent constitutive equations), at the initial time ($t = 0$) there is no vertical strain in the clay and therefore all the loading is borne by the clay. As consolidation progresses, part of the loading bore by the clay is shifted to the drain column and eventually, at the end of consolidation ($t \to \infty$), the loading stress on the clay is the same as on the drain.

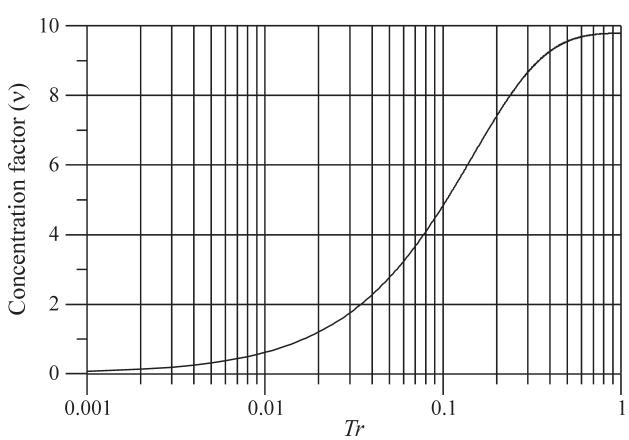

Figure 16 - Progress of the concentration factor (ν) with T_r for $a_s = 0.02$ and $\beta = 0.2$.

6. Conclusions

The Linear Viscoelasticity theory is a powerful tool to solve one-dimensional consolidation problems under variable loading. Although primary consolidation is strictly a hydrodynamic phenomenon, it may be successfully treated as a viscoelastic problem in terms of total stresses. This approach is similar to considering saturated clay soil exhibiting Tresca yield envelope when submitted to undrained loading, in terms of total stresses, when its plastic behaviour is analysed. This first and certainly the main conclusion of this work resulted from the straightforward way that three study cases involving consolidation of soft soils under variable loading were solved. The closed form solutions obtained are also relevant for both design practice and validation of numerical models.

The expressions obtained for one-dimensional consolidation under a number of linear variable loads are applicable to any loading history prescribed as long as it can be subdivided into several increments of load. It is worth mentioning that it may be very useful in embankment design to plan the most suitable loading history to achieve pre-set degrees of consolidation at particular times.

The diagrams U x T produced from the solutions allow a general overview of the progress of consolidation for a loading programme of three ramp loadings with two resting intervals. They also evidence how parameters n (radial drainage) and θ (combined drainage) affects the consolidation, although the logarithmic scale attenuates the differences.

The Viscoelasticity theory provides closed form solutions for the problem of one-dimensional consolidation of a deposit of clay under embankment loading when partial submersion of the fill occurs. As far as vertical drainage is concerned, classical approximate solutions were employed to obtain the corresponding creep function. Thus, in this case, two different expressions were derived for early and late stages of consolidation. For radial drainage, however, an exact solution was obtained from Barron's equation. For combined vertical and radial drainage only one expression was derived, regarding late stages of consolidation.

The non-dimensional parameter α is quite important in the analysis of submersion since it affects not only the amount of final settlement, but also the consolidation rate. In general, larger α implies faster consolidation, although this may not be true when vertical consolidation takes place.

The consolidation of a clay layer with drain columns of finite stiffness is also a variable loading problem easily tackled by Linear Viscoelasticity. The solution provides equations to determine stresses and strain on the soil and

columns and the average degree of consolidation at any time taking into account the area replacement ratio and the modulus of deformation of the drain column.

The parameter β represents the relative stiffness between the drain column and a fictitious column of soil, influencing both the amount of settlement and the consolidation rate.

Acknowledgments

This work was carried out at Instituto Alberto Luiz Coimbra de Pós-Graduação e Pesquisa de Engenharia (COPPE/UFRJ) under a grant from Fundação Coordenação de Aperfeiçoamento de Pessoal de Nível Superior (CAPES) and Conselho Nacional de Desenvolvimento Científico e Tecnológico (CNPq). The authors are grateful to Prof. Dirceu de Alencar Velloso, Prof. Fernando Arthur Brasil Danziger and Prof. Willy Alvarenga Lacerda for valuable discussions and comments on the work and to Renato Marques Bastos and Luiz de França for having carefully carried out some of the illustrations.

References

Barksdale, R.D. and Bachus, R.C. (1983) Design and Construction of Stone Columns. v. 1. Federal Highway Administration, Washington, D.C., Report n. FHWA/RD-83-026.

Barron, R.A. (1948) Consolidation of fine-grained soils by drain wells. Journal of the Geotechnical Engineering, Transactions, v. 113, p. 718-742.

Bland, D.R. (1960) The Theory of Linear Viscoelasticity. Pergamon Press, New York, 125 pp.

Carrillo, N. (1942) Simple two and three dimensional cases in the theory of consolidation of soils. Journal of Mathematics and Physics, v. 21:1, p. 1-5.

Da Mota, J.L.C.P. (1996) Study of One-Dimensional Consolidation Under Gradual Application of Load. M.Sc. Dissertation, COPPE/UFRJ (in Portuguese).

Findley, W.N.; Lai, J.S. & Onaran, K. (1976) Creep and Relaxation of Nonlinear Viscoelastic Materials. North-Holland Publishing Company, Amsterdam, 384 pp.

Kurma Rao, K. and Vijaya Rama Raju, M. (1990) One-dimensional consolidation with three-dimensional flow for time-dependent loading. Journal of Geotechnical Engineering, v. 116:10, p. 1576-1580.

Lekha, K.R.; Krishnaswamy, N.R. & Basak, P. (1998) Consolidation of clay by sand drain under time-dependent loading. Journal of Geotechnical and Geoenvironmental Engineering, v. 124:1, p. 91-94.

Olson, R.E. (1977) Consolidation under time dependent loading. Journal of the Geotechnical Engineering Division, v. 103:GT1, p. 55-60.

Santa Maria, F.C.M. (1997) The Linear Viscoelasticity Applied to Problems of Consolidation and Soil-Structure Interaction. D.Sc. Qualifying Examination Report, COPPE/UFRJ (in Portuguese).

Schiffman, R.L. (1958) Consolidation of soil under time-dependent loading and varying permeability. Proceedings, Highway Research Board, v. 37, p. 584-617.

Taylor, D.W. (1942) Research on Consolidation of Clays, Serial 82. Department of Civil and Sanitary Engineering - MIT, Massachusetts, 147 pp.

Terzaghi, K. & Frölich, O.K. (1936) Theorie der setzung von tonschichten. Leipzig, Franz Deuticke, 265 pp.

List of Symbols

a_s = area replacement ratio
c_r = coefficient of consolidation for radial flow
c_v = coefficient of consolidation for vertical flow
C_t = constant dependent upon the pattern of drain columns used
C_c = compression index
d_e = diameter of zone of influence of the soil mass
d_s = diameter of the drain column
e_0 = initial void ratio
erfc ( ) = complementary error function
h = height of an embankment constructed on the surface of a clay deposit
H = thickness of a clay layer
$H(t)$ = Heaviside function
$J(t)$ = creep function
$J_r(t)$ = creep function for one-dimensional consolidation with radial drainage
$\bar{J}_v(t)$ = average creep function for one-dimensional consolidation with vertical drainage
$\bar{J}_{vr}(t)$ = average creep function for one-dimensional consolidation with combined vertical and radial drainage
K_s = modulus of deformation of the drain column
m_v = coefficient of volume compressibility
n = ratio between radius of the zone of influence of a vertical drain and its radius
p'_0 = initial effective stress
q_0 = inicial surcharge on the surface of a clay layer
q_c = vertical loading stress acting on the surface of the clay layer
q_s = vertical loading stress acting on the top of the drain column
r_d = radius of a vertical drain
r_e = radius of the zone of influence of a vertical drain
$R(t)$ = relaxation function
s = centre-to-centre spacing of the drain columns
s = auxiliar variable in the Laplace transformation
$s(t)$ = settlement of the top of a clay layer at time t
$s(\infty)$ = final settlement of the top of a clay layer, at infinite time
t = time
T_r = time factor for one-dimensional consolidation with radial drainage
T_v = time factor for one-dimensional consolidation with vertical drainage
U_r = degree of consolidation for one-dimensional consolidation with radial drainage
U_v = average degree of consolidation for one-dimensional consolidation with vertical drainage
U_{vr} = average degree of consolidation for one-dimensional consolidation with combined vertical and radial drainage
$\alpha = m_v \Delta\gamma H$ (non-dimensional parameter related to consolidation with partial submersion of the fill)
$\beta = a_s k_s m_v$ (non-dimensional parameter related to consolidation with drain columns)
$\hat{\bar{\varepsilon}}(s)$ = Laplace transform of $\bar{\varepsilon}(t)$
$\bar{\varepsilon}(t)$ = average vertical strain at time t
$\bar{\varepsilon}(\infty)$ = final average vertical strain, at infinite time
γ_b = submerged unit weight of a fill
γ_t = unit weight of a fill
ν = stress concentration factor
$\theta = \dfrac{2c_r H^2}{c_v f(n) r_e^2}$ (non-dimensional parameter related to consolidation with combined radial and vertical drainage)
ρ = ratio between increment of load and total load applied
σ_0 = total stress applied, constant with time

Laboratory Study on the Mobility of Heavy Metals in Residual Compacted Soil

Rejane Nascentes, Izabel Christina Duarte de Azevedo, Antonio Teixeira de Matos, Maurício Paulo Ferreira Fontes, Roberto Francisco de Azevedo, Lucas Martins Guimarães

Abstract. Studies on heavy metal behavior in soil have received considerable attention and have helped to increase the understanding of their mobility and retention in the environment. Given the scarcity of information available in the literature on heavy metal transport parameters in Brazilian tropical soils, the main contribution of this paper is improving the knowledge about the mobility of some of these elements in compacted residual gneissic soil. Laboratory soil column tests together with chemical, physical and micromorphological analyses were performed on soil samples. The artificial contaminant solution used in the tests was prepared by addition of nitrate salts of Mn^{2+}, Zn^{2+}, Cd^{2+}, Cu^{2+}, Pb^{2+} and Cr^{3+}. The main conclusions were as follows. Initial percolation of distilled water to saturate the soil without counter pressure influenced the column test results since the soil structure was altered, especially when a large pore volume was percolated. Hydraulic conductivity values decreased significantly in all soil columns with contaminant solution percolation. The metals Cu, Pb and Cr remained totally retained in the soil. Comparison of Mn transport parameters determined in the present study with those obtained in a previous one showed that for the tests performed Mn mobility was practically independent of soil hydraulic conductivity when all other factors were held constant.

Key words: mobility, heavy metals, compacted soil, laboratory studies.

1. Introduction

There is a growing consciousness worldwide that progress must be linked to environmental preservation. However, in order to preserve the environment it is necessary to know it and only with an understanding of the mechanisms that regulate the integration of man with nature it is possible to use the environment without degrading or destroying it.

Heavy metals are important environmental contaminants that are toxic above a given concentration. Causes of soil contamination by metals include domestic and industrial solid waste disposal, atmospheric deposition of vehicular and industrial emissions, agricultural use of fertilizers, soil additives and pesticides and disposal of crop wastes (Alloway, 1995). Underground waters may be contaminated when metals levels exceed the maximum soil retention capacity.

Population growth and the consequent increase in waste generation has led to an increased demand for technologies that decrease the environmental impact of these wastes, especially with regard to barrier systems used to minimize the infiltration of waste leachates and contain migration of contaminants through soils and underground water in areas of waste disposal.

Tropical residual soils are common in Brazil. Compacted soils of this type alone or associated with geomembranes have been used as liners in industrial and urban solid waste disposal areas. However, a great deal of uncertainty exists with regard to the use of these soils since few studies have been undertaken to evaluate their applicability. More studies on the interactions that occur between tropical residual soils and contaminant solutions are therefore necessary because these interactions may modify properties, such as hydraulic conductivity, which are important in controlling contaminant transport through soils.

Sensibility to contaminants of the soil used as barrier may affect its structure and modify the liner layer by increasing its hydraulic conductivity, thus favoring contamination (Kaczmarek *et al.*, 1997). In this sense, laboratory testing of soils used in liner layers should have duration long enough to allow for long term interactions between soil and leachate to occur.

Some of the most important parameters used to express solute mobility through a soil are the diffusion and hydrodynamic dispersion coefficients and the retardation

Rejane Nascentes, D.Sc., Departamento de Engenharia Civil, Universidade Federal de Mato Grosso, Av. Fernando Corrêa da Costa s/n, 78.060-900 Cuiabá, MT, Brazil. e-mail: rejanenascentes@yahoo.com.br.
Izabel Christina Duarte de Azevedo, D.Sc., Associate Professor, Departmento de Engenharia Civil, Universidade Federal de Viçosa. Campus Universitário s/n, 36571-000 Viçosa, MG, Brazil. e-mail: iazevedo@ufv.br.
Antonio Teixeira de Matos, D.Sc., Associate Professor, Departmento de Engenharia Agrícola, Universidade Federal de Viçosa. Campus Universitário s/n, 36571-000 Viçosa, MG, Brazil. e-mail: atmatos@ufv.br.
Maurício Paulo Ferreira Fontes, PhD., Professor, Departmento de Solos, Universidade Federal de Viçosa. Campus Universitário s/n, 36571-000 Viçosa, MG, Brazil. e-mail: mpfontes@ufv.br.
Roberto Francisco de Azevedo, Ph.D., Professor, Departmento de Engenharia Civil, Universidade Federal de Viçosa. Campus Universitário s/n, 36571-000 Viçosa, MG, Brazil. e-mail: razevedo@ufv.br.
Lucas Martins Guimarães, MSc. Student, Departmento de Engenharia Civil, Universidade Federal de Viçosa. Campus Universitário s/n, 36571-000 Viçosa, MG, Brazil. e-mail: lucasmguimaraes@bol.com.br.
Submitted on January 23, 2007; Final Acceptance on June 11, 2007; Discussion open until August 29, 2008.

factor. Given the scarcity of information on these parameters in Brazilian tropical residual soils, especially in subsurface horizons and under compacted soil conditions, the main objectives of this study were to evaluate mobility of six heavy metals (Mn^{2+}, Zn^{2+}, Cd^{2+}, Cu^{2+}, Pb^{2+} and Cr^{3+}) in residual compacted soil and to study the variation in soil hydraulic conductivity during percolation of a multispecies metal contaminant solution through the soil.

2. Background

Underground water deposits are generally more protected from pollution processes than surface water since in the former the overlying soil layer acts as a chemical and physical filter. The ease with which a contaminant reaches the underground water will depend on whether the aquifer is freatic or confined, on the aeration zone depth, the aeration zone and aquifer permeability, the level of organic matter present in the soil and on the types of oxides and clay minerals existing in the soil. Deeper aeration zones permit a longer filtration time and also increase the exposure time of contaminants to oxidizing and adsorbing agents present in this layer. Soil with a higher organic fraction has a higher capacity to adsorb heavy metals.

A contaminant may go through a series of chemical, biochemical and photochemical reactions and physical interactions with soil constituents before reaching underground water. These reactions may neutralize, modify or retard the polluting effect.

The main functions of liner systems are to minimize infiltration of percolates and contain migration of contaminants to the soil and underground water. To properly design liner systems, not only must contaminant flux be determined but the different physicochemical mechanisms that influence transport in contamination evolution must also be known. Although legal requirements for liner materials establish limits for hydraulic conductivity (maximum value typically limited to 10^{-8} or 10^{-9} m/s), at least four mechanisms control contaminant transport across impermeable layers: advection, diffusion, dispersion and sorption. For practical and economic reasons natural soils alone or combined with geomembranes are being used in these barrier systems in domestic and industrial waste disposal areas.

Mineralogical composition has a profound affect on metals retention in soils. In most tropical residual soils the adsorption of metals is quite intense due to the oxide composition, since iron and aluminum oxides retain heavy metals with high energy in both specific and non-specific interactions.

Besides the knowledge of soil components, their physicochemical properties and soil retention mechanisms, the variation in permeability of the impermeabilization layers is an important aspect of soil and underground water contamination. Contact between the contaminant solution and soil that can cause spatial redistribution because of clay particle rearrangement (flocculation, dispersion, peptization and micro-migration) together with chemical reactions between contaminants and clay minerals, such as solids dissolution and precipitation, are the most important causes of variations in permeability.

The initial soil structure varies with compaction humidity, energy and degree of compaction. According to Boscov (1997), significant variations in permeability may occur within a relatively small range of compaction humidity and density because of the formation of different structural arrangements.

In order to better understand the interactions that occur between tropical residual soils and contaminant solutions and how these interactions can alter soil properties it is necessary to perform laboratory tests for sufficient time so that long term interactions between soil and the percolating solution may occur.

2.1. Heavy metals

The meaning of the term heavy metals is controversial and a variety of definitions based on different criteria can be found in the literature. In the density based definition, heavy metals are high density ($\geq 6 \times 10^3$ kg/m^3) chemical elements and their ions belonging to the transition and non-transition groups of the periodic table (Matos *et al.*, 1999). According to Guilherme *et al.* (2005), the term trace element has been preferred over heavy metal in several recent publications since the latter has never been formally defined by an official organization of chemistry professionals.

Some heavy metals, such as Co, Cu, Fe, Mn, Mo, Ni and Zn, are essential human, animal and plant elements. Other elements, such as Cd, Hg and Pb, have no known biological function (Srivastava & Gupta, 1996). Both essential and non-essential metals can cause metabolic problems in living beings if absorbed above a certain amount (McBride, 1994). These elements capacities to accumulate in living tissue and to concentrate along the food chain increases the chance of their causing disturbances in ecosystems that may occur even after the release of the metals is stopped. (Tavares & Carvalho, 1992).

Studies on the behavior of heavy metals in soils have concluded that soil retention of these elements depends on the nature of the solid phase and the proportions of its constituents, the properties of the liquid phase and the metal species present in the soil solution (Sposito, 1984; Yuan & Lavkulich, 1997; Naidu *et al.*, 1998).

The concentration of heavy metals in the soil solution results from equilibrium between precipitation, dissolution, complexation and adsorption reactions and is affected by various factors, such as soil type, climate, vegetative cover, and chemical form of the elements (Cooker & Matthews, 1983). However, given the equilibrium changes and chemicals forms of metals in wastes and soil and the possibility of exceeding the soil pollutant retention capacity, the metals may be leached, especially under acid conditions, and may

thus reach the groundwater. The specific surface area, texture, apparent density, temperature, pH, redox potential, cation exchange capacity (CTC), organic matter content, amount and type of clay minerals and metals and ion competition are among the soil properties that affect the metals reactions and their mobility in soil (Matos, 1995).

The existence of competition for adsorption sites between ions has been recognized by many researchers (Matos, 1995, 1999; Azevedo *et al.*, 2003; Nascentes, 2003, 2006), and it has been observed that the rate of adsorption of any ionic species decreases with the increase in number of competing species. Factors such as solution pH, concentration and the nature of competing species affect the competitive adsorption.

Soils generally have a large variety of adsorption sites with different bonding properties and contain abundant aqueous ionic and non-ionic complexes capable of participating in adsorption processes and possibly in metals precipitation processes.

The soil CTC is one of the most important indicators of heavy metals retention capacity in the soil solid phase. Soils with higher CTC values generally have greater metals adsorption capacity than those with lower CTC values (Rudd, 1987).

2.2. Mass transport mechanisms in porous media

The accumulation of contaminants in soil is a consequence of soil-solute physicochemical interactions arising from transport through the soil. Physical, chemical and biochemical mechanisms can govern solute transport in hydrogeological environments. The most important mechanisms in contaminant transport across saturated clay soil layers are the physical mechanisms of advection and diffusion. In the case of transport in aquifers, advection and dispersion are usually the most important mechanisms.

The transfer of the solute from the interstitial fluid to the solid soil particles is as important as the physical mechanisms. The transfer processes depend on the chemical composition of the solute, its reactivity and organic and inorganic content as well as on soil constituents and characteristics and system pH. These processes may include ion exchange sorption reactions (adsorption and desorption), precipitation and complexation. Biodegradation and radioactive decay are other mechanisms that may be involved.

According to Rowe *et al.* (1995), perhaps the most important factor in soil-contaminant interaction processes and substance transport through soil is probably the diffuse double layer expansion-contraction phenomenon.

2.3. Diffuse double layer

The effective thickness of the diffuse double layer (Eq. (1)) depends on charge density, surface electric potential, electrolyte concentration, valence, pH, dielectric constant of the medium and temperature. Changes in any of these variables may cause alterations in system behavior since forces of repulsion and attraction depend on interaction between adjacent double layers. An increase in thickness of the diffuse double layer corresponds to a lower tendency of the particles in suspension to flocculate. That is, the thicker the double layer, the thinner and more torturous will be the path of percolating solutions in the soil and consequently, the lower the hydraulic conductivity will be:

$$\frac{1}{K} = \left(\frac{\varepsilon_0 \, D \, k \, T}{2 n_0 \, e^2 \, \nu^2} \right)^{1/2} \qquad (1)$$

where $1/K$ is the electric effective double layer thickness; $\varepsilon = 8{,}8542 \times 10^{-12}\ C^2\ J^{-1}\ m^{-1}$; D is the dielectric constant; k is the Boltzman constant; T is the absolute temperature (K); n_0 is the ionic concentration and v is the cationic valence and e is the electron charge.

For a constant void volume, contraction or flocculation of the diffuse double layer causes an increase in voids between soil particles, and increases the hydraulic conductivity and accelerates the advance of percolating fluid. If, on the contrary, an ion exchange reaction that favors expansion of the diffuse double layer takes place, the hydraulic conductivity will decrease and the percolating fluid will be slowed. At a constant void volume, substitution of monovalent cations by bivalent or trivalent cations on the clay particle surface and an increase in temperature are among the factors that cause diffuse double layer contraction and can lead to dramatic increases in hydraulic conductivity (Rowe *et al.*, 1995).

Hydraulic conductivity is inversely proportional to resistance that the medium offers to fluid flow caused by a hydraulic gradient and depends on the characteristics of both the fluid and the porous medium. According to Lambe (1969), the factors with greatest effect on soil permeability are its composition, void ratio, structure, degree of saturation as well as fluid characteristics, including chemical composition, since the compounds present in the fluid interact with the minerals that form the soil (Mesri & Olson, 1971; Folkes, 1982).

3. Material and Methods

3.1. Soil

The material used in this study was collected from the B horizon of a red-yellow latosol classified according to Unified Soil Classification (USC) as high plasticity clay, located on line A (MH/CH), and according to the Highway Review Board (HRB) system as A-7 soil with group index 12 (Nascentes, 2006). The geotechnical soil characterization is presented in Tables 1 and 2.

X-ray analyses were performed on three sample types: (i) natural clay randomly placed in powdered form on a glass well slide, (ii) an oriented sample, prepared with natural clay spread as a paste to orient minerals and clay and (iii) an oriented sample, after treatment to remove ferric oxides in order to better identify clay silicates and alumi-

Table 1 - Grain size distribution and Atterberg limits for the soil used in this study.

Grain size distribution				Atterberg limits		
Clay (%)	Silt (%)	Sand (%)	Gravel (%)	LL (%)	LP (%)	PI (%)
42	10	47.1	0.9	52	30	22

LL - liquid limit; LP - plasticity limit; PI - plasticity index.

Table 2 - Physical indexes of the soil used in this study.

γ_s (kN.m^{-3})	Activity	γ_{dmax} [1] (kN.m^{-3})	$w_{optimum}$ [1] (%)	γ_{dmax} [2] (kN.m^{-3})	$w_{optimum}$ [2] (%)
27	0.52	16.45	22.3	15.82	24.1

γ_s - specific weight of solids; γ_{dmax} and $w_{optimum}$ - dry soil specific weight and optimum soil humidity: [1]at Standard Proctor energy; [2]at an energy of 233 kJ/m^3.

num oxides possibly present in the soil sample. Analyses were performed in the Mineralogy Laboratory of the Soils Department of the Federal University of Viçosa using a Rigaku D-Max X-ray difractometer. A cobalt tube and curved graphite monochromator was used to obtain Co-Kα radiation. The difractometer was operated at 40 kV and 30 mA.

The presence of various peaks that permit identification of kaolinite, goethite and small quantities of hematite can be observed in the difractogram of the random natural clay fraction (Fig. 1a). Given its yellow color, it was assumed that only a very small amount of hematite was present in this soil since the presence of hematite, even in small quantities imparts a reddish color to the soil (Fontes & Carvalho Jr., 2005), which was not the case for the sample used.

The attempt to orient the clay minerals in the presence of ferric oxides was not successful, as can be seen in Fig. 1b. Face to face alignment of kaolinite minerals was not possible due mainly to the presence of goethite, resulting in a large series of peaks characteristic of kaolinite. The difractogram of the clay fraction of the soil after removing ferric oxides is presented in Fig. 1c. Only two large kaolinite peaks (1st and 2nd order) were observed proving that when the kaolinite is perfectly aligned only peaks characteristic of this mineral's base atomic planes will appear.

Through combined evaluation of the difractograms the soil's clay fraction composition was defined as kaolinite and goethite with very little hematite.

The Fe content was determined using the dithionite extraction method (Coffin, 1963) to quantify iron oxides. Iron oxides corresponded to 13.3% of the clay fraction and were assigned to goethite. It is important to determine the presence of iron oxides since they have the capacity to retain heavy metals with high energy even when present in small quantities. Important chemical and physicochemical characteristics of the soil are presented in Table 3.

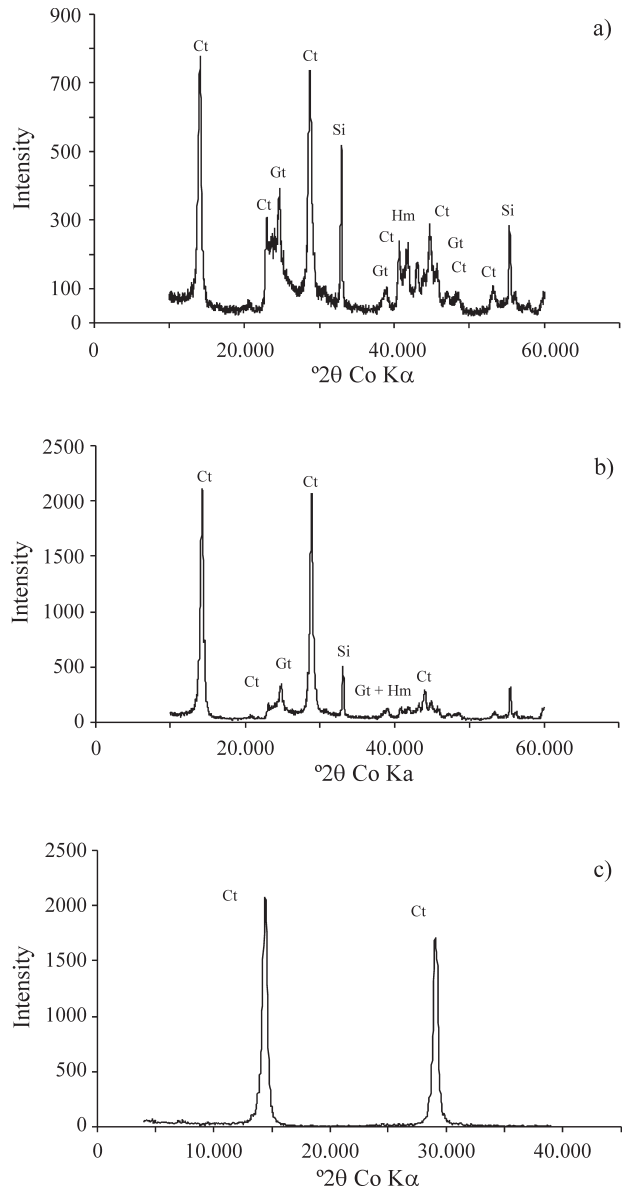

Figure 1 - Difractogram of the clay fraction. (a) Randomly oriented natural clay in a well slide; (b) Oriented natural clay (c) Oriented clay after iron removal.

3.2. Contaminant solution

A contaminant solution was prepared by mixing nitrates of manganese, zinc, cadmium, copper, lead and

Table 3 - Results of chemical and physicochemical soil analyses.

Ca^{2+}	Mg^{2+}	K^{+}	Al^{3+} $cmol_c$	$H^{+}+Al^{3+}$ kg^{-1}	CTC_{ef}	CTC_{pot}	pH	MO dag kg^{-1}
1.23	0.11	0.026	0.0	0.7	1.37	2.07	6.01	0.0

CTC_{ef} - Effective cation exchange capacity at natural soil pH; CTC_{pot} - Cation exchange capacity at pH 7.

chrome since these are the metals most commonly found in urban landfill leachates. The pH and concentrations of the heavy metals in the leachate (Table 4) are within the range cited in the literature for Brazilian landfill leachates (Oliveira & Jucá, 1999; Barbosa & Otero, 1999).

3.3. Column tests

Column tests were performed on eight soil samples (three repetitions and one reference, respectively, for gradients 7.3 m/m and 13.4 m/m) adjusted to 22.5% humidity to evaluate hydraulic conductivity of compacted soil leached by the contaminant solution and to determine the transport parameters of the metals studied.

All samples were compacted to a specific weight of approximately 15.63 kN/m^3 (95% of the maximum standard Proctor compaction degree). Compaction energy was such that the samples were compacted until reaching 0.10 m height and 0.05 m diameter (233 kJ/m^3). Compaction data for each sample are presented in Table 5.

Soil columns were saturated with distilled water until a constant flow was obtained (after 24 days) before percolating the contaminant solution. A flexible walled permeameter that resembled a triaxial chamber (Azevedo *et al.*, 2003), constructed in the Geotechnical Laboratory of the Civil Engineering Department of the Federal University of Viçosa was used for the tests. Tests were conducted in a temperature controlled room (17 to 20 °C) and lasted nine months and 15 days.

3.4. Analyses

Chemical, physical and micromorphological analyses of the samples were performed at the end of the column tests to evaluate soil retention of the heavy metals and variation in hydraulic conductivity caused by the percolating contaminant solution. The following determinations were made: hydraulic conductivity when percolating distilled water; hydraulic conductivity when percolating contaminant solution; leachate cation (Na^{+}, Ca^{2+}, Mg^{2+}) concentrations; effluent pH; effluent electric conductivity; metals retardation factors of (R_d); metals hydrodynamic dispersion coefficients (D_h); sequential extraction; dispersed clay; scanning microphotography.

3.5. Chemical analyses

Samples from columns CP01 (control), CP03, CP05 and CP07 were sliced into five 0.02 m thick layers, placed in plastic bags to avoid water loss and kept in a humidity chamber for up to 24 h for chemical analyses. Sequential extraction used to determine speciation of each heavy metal in the compacted samples was performed in four steps: i) distilled water; ii) $CaCl_2$ 0.1 mol L^{-1} solution; iii) Na_2HPO_4 0,167 mol L^{-1}, NaF 0,03 mol L^{-1} and EDTA 0,0083 mol L^{-1} solution; iv) nitric-percloric digestion (Nascentes, 2006).

At the end of the column tests three samples of distilled water were collected from each permeameter used to apply the confining pressure and analyzed for the six heavy

Table 4 - Contaminant solution.

Parameter	pH	Cr^{3+} (mgL^{-1})	Cd^{2+} (mgL^{-1})	Pb^{2+} (mgL^{-1})	Cu^{2+} (mgL^{-1})	Mn^{2+} (mgL^{-1})	Zn^{2+} (mgL^{-1})
Value	5.2	0.7	1.6	1.6	5.0	36.0	62.0

Source: Azevedo *et al.* (2006).

Table 5 - Compaction tests results.

	CP 01	CP 02	CP 03	CP 04	CP 05	CP 06	CP 07	CP 08
GC (%)	94.9	94.8	95.1	94.5	94.5	94.9	95.1	94.8
Gradient	13.4	13.4	7.3	7.3	13.4	13.4	7.3	7.3
Void ratio	0.729	0.731	0.726	0.737	0.737	0.729	0.726	0.731
Porosity	0.422	0.422	0.421	0.424	0.424	0.422	0.421	0.422
Void vol. (mL)	81.4	81.4	80.7	82.0	81.7	81.5	81.0	81.3
Degree of saturation (%)	83.2	83.0	83.6	82.4	82.4	83.3	83.6	83.0
Δh (%)	-1.6	-1.6	-1.6	-1.6	-1.6	-1.6	-1.6	-1.6

Δh - optimum water content deviation.

metals (Mn, Zn, Cd, Cu, Pb and Cr). No differences were detected among the samples indicating that no contaminant migration occurred into the water chamber.

3.6. Physical analyses

Percentage of dispersed clay was determined in the upper half of samples CP02, CP04, CP06 (control) and CP08. Slow and fast mechanical dispersion were employed to examine the effect of type of dispersion on the results. The methodology used was described by Ruiz (2005).

3.7. Micromorphological analyses

The lower half of samples CP02, CP04, CP06 and CP08 were used for micromorphological analyses. Samples were oven dried at 60 °C, for 48 h and then impregnated with a mixture of acrylic resin (60%) and styrene (40%) plus 5 mL of catalyst for each 1000 mL of mixture. The samples were left to soak in a well vented environment for 20 days to permit penetration in all the sample pores. Thin slices were prepared for optical and scanning electron microscope observations. The microphotographs were taken in the Microscopy Laboratory of the Geology Department of the Federal University of Ouro Preto. Some microphotographs were also taken of carefully withdrawn 10^{-6} m^3 subsamples from the compacted samples. These subsamples were oven dried at 50 °C and fixed on aluminum stubs using double faced adhesive tape, covered with about 20 nm of a gold-palladium mix using a model FDU 010 (Balzers, Inc, USA) metalizer and observed under a VP 1430 scanning electron microscope (LEO Electron Microscopy, Oberkochen, Germany) operated at a voltage of 15 kV. This procedure was performed at the Center for Microscopy and Microanalysis of the Federal University of Viçosa. The images obtained were used to observe changes in soil microstructure.

4. Results

4.1. Column tests

4.1.1. Distilled water percolation

Soil hydraulic conductivity curves (corrected to 20 °C) *vs.* number of pore volumes percolated (T) for distilled water percolation are presented in Fig. 2. Electrical conductivity and pH values measured in the column leachates are presented in Figs. 4 and 5, respectively.

The significant variation (up to one order of magnitude) in hydraulic conductivity with the number of pore volumes percolated (T) is shown in Fig. 2. The increase in hydraulic conductivity at the beginning of the test may have been caused by the gradual increase in degree of sample saturation due to expulsion of air from the voids.

Distilled water percolated through the soil led to a decrease in ionic concentration (Na^+, Ca^{2+}, Mg^{2+} etc.) of the soil solution (Figs. 3 (a), (b), (c)) as a result of expansion of the diffuse double layer. This expansion, which results in a

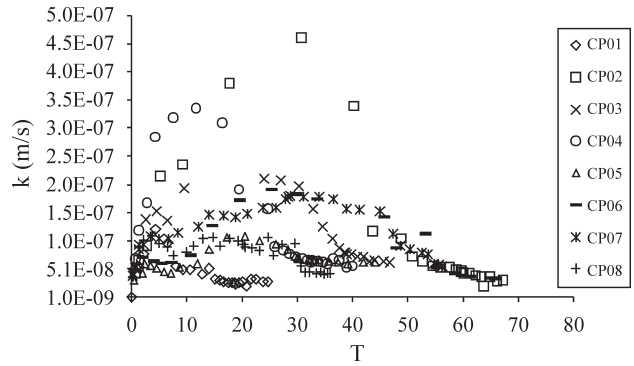

Figure 2 - Hydraulic conductivity in samples percolated with distilled water.

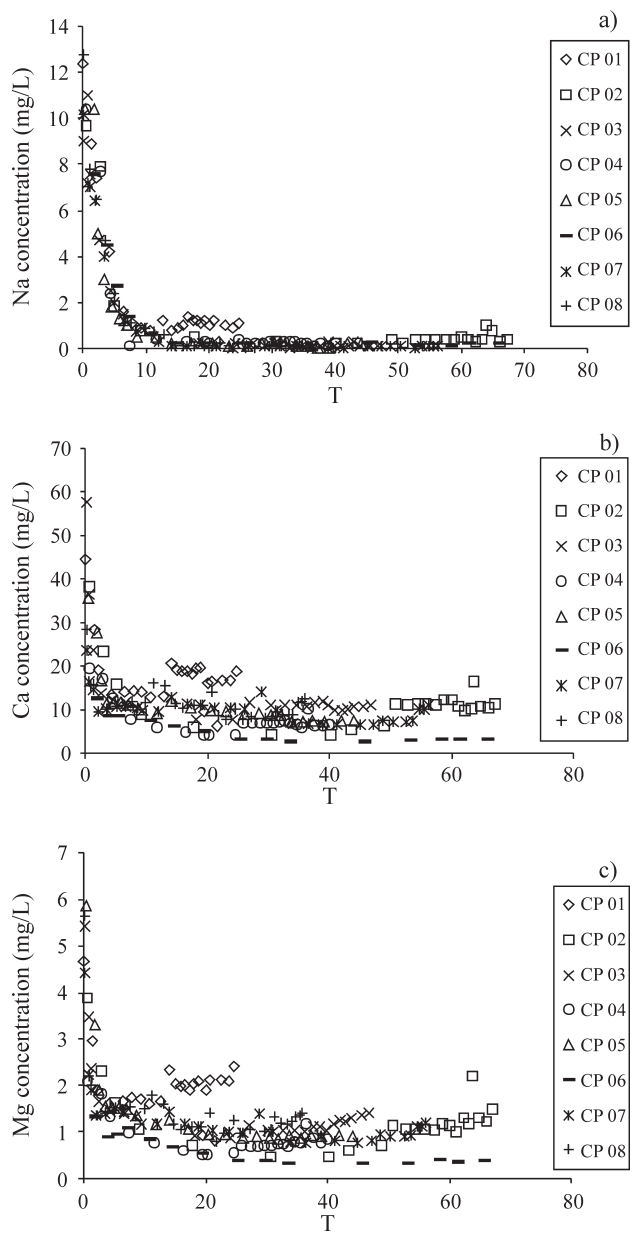

Figure 3 - Cations in soil column leachates percolated with distilled water (a) sodium, (b) calcium, (c) magnesium.

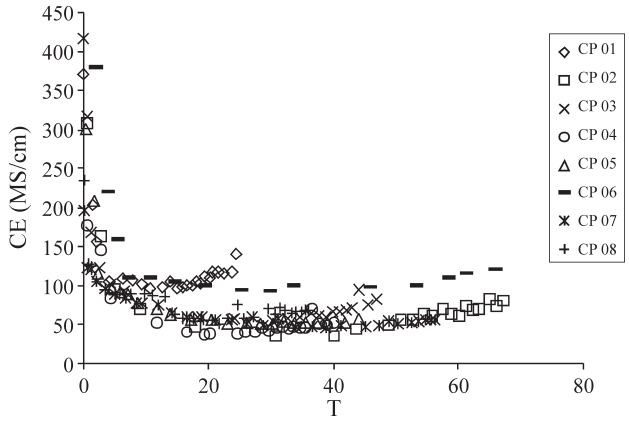

Figure 4 - Electrical conductivity (CE) in soil columns percolated with distilled water.

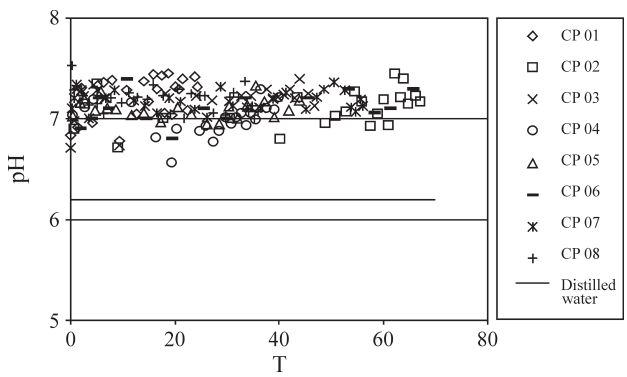

Figure 5 - Leachate pH of soil column percolated with distilled water.

narrower and more tortuous solution percolation path, may have contributed to colloidal dispersion including that of material that acted as cementing agent of primary particles. The dispersion of cementing agents led to partial disaggregation of the soil structure, causing the greatest effect on soil macroporosity. Given the high correlation between soil hydraulic conductivity and macroporosity, it is clear that a decrease in macroporosity would lead to a proportional reduction in hydraulic conductivity.

Values of electrical conductivity were higher at the beginning of the column test (Fig. 4) when greater leaching of basic cations occurred.

Leachate pH values varied somewhat during soil saturation with distilled water. All sample leachate pH values were higher than the influent water (pH = 6.2) due to leaching of the bases Na^+, Mg^{2+}, Ca^{2+} adsorbed on the soil exchange complex. Their leaching to the aqueous solution resulted in an increase in hydroxide concentration (OH^-), and consequently in leachate pH.

4.1.2 Percolation of contaminant solution

Soil hydraulic conductivity curves for all samples percolated with the contaminant solution are presented in Fig. 6. Control samples CP01 and CP06 were percolated with distilled water and served as references. Concentration curves for the leached cations *vs.* pore volumes are presented in Figs. 7a, 7b and 7c. Graphs of effluent electrical conductivity and pH *vs.* pore volumes are presented in Figs. 8 and 9, respectively.

A significant decrease in hydraulic conductivity with percolation of contaminant solution was seen for all samples (Fig. 6). The decrease was not homogeneous among samples due to the different structures formed after the initial percolation with distilled water (Fig. 2). The large difference in water volume percolating the samples had a strong influence in the hydraulic conductivity behavior when the contaminant solution was percolated. In samples CP04 and CP05, the small difference observed between number of pore volumes and amount of leached cations when percolating water led to a similar hydraulic conductivity behavior when the contaminant solution was percolated through these columns.

The decrease in hydraulic conductivity in all samples was caused by obstruction of soil pores by heavy metals precipitation. According to Alloway (1995), the solubility of Cr^{3+} decreases at pH values greater than 4, with complete precipitation of the metal at values above 5.5. Evidence of metals precipitation from the contaminant solution are indicated by the pH *vs. T* curves in Fig. 9. Curves obtained for samples CP04 and CP05 are shown in Fig. 10 because of the large amount of data overlay in Fig. 9.

Hydraulic conductivity *vs. T* curves presented the same trend in variation as the pH *vs. T* curves in all samples tested.

Column CP04 presented lower hydraulic conductivity than CP05 for number of pore volumes between 13 and 50 (Fig. 6). CP04 leachate pH was greater than that of CP05 over this pore volume interval, indicating greater precipitation in CP04. From that point on the pH values approached the hydraulic conductivity values up to T = 104. At that point CP05 leachate pH started to increase compared to that of CP04 and consequently the hydraulic conductivity of CP05 (6.0 x 10^{-9} m/s) decreased more than that of CP04 (1.5 x 10^{-8} m/s). This occurred in all samples.

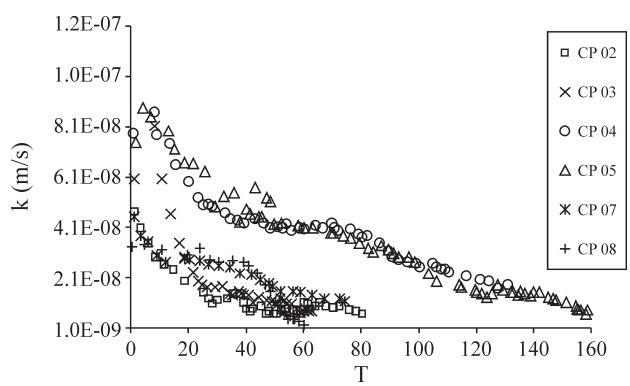

Figure 6 - Hydraulic conductivity in soil samples percolated with contaminant solution.

Column CP08 presented the highest leachate pH value (Fig. 11) and lowest final hydraulic conductivity (Fig. 6) of all samples. Higher pH values were observed at the beginning of the test (maximum of 7.6) for *T* values up to about 17, decreasing afterwards to *T* = 38. From that point on, the pH increased indicating an increase in metals precipitation and consequent decrease in hydraulic conductivity.

More colloidal dispersion also occurred in the samples after percolation with contaminant solution than after percolation with distilled water. Microphotographs of sample CP06 (control) and CP02 are presented in Figs. 12 and 13. It can be seen that the soil mass was more uniform in sample CP02 than in sample CP06, indicating more clay dispersion in the former. It is therefore possible to conclude that clay dispersion occurred during contaminant solution percolation and the dispersion contributed to the decrease in hydraulic conductivity.

Alterations in of all sample leachate pH values were attributed to an initial washing of the bases Na^+, Mg^{2+}, Ca^{2+} present in the soil solution exchange complex (Figs. 7a, 7b and 7c). In aqueous solution the bases promoted an increase in hydroxide concentration (OH^-), and thus an increase in solution pH. The fact that the leachate pH value remained above that of the influent solution may be due to the fact that ion exchange of metals by the bases adsorbed in the soil solid phase continued over the course of the test. This

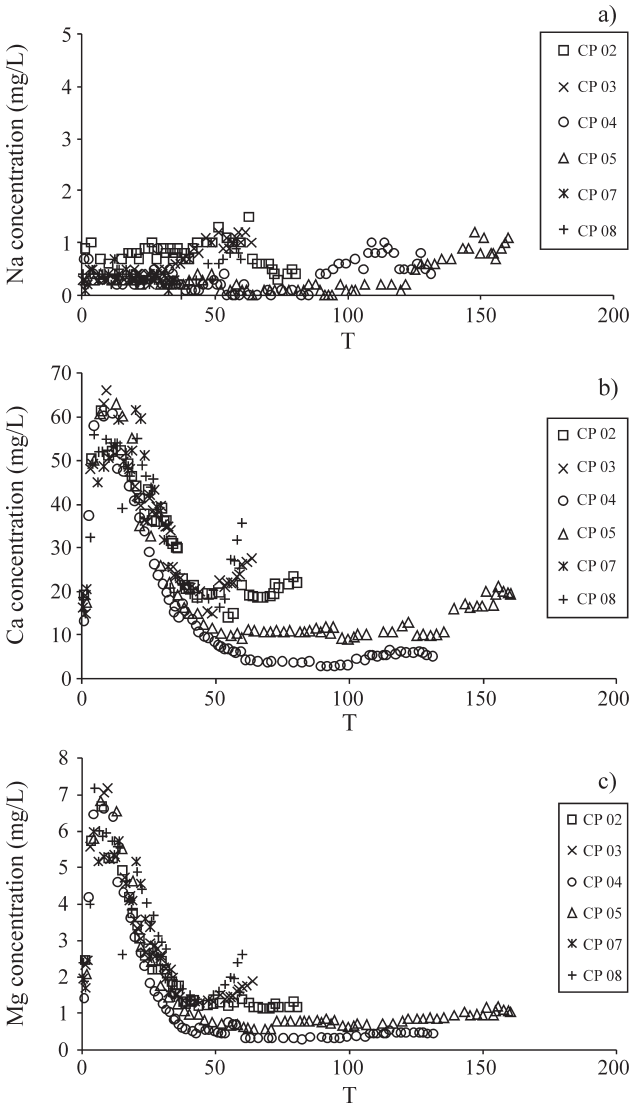

Figure 7 - Cation concentrations concentration in leachates from soil columns percolated with contaminant solution: a) sodium, b) calcium e c) magnesium.

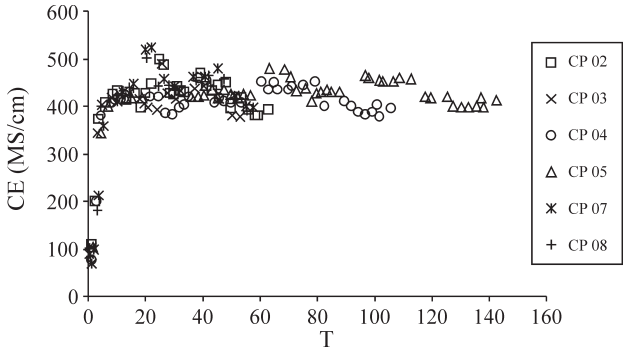

Figure 8 - Electrical conductivity in leachate from soils columns percolated with contaminant solution.

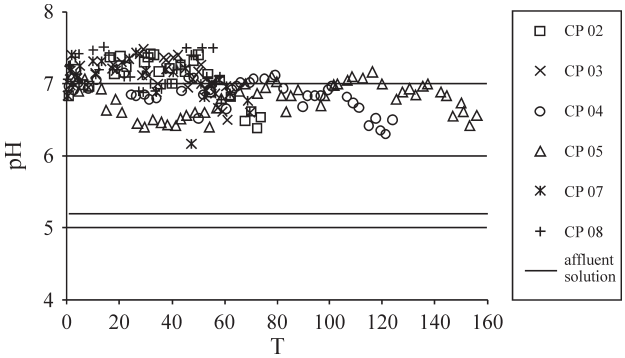

Figure 9 - pH of leachate from soil columns percolated with contaminant solution.

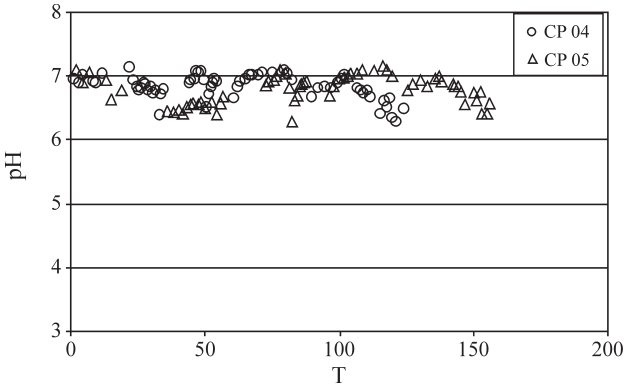

Figure 10 - Comparison of pH values of leachate collected from soil columns CP04 and CP05 percolated with contaminant solution.

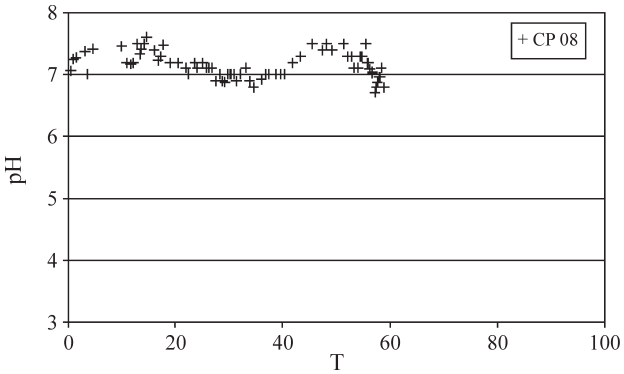

Figure 11 - pH values of leachate collected from soil column CP08 percolated with contaminant solution.

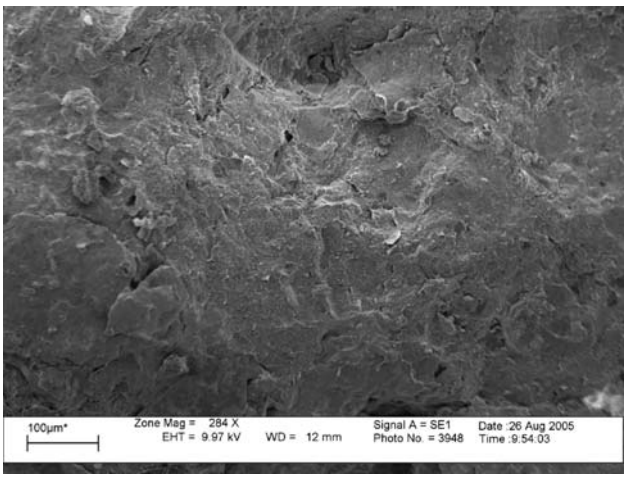

Figure 12 - Microphotograph of sample CP02.

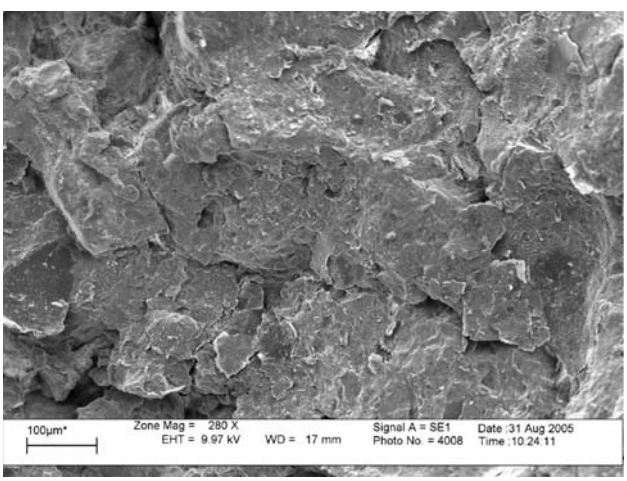

Figure 13 - Microphotograph of sample CP06 (control).

means that if sample saturation was reached with all the metals the leachate pH would be equal the influent pH, as was observed by Azevedo *et al.* (2005).

Cation leaching occurred due to substitution by heavy metals added to the soil. The initially high exchange of Ca^{2+} and Mg^{2+} decreased as the exchange sites occupied by these cations were occupied and their soil concentration decreased. Na^{+} was leached in small concentrations during almost the entire test. The concentrations of Ca^{2+}, Mg^{2+} and Na^{+} in the leachate of some samples tended to increase at the end of the test, indicating greater leaching of these cations caused by adsorption of metals with greater affinity for the soil matrix.

Electrical conductivity values presented fluctuations. The final portion of the curve in Fig. 8 presented a decline that indicates that a greater adsorption and/or precipitation of metals occurred.

4.1.3 Determination of transport parameters

Only the metals Mn (in all samples) and Zn (only in CP04) reached a steady state concentration (Figs. 14 and 15c) in the column tests, that is, they saturated the soil adsorption sites. Therefore it was only possible to determine the retardation factor (R_d) and hydrodynamic dispersion coefficient (D_h) using the cumulative mass method (Shackelford, 1995) for these two metals. The curves of cumulative mass ration (CMR) *vs.* theoretical and experimental *T* values are presented in Figs. 17 and 18.

Mn, Zn and Cd elution curves are presented in Figs. 14 to 16. The desorption of Mn (Fig. 14) and the increase in adsorption of Zn (Figs. 15a, b, d, e, f) and Cd (Figs. 16c, d, f) at the end of the column tests were observed in some samples.

The metals Cu, Pb and Cr remained totally retained in the soil, since these metals have low mobility and high affinity for iron oxides present in the soil. These elements can also form precipitates depending on their concentrations as well as on soil and solution pH.

Low data dispersion was observed in the CMR *vs. T* curves (Figs. 17 and 18) and the experimental curves adjusted well to the theoretical curves. The transport parameters R_d and D_h are presented in Table 6.

The relative Mn concentration (C/Co) in the elution curve (Fig. 14) was greater than unity, evidence of desorption. For Zn (except CP04) and Cd, the C/Co ratio never reached unity (and decreased in some cases), due to the decrease in hydraulic conductivity, mainly in CP08. It is thus possible to conclude that Zn and Cd replaced the desorbed Mn on the soil adsorption sites.

A Mn retardation factor of 18.8 was reported by Azevedo *et al.* (2005), close to the average value presented in Table 6. Given the greater hydraulic conductivity values (10^{-7} to 10^{-8} m s^{-1}) in the work by Azevedo *et al.* (2005) as compared to those in the present study (10^{-8} to 10^{-9} m s^{-1}), the mobility of Mn was found to be practically independent of soil hydraulic conductivity. The average D_h value equal to 4.3 x 10^{-8} m^2 min^{-1} (Table 6) was a little lower than the 8.64 x 10^{-7} m^2 min^{-1} presented in Azevedo *et al.* (2006), probably because the lower average percolation velocity used in that study caused less Mn dispersion.

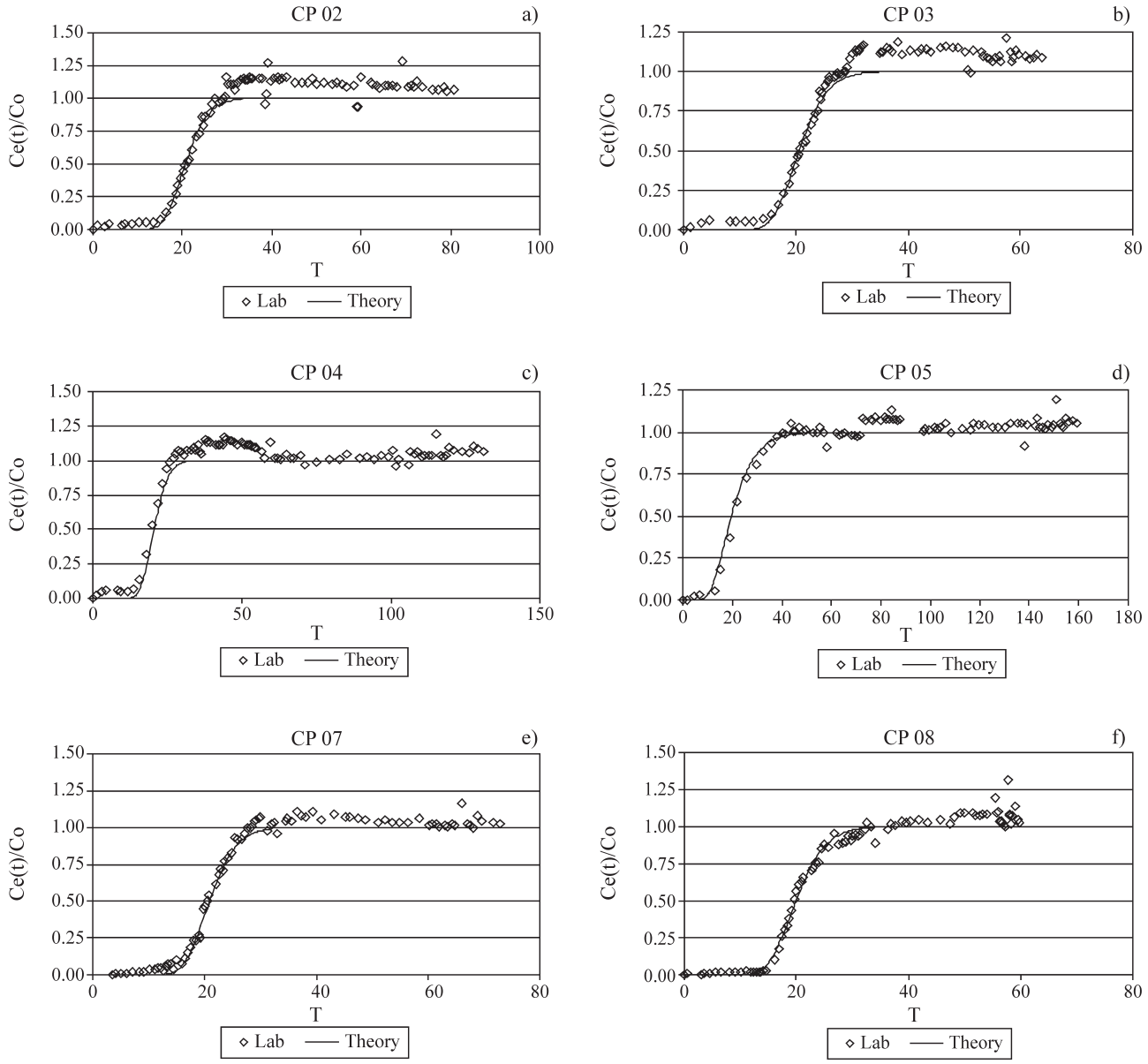

Figure 14 - Manganese elution curves from soil columns: (a) CP02, (b) CP03, (c) CP04, (d) CP05, (e) CP07, (f) CP08.

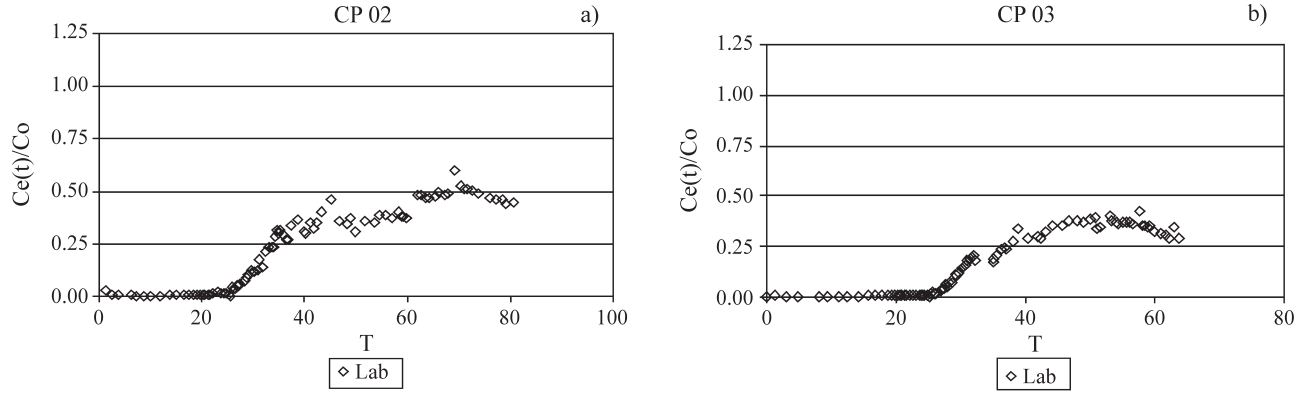

Figure 15 - Zinc elution curves from soil columns: (a) CP02, (b) CP03.

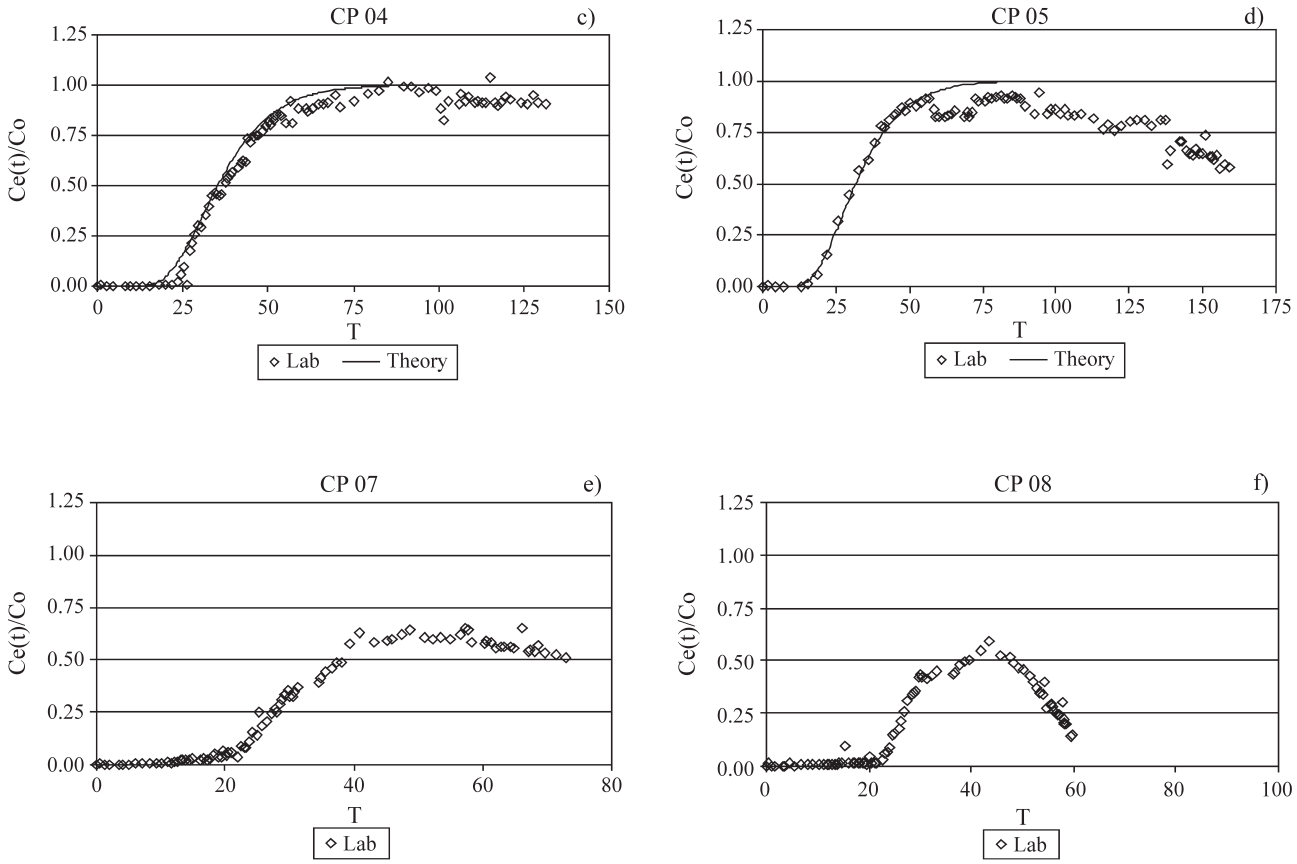

Figure 15 (cont.) - Zinc elution curves from soil columns: (c) CP04, (d) CP05, (e) CP07, (f) CP08.

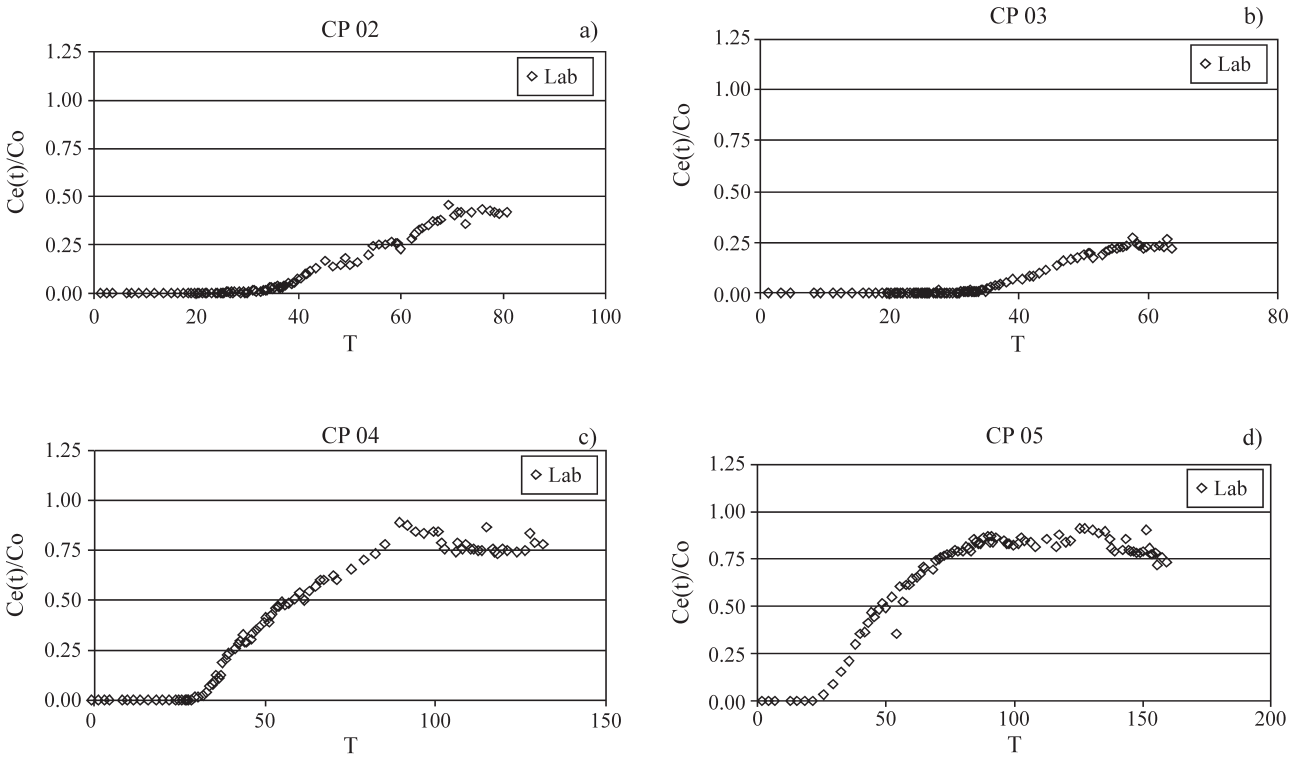

Figure 16 - Cadmium elution curves from soil columns: (a) CP02, (b) CP03, (c) CP04, (d) CP05.

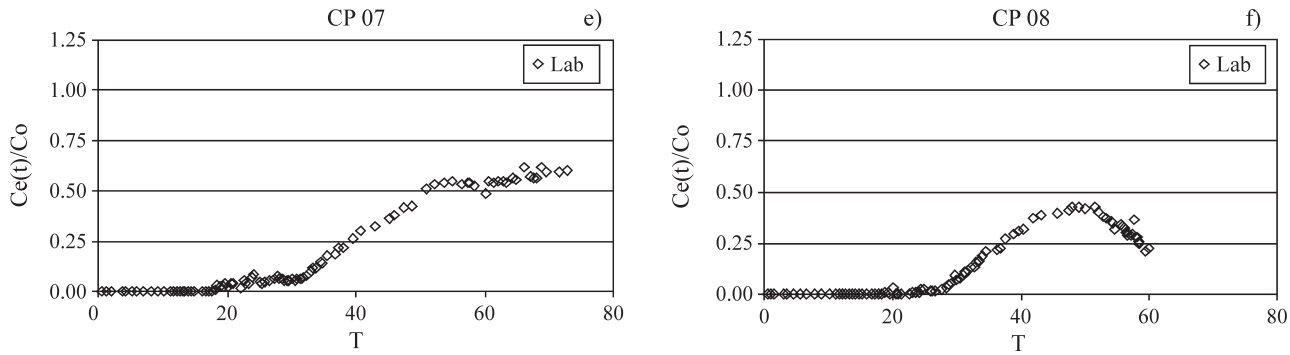

Figure 16 (cont.) - Cadmium elution curves from soil columns: (e) CP07, (f) CP08.

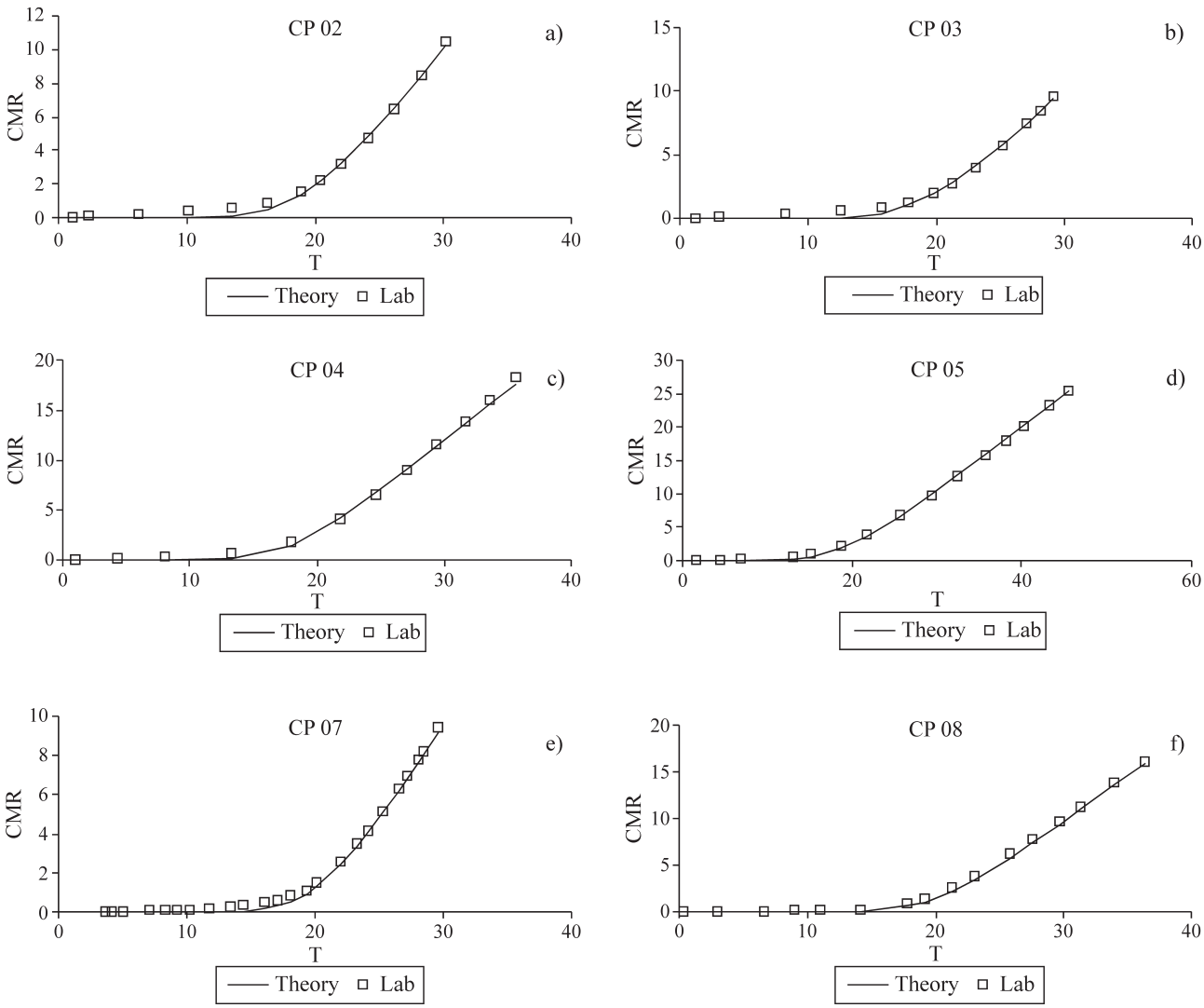

Figure 17 - Manganese cumultative mass ratio curves. CP02, (b) CP03, (c) CP04, (d) CP05, (e) CP07 e (f) CP08.

4.1.4 Soil physical analyses

Results of dispersed clay in samples withdrawn from the soil columns were quite similar for both fast and slow dispersal methods. Average results are indicated in Table 7. The values of dispersed clay indicated little dispersion of fine material in the soil samples analyzed. Greater values were expected since the hydraulic conductivity results indicated that clay dispersion occurred when distilled water was percolated through the columns. However, the samples

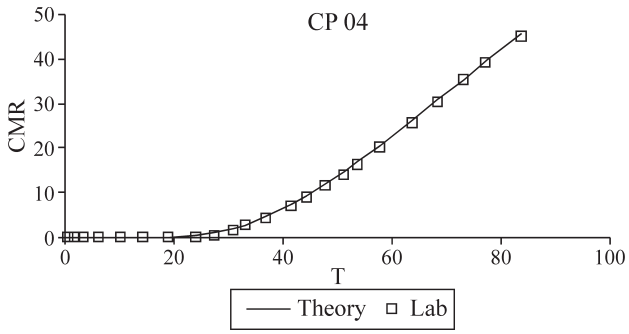

Figure 18 - Zinc cumultative mass ratio curve (CP04).

Table 6 - R_d and D_h obtained by the cumulative mass method.

Metal	Sample	R_d	D_h (m^2 min^{-1})
	CP02	20	4.6E-08
	CP03	20	3.9E-08
	CP04	18	4.4E-08
Manganese	CP05	20	8.0E-08
	CP07	20.5	2.0E-08
	CP08	20.4	2.7E-08
	Average	19.8	4.3E-08
Zinc	CP04	38	1.4E-07

were stored for two months and 23 days (justified by the time necessary to decide on the appropriate sample analyses) and it is believed that they suffered a tixotropic effect. Compacted clays may exhibit a considerable tixotropic effect (increase in resistance and rigidity with time) leading to a natural tendency to flocculate during storage. According to Boscov (1997), the structure of adsorbed water may change in stored compacted samples and can be detected by measurements that show the decrease in pore pressure with time after compaction.

Table 7 - Dispersed clay in samples withdrawn from the soil columns.

Sample	CP02	CP04	CP06	CP08
Dispersed clay (kg/kg)	0.002	0.002	0.005	0.003
FI*	0.99	0.99	0.988	0.99

*Floculation index.

4.1.5 Micromorphological analyses

Mosaics were prepared from 50% of the photos of slices taken in the optical microscope to better visualize pores. The photos taken with the scanning electron microscope (SEM) permitted visualization of a greater quantity of sample fissures in the control (CP06) than in the columns percolated with contaminant solution (CP02, CP04 and CP08). Mosaics of samples CP02, CP04 and CP06 are presented in Fig. 19. No mosaic was made of CP08 due to insufficient sample quantity for evaluation.

A greater quantity of blue stained macropores can be observed in control column CP06 that had the greatest hydraulic conductivity. Sample CP04 presented larger pores than sample CP02, consistent with the larger final hydraulic conductivity of sample CP04, which could be attributed to less plugging of macropores.

The presence of fissures in photos of samples CP06 (control), CP02, CP04 and CP08 obtained by SEM are indicated by arrows in Figs. 20, 21, 22 and 23. More fissures are present in CP06 (Fig. 20) than in the other samples. The fissures in the other samples may possibly have been blocked by precipitates formed during the percolation of the contaminant solution in the soil columns and also by particle washout during the test (Figs. 21, 22 and 23).

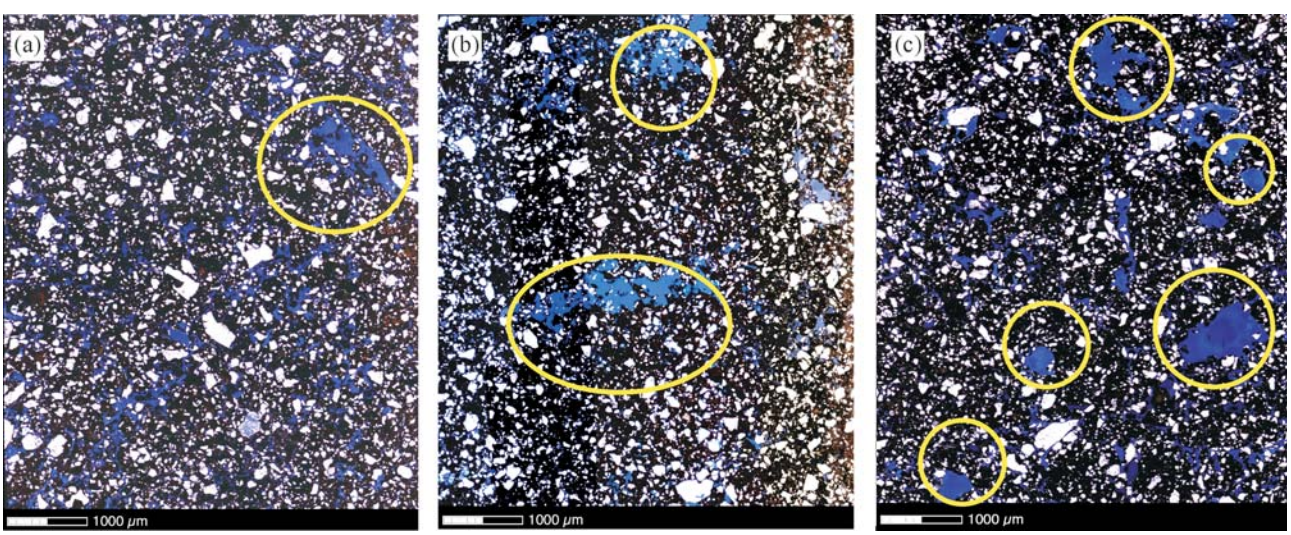

Figure 19 - Optical microscope mosaic of samples withdrawn from soil column: (a) CP02; (b) CP04; (c) CP06 (control.)

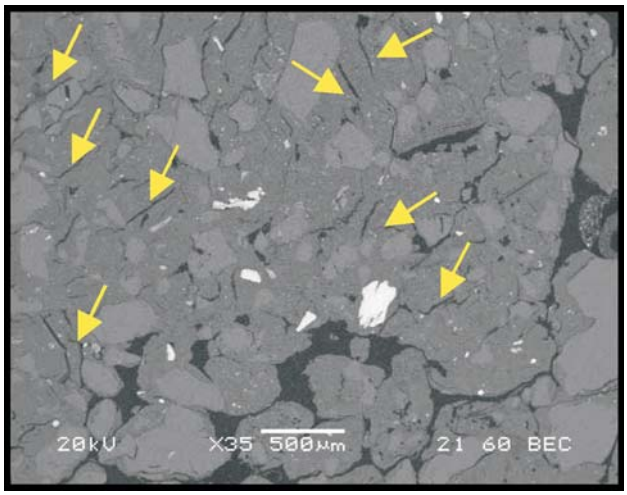

Figure 20 - Various fissures present - CP06.

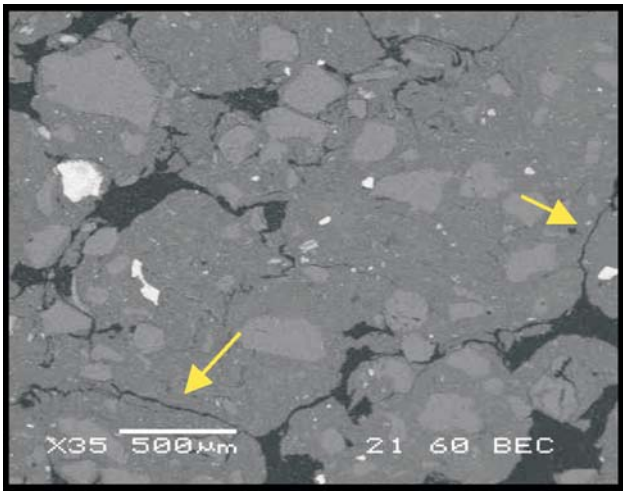

Figure 21 - Few fissures present - CP02.

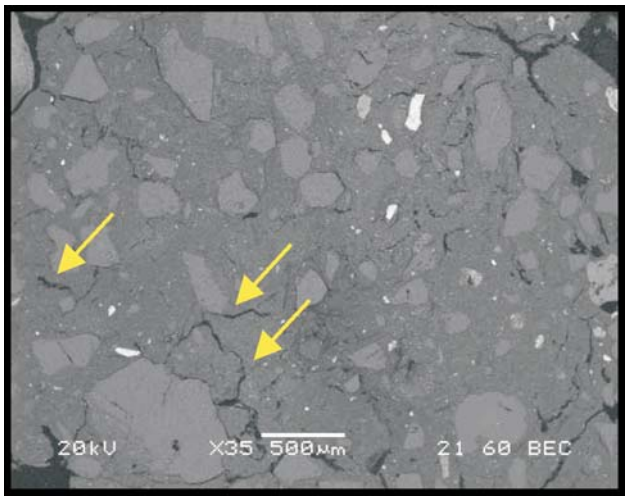

Figure 22 - Few fissures present - CP04.

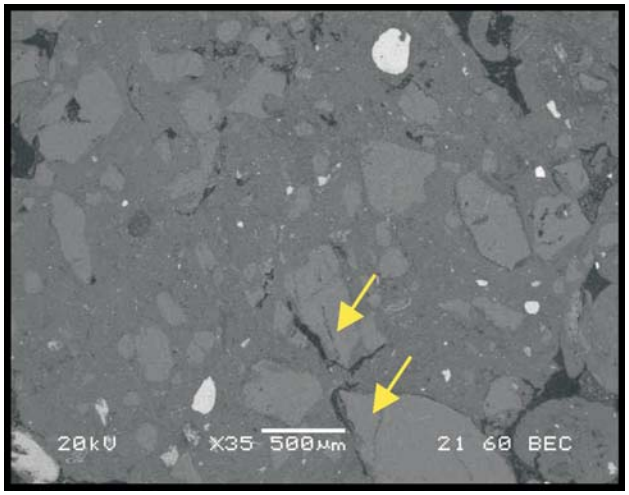

Figure 23 - Few fissures present - CP08.

5. Conclusions

Of the various conclusions to be drawn, it should be emphasized that initial percolation of distilled water to saturate the soil without back-pressure influenced the column test results since the soil structure was altered, especially when a large pore volume was percolated.

Hydraulic conductivity values decreased significantly in all soil columns with contaminant solution percolation, although the decrease differed among the samples.

The difference in number of pore volumes percolated (T) and the amount of cations leached during percolation of distilled water in the soil columns directly affected hydraulic conductivity when the contaminant solution was percolated possibly because of an alteration in soil structure caused by initial percolation with distilled water.

Evidence of pore obstruction caused by heavy metal precipitation was observed, explaining in part the decrease in hydraulic conductivity. The decrease was also partially attributed to dispersion of colloidal material

Greater leaching of Ca^{2+}, Mg^{2+} and Na^{+} was observed at the end of the soil column tests resulting in greater adsorption of some metals.

At the end of the column test, Mn was desorbed and a proportionally greater amount of Zn (except for CP04) and Cd were adsorbed due to decrease in hydraulic conductivity (especially in CP08), suggesting that Zn and Cd dislocated Mn from the adsorption sites.

The metals Cu, Pb and Cr remained totally retained in the soil, since these metals have low mobility and high affinity for iron oxides present in the soil.

Dispersed clay measurements indicated high flocculation indexes but the results may have been influenced by a trixotropic effect occurring in the stored samples.

Comparison of Mn transport parameters determined in the present study with those obtained in a previous one (Nascentes, 2003) showed that for the tests performed Mn

mobility was practically independent of soil hydraulic conductivity when all other factors were held constant. Nevertheless, for other five metals studied, results show correlation of hydraulic conductivity and metal mobility.

The mobility sequence obtained was $Mn^{2+} > Zn^{2}$.

Average values of R_d and D_h determined for Mn were, respectively, 19.8 and 4.3E-08 (m^2 min^{-1}), while for Zn these values were 38 and 1.4E-07, respectively.

Acknowledgments

The authors would like to acknowledge CNPq and CAPES for financial support and the Civil Engineering, Agricultural Engineering, and Soil Departments of the Federal University of Viçosa, MG, Brazil, for carrying out tests.

References

Alloway, B.J. (1995) Heavy Metals in Soils. 2nd ed. John Wiley & Sons, New York, chap. 1, pp. 3-10.

Azevedo, I.C.D.A.D.; Nascentes, R.; Azevedo, R.F.; Matos, A.T. & Guimarães, L.M. (2003) Hydrodynamic dispersion coefficient and retardation factor for heavy metals in residual compacted soils. (In Portuguese). Solos e Rochas - Revista Brasileira de Geotecnia, v. 26:3, p. 229-249.

Azevedo, I.C.D.; Nascentes, C.R.; Matos, A.T. & Azevedo, R.F. (2005) Determination of heavy metal transport parameters in residual compacted soil. (In Portuguese). Revista Brasileira de Engenharia Agrícola e Ambiental, v. 9:4, p. 623-630.

Azevedo, I.C.D.A.D.; Nascentes, C. R.; Matos, A.T. & Azevedo, R.F. (2006). Determination of transport parameters for heavy metal in residual compacted soil using two methodologies. Canadian Journal of Civil Engineering, v. 33:7, p. 912-917.

Barbosa, R.M. & Otero, O.M.F. (1999) Characterization of a pollution plume caused by urban waste disposal. (In Portuguese). Geochimica Brasiliensis, Rio de Janeiro, v. 13:1, p. 51-65.

Boscov, M.E.G. (1997) Contribution of design of systems of hazardous waste containment using lateritic soils. PhD Thesis (In Portuguese). Universidade de São Paulo, Escola Politécnica. São Paulo, 259 pp.

Coffin, D.E. (1963) A method for determination of free iron oxides in soils and clays. Can. Journal of Soil Science, v. 43, p. 9-17.

Cooker, E.G. & Matthews, P.J. (1983) Metals in sewage sludge and their potential effects in agriculture. Water Sci. Technol., v. 15, p. 209-225.

Folkes, D.J. (1982) Fifth Canadian Geotechnical Colloquium: Control of contaminant migration by the use of liners. Canadian Geotechnical Journal, v. 19, p. 320-344.

Fontes, M.P.F. & Carvalho Jr., I. (2005) Color attributes and mineralogical characteristics, evaluated by radiometry, of highly weathered tropical soils. Soil Science Society of America Journal, v. 69, p. 1162-1172.

Guilherme, L.R.G.; Marques, J.J.; Pierangeli, M.A.P.; Zuliani, D.Q.; Campos, M.L. & Marchi, G. (2005) Trace elements in soils and aquatic systems. (In Portuguese). Topics in Soil Science. Soc. Bras. de Ciência do Solo, v. 5, p. 345-390.

Kaczmarek, M.; Hueckel, T.; Chawla, V. & Imperiali, P. (1997) Transport Through a Clay Barrier with the Contaminant Concentration Dependent Permeability. Transport in Porous Media, v. 29, p. 159-178.

Lambe, T.W. (1979) Soil Mechanics. John Wiley & Sons Inc., New York, 553 pp.

McBride, M.B. (1994) Environmental Chemistry of Soils. Oxford University Press, New York, 406 pp.

Matos A.T. (1995) Retardation Factors and Dispersion-Diffusion Coefficients for Zinc, Cadmium, Copper and Lead in Soils from the County of Viçosa, Minas Gerais. Doctoral Thesis, Universidade Federal de Viçosa, Viçosa, 183 pp. (In Portuguese)

Matos, A.T.; Costa, L.M.; Fontes, M.P.F. & Martinez, M.A. (1999) Retardation factors and the dispersion-diffusion coefficients of Zn, Cd, Cu and Pb in soils from Viçosa - MG, Brazil. Transaction of the ASAE, v. 42:4, p. 903-910.

Mesri, G. & Olson, R.E. (1971) Mechanisms controlling the permeability of clays. Clay and Clay Minerals, v. 19:3, p. 151-158.

Nascentes, R. (2006) Mobility Study of Heavy Metals in Compacted Residual Soil. Master Thesis, Universidade Federal de Viçosa, Viçosa, 111 pp. (In Portuguese).

Nascentes, C.R. (2003) Heavy Metal Hydrodinamic Dispersion Coefficient and Retardation Factor in Compacted Residual Soil. Doctoral Thesis, Universidade Federal de Viçosa, Viçosa, 153 pp. (In Portuguese).

Naidu, R.; Sumner, M.E. & Harter, R.D. (1998) Sorption of heavy metals in strongly weathered soils: An overview. Environ. Geochem. Health., v. 20:1, p. 5-9.

Oliveira, F.J.S. & Jucá, J.F.T. (1999) Study on contamination of subsoil of the landfill region in Muribeca, Pernambuco. Proc. Brazilian Environmental Geotechnology Congress, REGEO IV, São José dos Campos, pp. 455-460 (In Portuguese).

Rowe, R.K.; Quigley, R.M. & Booker, J.R. (1995) Clayey Barrier Systems for Waste Disposal Facilities. E&FN Spon, London, 390 pp.

Rudd, T. (1987) Heavy Metals in Wastewater and Sludge Treatment Process. Sources, Analysis and Legislation. CRC Press, London v. 1, p. 2.

Ruiz, H.A. (2005) Accuracy increment of soil granulometric analysis through suspension collection (silt + clay). Rev. Bras. Ciência do Solo, v. 29:2, p. 297-300 (In Portuguese).

Shackelford, C.D. (1995) Cumulative Mass Approach for Column Testing. Journal of Geotechnical Engineering.

American Society for Civil Engineers v. 121:10, p. 696-703.

Sposito, G. (1984) The Surface Chemistry of Soils. Oxford University Press, New York, 234 pp.

Srivastava, P.C. & Gupta, U.C. (1996) Trace Elements in Crop Production. Science Publishers, Lebanon, 356 pp.

Tavares, T.M. & Carvalho, F.M. (1992) Evaluation of human exposure to heavy metals in the environment: Examples from the Recôncavo Baiano. Química Nova, v. 15:2, p. 147-153 (In Portuguese).

Yuan, G. & Lavkulich, L.M. (1997) Sorption behavior of copper, zinc and cadmium in response to simulated changes in soil properties. Comm. Soil Sci. Plant Anal., v. 28:6-8, p. 571-587.

Analytical Solution for Luscher's Problems on Two-Layer Consolidation

Paulo Ivo Braga de Queiroz, Delma de Mattos Vidal

Abstract. In this work, the problem of consolidation of two layers is discussed and analytical solutions for the specific case of Luscher's problems are developed. Literature suggests that they are the first analytical solutions for problems that cannot be solved by the Gray-Barber closed form solutions for calculation of equivalent thickness. Luscher's problems are solved using a generalization of the Sturm-Liouville problems for the solution of the partial differential equations. A discussion about the difficulties in generalizing these solutions is also presented. The solution obtained in this work is quantitatively different from that obtained by Luscher via integrated circuits.

Key words: consolidation, analytical solutions, unidirectional flow, heterogeneous media.

1. Introduction

Although the development of new analytical solutions seems to be an outdated subject of study, it may still be justified by the growing use of numerical methods in engineering practice. As newer and more sophisticated numerical programs for geotechnics are developed, the accuracy of their results needs to be assessed somehow. One of the most straightforward procedures to obtain this purpose is to compare numerical results to analytical solutions. In particular, programs that calculate consolidation by coupling flow and effective stresses may be assessed with the help of analytical solutions like the ones presented in this work.

The linear consolidation of two or more layers does not have simple general solutions, despite what might appear at first glance. The illusory simplicity of this problem may be explained by historical reasons.

The formulation of a homogeneous stratum consolidation, attributed to Karl Terzaghi, may be considered as the beginning of modern soil mechanics. Even undergraduate students in civil engineering must know the solution to this problem. The consolidation of a homogeneous soil layer subject to a uniform load is governed by the equation

$$\frac{\partial u_e}{\partial t}(z,t) = c_v \frac{\partial^2 u_e}{\partial z^2}(z,t) \tag{1}$$

where u_e is the excess pore pressure, t is the time elapsed from the start of load application and z is the depth from soil surface. The coefficient of consolidation c_v is given by

$$c_v = \frac{k_w}{\gamma_w m_v} \tag{2}$$

where k_w is the soil permeability to water, γ_w is the unit weight of water and m_v is the coefficient of volume change of the soil. In classic consolidation problems, the following conditions are frequently defined: as initial condition, excess pore pressure is constant ($u_e = u_0$); boundary conditions, excess pore pressure is null at $z = 0$ (top of the consolidating layer) and no flow takes place at $z = H$ (bottom of the consolidating layer). The solution of this boundary value problem may be written in dimensionless terms as

$$\frac{u_e}{u_0} = \sum_{m=0}^{\infty} \frac{2}{M} \sin(MZ) e^{-M^2 T} \tag{3}$$

where the following dimensionless numbers are defined (Lambe & Whitman, 1979):

$$Z = \frac{z}{H}, \quad T = \frac{c_v t}{H^2} \quad \text{and} \quad M = \frac{\pi}{2}(2m+1) \tag{4}$$

The consolidation of two or more layers is governed by the same equation, with the difference that each layer i may have a different coefficient of consolidation (c_{vi}). Moreover, compatibility conditions regarding settlements (ρ), groundwater flow (q) vertical normal stresses (σ_v) and excess pore pressure (u_e) must be imposed at the interface between layers. Even in a two-layer consolidation problem with the same initial and boundary conditions as those presented previously (in the problem of homogeneous stratum), excess pore pressure and effective stress at the interface between layers will change in time. So, two-layer consolidation problems just cannot be divided into two simple problems of single layer consolidation, except in very special cases.

In this work, the problem of consolidation of two layers is discussed and the analytical solutions for Luscher's problems are developed. Although these solutions have already been published (Queiroz, 2002; Queiroz & Vidal, 2002; Queiroz & Vidal, 2003), their complete development and discussion are published herein for the first time. Moreover, recent studies have led to a new form for these solu-

Paulo Ivo Braga de Queiroz, DSc., Instituto Tecnológico de Aeronáutica, Praça Marechal Cândido s/n, São José dos Campos, SP, Brazil. e-mail: pi@ita.br.
Delma de Mattos Vidal, DSc., Instituto Tecnológico de Aeronáutica, Praça Marechal Cândido s/n, São José dos Campos, SP, Brazil.
Submitted on August 14, 2006; Final Acceptance on January 28, 2008; Discussion open until August 29, 2008.

tions, which are simpler than the previously published ones.

A short survey of works in analytical solutions for consolidation of two layers follows. Some of these works were not carried out in geotechnics, but in other fields of engineering that use the same equation for one-dimensional problems, like heat and mass diffusion. Luscher's problems are then solved using a generalization of the Sturm-Liouville problems, which is the standard technique to solve linear partial differential equations (Arfken & Weber, 2001). A discussion about the difficulties in generalizing these solutions is also presented.

2. Consolidation of Heterogeneous media

The subject of consolidation of heterogeneous media is not covered in most textbooks on Soil Mechanics, despite the fact that it has been investigated for more than fifty years. Gray (1945) and Barber (1945) proposed a simplified technique to solve this problem in an approximate way. To do so, the ith soil layer is taken as reference, and an equivalent thickness H'_j for each other layer can be calculated with the help of the following equation, (Urzua & Christian, 2002),

$$H'_j = H_j \sqrt{\frac{c_{vi}}{c_{vj}}} \tag{5}$$

where H_j is the real thickness of the j_{th} layer, and c_{vi} and c_{vj} are respectively the coefficients of consolidation of the reference layer and of the layer whose equivalent thickness is being calculated. The equivalent thickness of several soil layers is calculated by summing up all the H'_js. The excess pore pressure at any depth may be obtained by using Fourier series, which is calculated over the equivalent thickness of the layers. However, this procedure is based on an implicit hypothesis that the following relationship between permeabilities k_{wi} and coefficients of consolidation of adjacent layers holds,

$$\frac{k_{wi}}{k_{wj}} = \sqrt{\frac{c_{vi}}{c_{vj}}} \tag{6}$$

otherwise, groundwater flow on either side of the interface between adjacent layers will not be equal. Urzua & Christian (2002) clearly show that, depending on the real value of k_{wi}/k_{wj}, appreciable discrepancies between the approximate and exact excess pore pressure may arise.

Domenico & Clark (1964) proposed the use of electric analog circuits to model the consolidation of two layers which have the same thickness and the same compressibility, with permeability for one layer being four times the value of the other. Figure 1 shows a scheme of the problem proposed by the authors, involving the layers' properties relevant to consolidation (k_{wi} and m_{vi}), the depth of the contact between layers, the depth of the bottom of the second

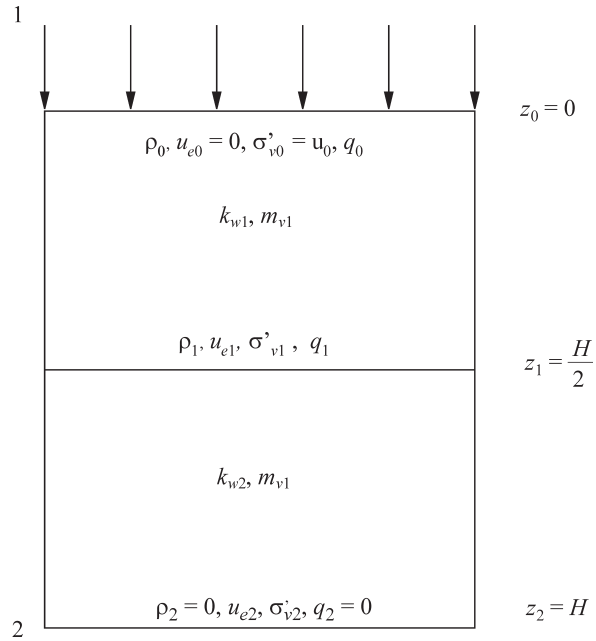

Figure 1 - Scheme of the consolidation of two layers.

layer and the boundary conditions (ρ_i, u_{ei}, σ'_{vi} and q_i). They considered as the initial condition a constant excess pore pressure u_0 and as boundary conditions, a draining frontier at the top (null excess pore pressure) and an impervious frontier at the bottom (no flow). So, two boundary value problems were defined. In the first problem, the upper layer has a higher permeability, while in the second one, the bottom layer is the one with higher permeability. Results obtained by Domenico & Clark were not accurate, which led Luscher (1965) to propose another approach to solve the problem, by using integrated circuits. The results obtained by Luscher were very convincing and his charts became an important reference in the study of consolidation involving multiple layers (Lambe & Whitman, 1979). For this reason, the problems previously described are called Luschers problem in this work, although they were proposed by Domenico & Clark.

Mikhailov & Özisik (1994) proposed a very general method to solve mass and heat diffusion problems in heterogeneous media, for Cartesian, cylindrical and spherical coordinates. Regarding the analogy between one-dimensional consolidation and diffusion in Cartesian coordinates, the methods proposed by these authors can be used to solve consolidation problems involving several layers. Nevertheless, it should be pointed out that this analogy is not valid for problems involving other symmetry conditions, in which consolidation needs to be treated as a tensor problem and its solution may be very different from the solutions of diffusion problems (Mandel, 1953; Abousleiman *et al.*, 1996).

The methods attributed to Mikhailov & Özisik generalize the concepts of eigenvalues and eigenfunctions (from

the Sturm-Liouville problems), in order to apply them to problems of diffusion in heterogeneous media. These authors propose that the eigenvalues be obtained by numerical methods such as Newton-Raphson or bisection together with the "sign count method".

3. Eigenvalues for Luscher's problems

3.1. General Formulation

In this section, the eigenvalues of Luscher's problems are obtained in their analytical form, without the use of iterative methods. In order to simplify their equations and the final form of their solution, Luscher's problems are written in their dimensionless forms. So, for each layer *j* showed in Fig. 1, Eq. (1) becomes

$$\frac{\partial U}{\partial T} = C_j \frac{\partial^2 U}{\partial z^2}, \; j = 1,2 \tag{7}$$

where, in analogy to the consolidation problem of a homogeneous medium, the following dimensionless numbers are defined:

$$U = \frac{u_e}{u_0}, \; Z = \frac{z}{H}, \; T = \frac{c_{v1} t}{H^2} \text{ and } C_j = \frac{c_{vj}}{c_{v1}} \tag{8}$$

Here, c_{v1} is the coefficient of consolidation of the upper layer. In order to define boundary and compatibility flow conditions, it will be also useful to put Darcy's law in a dimensionless form,

$$Q = -K_i \frac{\partial U}{\partial Z} \tag{9}$$

where the following dimensionless numbers are defined:

$$Q = \frac{\gamma_w H}{k_{w1} u_0} q \text{ and } K_j = \frac{k_{wj}}{k_{w1}} \tag{10}$$

The eigenvalue problem related to Eq. (7) may be described by equations (Mikhailov & Özisik, 1994)

$$-\mu_i^2 \psi_{ij}(Z) = C_j \frac{d^2 \psi_{ij}}{dZ^2}(Z), \; j = 1,2 \tag{11}$$

and by the boundary conditions

$$\psi_{i1}(0) = 0 \tag{12}$$

$$K_2 \frac{d\psi_{i2}}{dZ}(1) = 0 \tag{13}$$

Here, $\psi_{ij}(Z)$ is the part of the C^1 piecewise continuous eigenfunction, related to the ith eigenvalue μ_i, defined over the depth range of the jth layer. It is also necessary to establish compatibility conditions for flow and excess pore pressure at the interface between layers:

$$Q\left(\frac{1}{2}\right) = -K_1 \frac{d\psi_{i1}}{dZ}\left(\frac{1}{2}\right) = -K_2 \frac{d\psi_{i2}}{dZ}\left(\frac{1}{2}\right) \tag{14}$$

$$U\left(\frac{1}{2}\right) = \psi_{i1}\left(\frac{1}{2}\right) = \psi_{i2}\left(\frac{1}{2}\right) \tag{15}$$

The general solution of Eq. (11) is

$$\psi_{ij} = a_{ij} \cos\left(\frac{\mu_i}{\sqrt{C_j}} Z\right) + b_{ij} \sin\left(\frac{\mu_i}{\sqrt{C_j}} Z\right) \tag{16}$$

From the boundary conditions (Eqs. (12) and (13)), this solution becomes:

$$\psi_{i1} = b_i \sin(\mu_i Z) \tag{17}$$

$$\psi_{i2} = a_i \cos\left(\frac{\mu_i}{\sqrt{C_2}}(1-Z)\right) \tag{18}$$

It should be remembered that $K_1 = C_1 = 1$, and which is the reason why these dimensionless numbers do not appear in the previous equations. The eigenvalues μ_i depend on the compatibility conditions (Eqs. (14) and (15)) in the first analysis, and depend on K_2 and C_2 in the second analysis. The following sections deals with the calculation of these eigenvalues.

3.2. Eigenvalues for non-null *Q* and *U* at the interface

In this section, the eigenvalues of Luscher's problems that are related to eigenfunctions that result in *Q* and *U* non-null at the interface will be calculated. These eigenfunctions are obtained by applying the compatibility conditions of *Q* (Eq. (14)) and *U* (Eq. (15)) on the eigenfunctions obtained from the previous section. As eigenfunctions they are "scalable", that is, they remain eigenfunctions after being multiplied by some real value, one can set $a_i = 1$ by convention.

Once a_i is determined, b_i can be calculated with the help of the compatibility equations for *Q* at the interface. In this case, by using Eqs. (14), (17) and (18), eigenfunctions become

$$\psi_{i2} = \cos\left(\frac{\mu_i}{\sqrt{C_2}}(1-Z)\right) \tag{19}$$

$$\psi_{i1} = \frac{K_2}{\sqrt{C_2}} \frac{\sin\left(\frac{\mu_i}{2\sqrt{C_2}}\right)}{\cos\left(\frac{\mu_i}{2}\right)} \sin(\mu_i Z) \tag{20}$$

These equations will be used later in this paper, in calculations related to Luscher's second problem.

Alternatively, b_i may be calculated with the help of compatibility equations for *U* at the interface. In this case, by using Eqs. (15), (17) and (18), eigenfunctions become

$$\psi_{i2} = \cos\left(\frac{\mu_i}{\sqrt{C_2}}(1-Z)\right) \tag{21}$$

$$\psi_{i1} = \frac{\cos\left(\dfrac{\mu_i}{2\sqrt{C_2}}\right)}{\sin\left(\dfrac{\mu_i}{2}\right)}\sin(\mu_i Z) \tag{22}$$

From the compatibility equation for Q at the interface (Eq. (14)), one has

$$\mu_i \frac{\cos\left(\dfrac{\mu_i}{2\sqrt{C_2}}\right)}{\sin\left(\dfrac{\mu_i}{2}\right)}\cos\left(\frac{\mu_i}{2}\right) = K_2 \frac{\mu_i}{\sqrt{C_2}}\sin\left(\frac{\mu_i}{2\sqrt{C_2}}\right) \tag{23}$$

which, after some algebraic operations, becomes

$$\tan\left(\frac{\mu_i}{2\sqrt{C_2}}\right)\tan\left(\frac{\mu_i}{2}\right) = \frac{\sqrt{C_2}}{K_2} \tag{24}$$

In Luscher's first problem, the permeability of the bottom layer is a quarter of the permeability of the upper layer, that is,

$$K_2 = \frac{1}{4} \rightarrow \sqrt{C_2} = \sqrt{\frac{c_{v2}}{c_{v1}}} = \frac{1}{2} \tag{25}$$

By replacing these values in Eq. (24), one obtains

$$\tan(\mu_i)\tan\left(\frac{\mu_i}{2}\right) = \frac{2\tan^2\left(\dfrac{\mu_i}{2}\right)}{1-\tan^2\left(\dfrac{\mu_i}{2}\right)} = 2 \tag{26}$$

The previous equation can be solved for $\tan(\mu_i/2)$:

$$\tan\left(\frac{\mu_i}{2}\right) = \pm\frac{\sqrt{2}}{2} \tag{27}$$

It should be pointed out that only positive values of μ_i are of interest, because they will provide a complete set of eigenfunctions of the problem. So, by considering the range $(-\pi/2, \pi/2)$ as image of the arc tangent function, the following series of eigenvalues are obtained as the solution of Eq. (27):

$$\mu_i = 2\left[\arctan\left(\frac{\sqrt{2}}{2}\right) + (i-1)\pi\right] \quad i = 1,2,3\ldots \tag{28}$$

$$\mu_i' = 2\left[\pi - \arctan\left(\frac{\sqrt{2}}{2}\right) + (i-1)\pi\right] \quad i = 1,2,3\ldots \tag{29}$$

In Luscher's second problem, the permeability of the bottom layer is four times the permeability of the upper layer, that is,

$$K_2 = 4 \rightarrow \sqrt{C_2} = \sqrt{\frac{c_{v2}}{c_{v1}}} = 2 \tag{30}$$

By replacing these values in Eq. (24), one obtains

$$\tan\left(\frac{\mu_i}{2}\right)\tan\left(\frac{\mu_i}{4}\right) = \frac{2\tan^2\left(\dfrac{\mu_i}{4}\right)}{1-\tan^2\left(\dfrac{\mu_i}{4}\right)} = \frac{1}{2} \tag{31}$$

The previous equation can be solved for $\tan(\mu_i/4)$:

$$\tan\left(\frac{\mu_i}{4}\right) = \pm\frac{\sqrt{5}}{5} \tag{32}$$

It should be pointed out that only positive values of μ_i are of interest, because they will provide a complete set of eigenfunctions of the problem. So, by considering the range $(-\pi/2, \pi/2)$ as image of the arc tangent function, the following series of eigenvalues are obtained as the solution of Eq. (32):

$$\mu_i = 4\left[\arctan\left(\frac{\sqrt{5}}{5}\right) + (i-1)\pi\right] \quad i = 1,2,3\ldots \tag{33}$$

$$\mu_i' = 4\left[\pi - \arctan\left(\frac{\sqrt{5}}{5}\right) + (i-1)\pi\right] \quad i = 1,2,3\ldots \tag{34}$$

3.3 On the general solution of the consolidation problem of two layers

It should be noted that the eigenvalues obtained in the previous section are valid only for the specific case that

$$\frac{1-Z_1}{Z_1\sqrt{C_2}} = 2 \quad \text{or} \quad \frac{1-Z_1}{Z_1\sqrt{C_2}} = \frac{1}{2} \tag{35}$$

where Z_1 is the dimensionless depth of the interface between layers (for Luscher's problems, $Z_1 = 1/2$). These particular values permit the use of the formula that calculates the tangent of a double arc, which transforms the compatibility equation into a polynomial in $\tan(\mu_i/2)$ (for Luscher's first problem), or in $\tan(\mu_i/4)$ (for Luscher's second problem). In truth, any rational relation between the factors that multiply μ_i in Eqs. (17) and (18) will produce a polynomial in $\tan(\kappa\mu_i)$, where κ is the greatest common divisor of $(1-Z_1)/\sqrt{C_2}$ and Z_1. If the degree of this polynomial is lower or equal to 4, or if the polynomial belongs to the Galois group of polynomials solvable by radicals (Birkhoff & MacLane, 1977), the problem can readily be solved. There are also methods to calculate the roots of polynomials of fifth and sixth degree using Generalized Hyper-

geometric and Kampé de Fériet functions (Weisstein, 1999a; Weisstein, 1999b). If $(1-Z_1)/Z_1\sqrt{C_2}$ is not a rational number, μ_i will have to be calculated by the iterative methods proposed by Mikhailov & Özisik (1994).

3.4 Eigenvalues for either *Q* or *U* null at the interface

When $\psi_{ij}(Z)$ causes either Q or U to be null at interface, some algebraic operations performed in section 3.2 might lead to trivial equalities like 0 = 0. These eigenfunctions were discarded by implicit hypotheses in eigenvalue calculations of that section. This section is dedicated to the calculation of eigenvalues related to eigenfunctions of this kind.

Initially, the eigenvalues that result in $U = 0$ at interface are calculated. For Luscher's first problem, this condition is equivalent to (see Eqs. (15), (17) and (18), with $C_2 = 1/4$)

$$\sin\left(\frac{\mu_i}{2}\right)=\cos(\mu_i)=0 \tag{36}$$

This is equivalent to say that $\mu_i/2$ must be an even multiple of $\pi/2$, while μ_i must be an odd multiple of $\pi/2$, which is a contradiction. So, Luscher's first problem does not have eigenvalues of this kind. For Luscher's second problem, the same condition of $U = 0$ at interface is equivalent to (see Eqs. (15), (17) and (18), with $C_2 = 4$)

$$\sin\left(\frac{\mu_i}{2}\right)=\cos\left(\frac{\mu_i}{4}\right)=0 \tag{37}$$

This is equivalent to say that $\mu_i/2$ must be an even multiple of $\pi/2$, while $\mu_i/4$ must be an odd multiple of $\pi/2$. These conditions are obtained by using

$$\mu_i''=4\left[\frac{\pi}{2}+(i-1)\pi\right] \quad i=1,2,3\ldots \tag{38}$$

This is the third series of eigenvalues for Luscher's second problem.

In the following, eigenvalues that result in $Q = 0$ at interface are calculated. For Luscher's first problem, this condition is equivalent to (see Eqs. (14), (17) and (18), with $C_2 = 1/4$)

$$\cos\left(\frac{\mu_i}{2}\right)=\sin(\mu_i)=0 \tag{39}$$

This is also equivalent to say that $\mu_i/2$ must be an odd multiple of $\pi/2$, while μ_i must be an even multiple of $\pi/2$. These conditions are obtained by using

$$\mu_i''=2\left[\frac{\pi}{2}+(i-1)\pi\right] \quad i=1,2,3\ldots \tag{40}$$

This is the third series of eigenvalues for Luscher's first problem. For Luscher's second problem, the same condition of $Q = 0$ at interface is equivalent to (see Eqs. (14), (17) and (18), with $C_2 = 4$)

$$\cos\left(\frac{\mu_i}{2}\right)=\sin\left(\frac{\mu_i}{4}\right)=0 \tag{41}$$

This is equivalent to saying that $\mu_i/2$ must be an odd multiple of $\pi/2$, while $\mu_i/4$ must be an even multiple of $\pi/2$, which is a contradiction. So, Luscher's second problem does not have eigenvalues of this kind.

It should be stressed that the eigenvalues obtained in this section arise only in problems where $(1-Z_1)/Z_1\sqrt{C_2}$ is a rational number, otherwise, no finite value of μ_i will simultaneously satisfy the conditions that both $\mu_i(1-Z_1)/\sqrt{C_2}$ and $\mu_i Z_i$ must be multiples of $\pi/2$.

4. Calculation of the coefficients A_i

After calculating the eigenvalues of Luscher's problems, one can calculate the coefficients $A_i(T)$ that, together with the eigenfunctions ψ_{ij}, will compose the solutions for Luscher's problems that have the following general form:

$$U(Z,T)=\begin{cases}\sum_{i=1}^{\infty} A_i(T)\psi_{i1}(Z)+A_i'(T)\psi_{i1}'(Z)+ \\ \quad A_i''(T)\psi_{i1}''(Z), \quad Z\le\frac{1}{2} \\ \sum_{i=1}^{\infty} A_i(T)\psi_{i2}(Z)+A_i'(T)\psi_{i2}'(Z)+ \\ \quad A_i''(T)\psi_{i2}''(Z), \quad Z>\frac{1}{2}\end{cases} \tag{42}$$

This solution form is slightly different from the original ones proposed by Mikhailov & Özisik (1994), because in this work three different series of eigenvalues were determined, while in the original work, all eigenvalues belong to only one series.

The eigenfunctions of the Sturm-Liouville problem solved in the previous section are orthogonal in relation to the internal product (Tang *et al.*, 1997)

$$(\psi_i,\psi_j)=\int_0^{1/2}\psi_{i1}\psi_{j1}\,dZ+\frac{K_2}{C_2}\int_{1/2}^{1}\psi_{i2}\psi_{j2}\,dZ \tag{43}$$

that is, once the norm is defined (Mikhailov & Özisik, 1994)

$$N_i=(\psi_i,\psi_i)=\int_0^{1/2}\psi_{i1}^2\,dZ+\frac{K_2}{C_2}\int_{1/2}^{1}\psi_{i2}^2\,dZ \tag{44}$$

the following equality holds:

$$\frac{(\psi_i,\psi_j)}{N_i}=\delta_{ij} \tag{45}$$

Here, δ_{ij} is the Kronecker Delta (Arfken & Weber, 2001). Hence, like in the Fourier series, $A_i(0)$ may be calculated by the formula (Mikhailov & Özisik, 1994)

$$A_i(T=0)=\frac{(\psi_i,U_0)}{N_i} \tag{46}$$

where $U_0(Z)$ is the dimensionless initial condition, that in Luscher's problem is equal to 1. So, $A_i(T)$ can be calculated by the formula

$$A_i(T)=A_i(T=0)e^{-\mu_i^2 T} \tag{47}$$

For Luscher's first problem, after some algebraic manipulations, one obtains

$$N_i=\int_0^{1/2}\left[\frac{\cos(\mu_i)}{\sin\left(\frac{\mu_i}{2}\right)}\sin(\mu_i Z)\right]^2 dZ+$$

$$\int_{1/2}^{1}\cos^2\left[2\mu_i(1-Z)\right]dZ=\frac{1}{4}+\frac{\cos^2(\mu_i)}{4\sin^2\left(\frac{\mu_i}{2}\right)} \tag{48}$$

$$\frac{\sin(2\mu_i)}{8\mu_i}\left[3-\frac{1}{\sin^2\left(\frac{\mu_i}{2}\right)}\right]$$

From Eqs. (27) and (40), all values of trigonometric functions in the previous equation can be calculated using double arc trigonometric functions, and the following results may be verified

$$N_i=N_i'=\frac{1}{3} \tag{49}$$

$$N_i''=\frac{1}{2} \tag{50}$$

for any integer i. So, A_i may be calculated as

$$A_i(T=0)=\frac{(\psi_i,U_0)}{N_i}=\frac{(\psi_i,1)}{N_i}=$$

$$\frac{1}{N_i}\left\{\int_0^{1/2}\frac{\cos(\mu_i)}{\sin\left(\frac{\mu_i}{2}\right)}\sin(\mu_i Z)dZ+\int_{1/2}^{1}\cos[2\mu_i(1-Z)]dZ\right\}= \tag{51}$$

$$\frac{1}{N_i\mu_i}\left\{\frac{\cos(\mu_i)}{\sin\left(\frac{\mu_i}{2}\right)}\left[1-\cos\left(\frac{\mu_i}{2}\right)\right]+\frac{\sin(\mu_i)}{2}\right\}$$

The absolute value of the trigonometric functions in the previous equation can be calculated from Eqs. (27) and (40). Their sign may be obtained from Eqs. (28), (29) and (40), which provide the quadrants to which the trigonometric operands belong. So, the following results may be verified

$$A_i(T=0)=\frac{1}{N_i\mu_i}\frac{\sqrt{3}}{3}(-1)^{i+1}=\frac{1}{\mu_i}\sqrt{3}(-1)^{i+1} \tag{52}$$

$$A_i'(T=0)=\frac{1}{N_i'\mu_i'}\frac{\sqrt{3}}{3}(-1)^{i+1}=\frac{1}{\mu_i'}\sqrt{3}(-1)^{i+1} \tag{53}$$

$$A_i''(T=0)=\frac{1}{N_i''\mu_i''}(-1)^{i+1}=\frac{1}{\mu_i''}2(-1)^{i+1} \tag{54}$$

For Luscher's second problem, by using ψ_{i1} as defined in Eq. (20), after some algebraic manipulations, one obtains

$$N_i=\int_0^{1/2}\left[2\frac{\sin\left(\frac{\mu_i}{4}\right)}{\cos\left(\frac{\mu_i}{2}\right)}\sin(\mu_i Z)\right]^2 dZ$$

$$+\int_{1/2}^{1}\cos^2\left[\frac{\mu_i(1-Z)}{2}\right]dZ=\frac{1}{4}+\frac{\sin^2\left(\frac{\mu_i}{4}\right)}{\cos^2\left(\frac{\mu_i}{2}\right)}+ \tag{55}$$

$$\frac{1}{\mu_i}\left[\sin\left(\frac{\mu_i}{2}\right)-\frac{\sin^2\left(\frac{\mu_i}{4}\right)}{\cos^2\left(\frac{\mu_i}{2}\right)}\sin(\mu_i)\right]$$

The absolute value of the trigonometric functions in the previous equation can be calculated from Eqs. (32) and (38) using double arc trigonometric functions. Their sign may be obtained from Eqs. (33), (34) and (38), which provide the quadrants to which the trigonometric operands belong. So, the following results may be verified

$$N_i=N_i'=\frac{5}{8} \tag{56}$$

$$N_i''=\frac{5}{4} \tag{57}$$

for any integer i. So, A_i may be calculated as

$$A_i(T=0)=\frac{(\psi_i,U_0)}{N_i}=\frac{(\psi_i,1)}{N_i}=$$

$$\frac{1}{N_i}\left\{\int_0^{1/2}2\frac{\sin\left(\frac{\mu_i}{4}\right)}{\cos\left(\frac{\mu_i}{2}\right)}\sin(\mu_i Z)dZ+\int_{1/2}^{1}\cos\left[\frac{\mu_i(1-Z)}{2}\right]dZ\right\}= \tag{58}$$

$$\frac{1}{N_i\mu_i}\left\{2\frac{\sin\left(\frac{\mu_i}{4}\right)}{\cos\left(\frac{\mu_i}{2}\right)}\left[1-\cos\left(\frac{\mu_i}{2}\right)\right]+2\sin\left(\frac{\mu_i}{4}\right)\right\}$$

The absolute value of the trigonometric functions in the previous equation can be calculated from Eqs. (32) and (38). Their sign may be obtained from Eqs. (33), (34) and

(38), which provide the quadrants to which the trigonometric operands belong. So, the following results may be verified

$$A_i(T=0)=\frac{1}{N_i\mu_i}\frac{\sqrt{6}}{2}(-1)^{i+1}=\frac{1}{\mu_i}\frac{4\sqrt{6}}{5}(-1)^{i+1} \quad (59)$$

$$A'_i(T=0)=\frac{1}{N'_i\mu'_i}\frac{\sqrt{6}}{2}(-1)^{i+1}=\frac{1}{\mu'_i}\frac{4\sqrt{6}}{5}(-1)^{i+1} \quad (60)$$

$$A''_i(T=0)=\frac{1}{N''_i\mu''_i}2(-1)^{i+1}=\frac{1}{\mu''_i}\frac{8}{5}(-1)^{i+1} \quad (61)$$

5. Solution formulas for Luscher's problems

5.1. Luscher's first problem

Based on the previously calculated values of the eigenvalues, eigenfunctions and series coefficients, the solution of Luscher's first problem is given by:

$$\frac{u_e}{u_0}=\sum_{i=1}^{\infty}\frac{2}{\mu''_i}\sin(\mu''_iZ)e^{-\mu''_i{}^2T}+\frac{1}{\mu'_i}\sin(\mu'_iZ)e^{-\mu'_i{}^2T}+\frac{1}{\mu_i}\sin(\mu_iZ)e^{-\mu_i^2T},\ Z\le\frac{1}{2} \quad (62)$$

$$\frac{u_e}{u_0}=\sum_{i=1}^{\infty}(-1)^i\left\{\frac{2}{\mu''_i}\cos[\mu''_i(1-Z)]e^{-\mu''_i{}^2T}-\frac{\sqrt{3}}{\mu'_i}\cos[2\mu'_i(1-Z)]e^{-\mu'_i{}^2T}-\frac{\sqrt{3}}{\mu_i}\cos[2\mu_i(1-Z)]e^{-\mu_i^2T}\right\},\ Z>\frac{1}{2} \quad (63)$$

where μ_i, μ'_i and μ''_i are given by Eqs. (40), (29) and (28) and Z and T are defined in Eq. (8).

Figure 2 shows the series solution for eight time instants T. They were calculated with five terms from each series of eigenvalues (i = 1,..., 5), summing up a total of fifteen terms. It may be observed that these curves differ quantitatively from those obtained by Luscher (1965), although the general aspect of the solution is the same. The solution obtained in this work fits very well with results from numerical analyses for C_2 = 1/4 (Queiroz, 2002). Studies under development lead to suppose that Luscher's circuits produced charts valid for C_2 = 1/16, due to a mistake in its project.

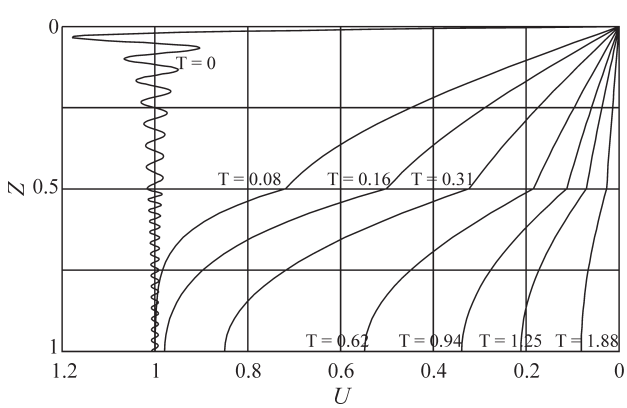

Figure 2 - Series solution for Luscher's first problem.

It should be noted that for $T = 0$, the series solution exhibits an oscillation near to origin, with an overshoot of about 18%. This is known as Gibbs Phenomenon (Arfken & Weber, 2001) and it also occurs in the Fourier series, like the one used by Terzaghi in the solution of consolidation of homogeneous media. Calculating U with more terms of the series solution does not decrease the magnitude of overshoot, but only moves it closer to Z = 0. This oscillation only vanishes for high values of T and is not noticeable for T = 0.08.

5.2. Luscher's second problem

Based on the previously calculated values of the eigenvalues, eigenfunctions and series coefficients, the solution of Lucher's second problem is expressed by:

$$\frac{u_e}{u_0}=\sum_{i=1}^{\infty}\frac{16}{5\mu''_i}\sin(\mu''_iZ)+\frac{12}{5\mu'_i}\sin(\mu'_iZ)e^{-\mu'_i{}^2T}+\frac{12}{5\mu_i}\sin(\mu_iZ)e^{-\mu_i^2T},\ Z\le\frac{1}{2} \quad (64)$$

$$\frac{u_e}{u_0}=\sum_{i=1}^{\infty}(-1)^i\left\{\frac{8}{5\mu''_i}\cos\left[\frac{1}{2}\mu''_i(1-Z)\right]e^{-\mu''_i{}^2T}-\frac{4\sqrt{6}}{5\mu'_i}\cos\left[\frac{1}{2}\mu'_i(1-Z)\right]e^{-\mu'_i{}^2T}-\frac{4\sqrt{6}}{5\mu_i}\cos\left[\frac{1}{2}\mu_i(1-Z)\right]e^{-\mu_i^2T}\right\},\ Z>\frac{1}{2} \quad (65)$$

where μ_i, μ'_i and μ''_i aregiven by Eqs. (38), (34) and (33) and Z and T are defined in Eq. (8).

Figure 3 shows the series solution for eight time instants T. They were calculated with five terms from each series of eigenvalues. It may be observed that these curves differ quantitatively from those obtained by Luscher (1965), although the general aspect of the solution is the same. The solution obtained in this work fits very well with results from numerical analyses for C_2 = 4 (*e.g.*, Queiroz, 2002). Studies under development lead to suppose that Luscher's circuits produced charts valid for C_2 = 16, due to a mistake in its project.

It should be noted that, as in the solution of first Luscher's problem, Gibbs Phenomenon occurs for T = 0.

6. Final Remarks

In this work, the problem of consolidation of two layers was discussed, and some techniques for its solution were commented. Analytical solutions for two special

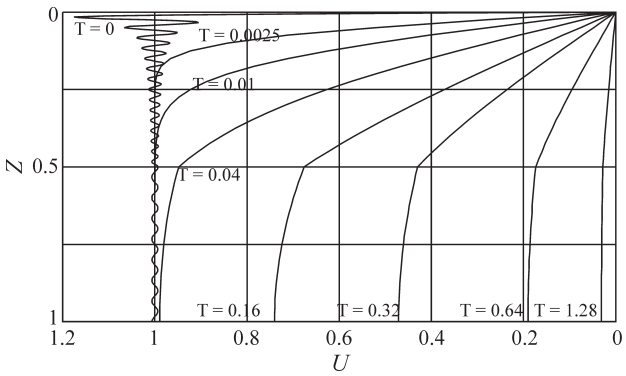

Figure 3 - Series solution for Luscher's second problem.

problems, the so-called Luscher's problems, were developed. These analytical solutions may be useful as benchmark for convergence analyses of numerical methods. As an example, the analytical solution of the first problem furnishes $U = 0.08$ for $T = 1.88$ and $Z = 1$. Luscher (1965) obtained via integrated circuits $U = 0.16$ for the same T and Z, which leads to an error of about 100% over the analytical solution. Future works will provide solutions for other problems in consolidation of heterogeneous media.

References

Abousleiman, Y.; Cheng, A.H.-D.; Cui, L.; Detournay, E. & Roegiers, J.-C. (1996) Mandel's problem revisited, Géotechnique, v. 46:2, p. 187-195.

Arfken, G.B. & Weber, H.J. (2001) Mathematical Methods for Physicists. 5th ed. Academic Press, San Diego, 1112 pp.

Birkhoff, G. & MacLane, S. (1977) A Survey of Modern Algebra. 4th ed. Macmillan Publishing Co., New York, 500 pp.

Barber, E.S. (1945) Discussion of 'Simultaneous consolidation of contiguous layers of unlike compressible soils' by H. Gray. Transactions of American Society of Civil Engineers 110, p. 1345-1349.

Domenico, P. & Clark, G. (1964) Electric analog in time-settlement problems. Journal of the Soil Mechanics and Foundations Division 90:SM3, p. 33-51.

Gray, H. (1945) Simultaneous consolidation of contiguous layers of unlike compressible soils. Transactions of American Society of Civil Engineers 110, p. 1327-1344.

Lambe, T.W. & Whitman, R.V. (1979) Soil Mechanics. John Wiley & Sons, New York, 553 pp.

Luscher, U. (1965) Discussion of 'Electric analogs in time-settlement problems' by Domenico & Clark. Journal of the Soil Mechanics and Foundations Division 91:SM1, p. 190-195.

Mandel, J. (1953) Consolidation des sols (etude mathématique). Géotechnique 3, p. 287-299.

Mikhailov, M.D. & Özisik, M.N. (1994) Unified Analysis and Solutions of Heat and Mass Diffusion. Dover, New York, 524 pp.

Queiroz, P.I.B. (2002) A Numerical Method for the Analysis of Consolidation and Contaminant Transport in Soils (in Portuguese). PhD. Thesis, Instituto Tecnológico de Aeronáutica, São José dos Campos, 150 pp.

Queiroz, P.I.B. & Vidal, D.M. (2002) SOLAM - a numerical formulation for parabolic problems. Mello, L.G. & Almeida, M. (eds) Proc. 4th International Congress on Environmental Geotechnics - 4ICEG, Balkema, Rotterdam, v. 1, pp. 151-156.

Queiroz, P.I.B. & Vidal, D.M. (2003) Applications of a localized adjoint method to the transport of contaminants. Azevedo,R.; Vargas Jr., E.; Sousa, L.R. & Fernandes, M. (eds) Proc. International Workshop on Applications of Computational Mechanics in Geotechnical Engineering, ABMS-NRMG, Ouro Preto, v. 1, pp. 21-28.

Tang, X.W.; Onitsuka, K. & Xie, K.H. (1997) Consolidation solution for double-layered ground with vertical ideal drains. Yuan, J.-X. (ed.) Computer Methods and Advances in Geomechanics, Balkema, Rotterdam, v. 1, pp. 447-456.

Urzua, A. & Christian, J.T. (2002) Limits on a common approximation for layered consolidation analysis. Journal of Geotechnical and Geoenvironmental Engineering v. 128(12), p. 1043-1045.

Weisstein, E.W. (1999a) Quintic equation. URL: http://mathworld.wolfram.com/QuinticEquation.html (downloaded at January 21, 2006).

Weisstein, E.W. (1999b) Sextic equation. URL: http://mathworld.wolfram.com/SexticEquation.html (downloaded at January 21, 2006).

List of Symbols

A_i, A'_i and A''_i: Coefficients of trigonometric series for i^{th} eigenfunction

c_v, c_{vi} and c_{vj}: Coefficients of consolidation (related to i^{th} or j^{th} soil layer)

C_i: Dimensionless coefficient of consolidation of ith soil layer

H, H_j: Thickness of soil layer (thickness of ith soil layer)

H'_j: Equivalent thickness of jth soil layer

k_w, k_{wi}, k_{wj}: Soil permeability related to water (permeability of ith or j^{th} soil layer)

K_i: Dimensionless permeability of ith soil layer

M and m: Multiplying factors of Fourier series

m_v: Coefficient of volume change

N_i, N'_i and N''_i: Norm of ith eigenfunction

q: Groundwater flow

Q: Dimensionless groundwater flow

t: Time

T: Dimensionless time

u_0: Initial excess of pore pressure

u_e: Excess of pore pressure

U: Dimensionless excess of pore pressure
z: Depth
Z and Z_i: Dimensionless depth (of the bottom of ith soil layer)
γ_w: Unit weight of water
μ_i: Eigenvalue related to i^{th} eigenfunction
ρ: Settlement
σ_v: Vertical tension
ψ_{ij}: C^1 Piecewise continuous eigenfunction, related to the ith eigenvalue μ_i, defined over the depth range of the jth layer.
$(\bullet,\bullet)$: Internal product of functions

SOILS and ROCKS
An International Journal of Geotechnical and Geoenvironmental Engineering

Publication of
ABMS - Brazilian Association for Soil Mechanics and Geotechnical Engineering
ABGE - Brazilian Association for Engineering Geology and the Environment
SPG - Portuguese Geotechnical Society

Volume 31, N. 1, January-April 2008

Author index

Instructions to Authors

Category of the Papers

Soils and Rocks is the scientific journal edited by the Brazilian Society of Soil Mechanics and Geotechnical Engineering (ABMS) and by the Brazilian Society of Engineering and Environmental Geology (ABGE). The journal is intended to the divulgation of original research works from all geotechnical branches.

The accepted papers are classified either as an Article paper, a Technical Note, a Case Study, or a Discussion according to its content. An article paper is an extensive and conclusive dissertation about a geotechnical topic. A paper is considered as a technical note if it gives a short description of ongoing studies, comprising partial results and/or particular aspects of the investigation. A case study is a report of unusual problems found during the design, construction or the performance of geotechnical projects. A case study is also considered as the report of an unusual solution given to an ordinary problem. The discussions about published papers, case studies and technical notes are made in the Discussions Section.

When submitting a manuscript for review, the authors should indicate the category of the manuscript, and is also understood that they:

a) assume full responsibility for the contents and accuracy of the information in the paper;

b) assure that the paper has not been previously published, and is not being submitted to any other periodical for publication.

Manuscript Instructions

Manuscripts must be written in English. The text is to be typed in a word processor (MS Word or equivalent), using ISO A4 page size, left, right, top, and bottom margins of 25 mm, Times New Roman 12 font, and line spacing of 1.5. All lines and pages should be numbered. The text should be written in the third person.

The fist page of the manuscript is to include the title of the paper in English, followed by the names of the authors with the abbreviation of the most relevant academic title. The affiliation, address and e-mail is to be indicated below each author's name. An abstract of 200 words is to be written in the language of the paper after the author's names. Translations of the abstract in the other languages are to follow the abstract. A list with up to six keywords at the end of the abstract and each translation is required.

Although alteration of the sequence and the title of each section may be required, it is suggested that the text contains the following sections: Introduction, Material and Methods, Results, Discussions, Conclusion, Acknowledgements, References and List of Symbols. A brief description of each section is given next.

Introduction: This section should indicate the state of the art of the problem under evaluation, a description of the problem and the methods undertaken. The objective of the work is to be clearly presented at the end of the section.

Materials and Methods: This section should include all information needed to the reproduction of the presented work by other researchers.

Results: In this section the data of the investigation should be presented in a clear and concise way. Figures and tables should not repeat the same information.

Discussion: The analyses of the results should be described in this section. **Conclusions**: The text of this section should be based on the presented data and in the discussions.

Acknowledgenments: If necessary, concise acknowledgements should be written in this section.

References: References to other published sources are to be made in the text by the last name(s) of the author(s), followed by the year of publication, similarly to one of the two possibilities below:

"*while Silva & Pereira (1987) observed that resistance depended on soil density*" or "*It was observed that resistance depended on soil density (Silva & Pereira, 1987).*"

In the case of three or more authors, the reduced format must be used, *e.g.*: Silva *et al.* (1982) or (Silva *et al.*, 1982). Two or more citations belonging to the same author(s) and published in the same year are to be distinguished with small letters, *e.g.*: (Silva, 1975a, b, c.). Standards must be cited in the text by the initials of the entity and the year of publication, *e.g.*: ABNT (1996), ASTM (2003).

Full references shall be listed alphabetically at the end of the text by the first author's last name. Several references belonging to the same author shall be cited chronologically. Some examples are listed next:

Papers: Bishop, A.W. & Blight, G.E. (1963) Some aspects of effective stress in saturated and unsaturated soils. Géotechnique, v. 13:2, p. 177-197.

Books: Lambe, T.W & Whitman, R.V. (1979) Soil Mechanics, SI Version, 2nd ed. John Wiley & Sons, New York, p. 553.

Book with editors: Sharma, H.D.; Dukes, M.T. & Olsen, D.M. (1990) Field measurements of dynamic moduli and Poisson's ratios of refuse and underlying soils at a landfill site. Landva A. & Knowles, G.D. (eds) Geotechnics of Waste Fills - Theory and Practice, American Society for Testing and Materials - STP 1070, Philadelphia, p. 57-70.

Proceedings (printed matter or CD-ROM): Jamiolkowski, M.; Ladd, C.C.; Germaine, J.T & Lancellotta, R. (1985) New developments in field and laboratory testing of soils. Proc. 11th Int. Conf. on Soil Mech. and Found. Engn., ISSMFE, San Francisco, v. 1, pp. 57-153.(specify if CD – ROM)

Thesis and dissertations: Lee, K.L. (1965) Triaxial Compressive Strength of Saturated Sands Under Seismic Loading Conditions. PhD Dissertation, Department of Civil Engineering, University of California, Berkeley, 521 p.

Standards: ASTM (2003) Standard Test Method for Particle Size Analysis of Soils - D 422-63. ASTM International, West Conshohocken, Pennsylvania, USA, 8 p.

Internet references: Soils and Rocks available at http://www.abms.com.br.

On line first publications must also bring the digital object identifier (DOI) at the end.

Figures shall be either computer generated or drawn with India ink on tracing paper. Computer generated figures must be accompanied by the corresponding digital file (.tif, .jpg, .pcx, etc.). All figures (graphs, line drawings, photographs, etc.) shall be numbered consecutively and have a caption consisting of the figure number and a brief title or description of the figure. This number should be used when referring to the figure in text. Photographs should be black and white, sharp, high contrasted and printed on glossy paper.

Tables shall be numbered consecutively in Arabic and have a caption consisting of the table number and a brief title. This number should be used when referring to the table in text. Units should be indicated in the first line of the table, below the title of each column. Abbreviations should be avoided. Column headings should not be abbreviated. When applicable, the units should come right below the corresponding column heading. Any necessary explanation can be placed as footnotes.

Equations shall appear isolated in a single line of the text. Numbers identifying equations must be flush with the right margin. International

System (SI) units are to be used. The symbols used in the equations shall be listed in the List of Symbols. It is recommended that the used symbols be in accordance with Lexicon in 8 Languages, ISSMFE (1981) and the ISRM List of Symbols.

The text of the submitted manuscript (including figures, tables and references) intended to be published as an article paper or a case history should not contain more than 30 pages formatted according to the instructions mentioned above. Technical notes and discussions should have no more than 15 and 8 pages, respectively. Longer manuscripts may be exceptionally accepted if the authors provide proper explanation for the need of the required extra space in the cover letter.

Discussion

Discussions must be written in English. The first page of a discussion paper should contain:

• The title of the paper under discussion in the language chosen for publication;

• Name of the author(s) of the discussion, followed by the position, affiliation, address and e-mail. The discusser(s) should refer himself (herself, themselves) as "the discusser(s)" and to the author(s) of the paper as "the author(s)".

Figures, tables and equations should be numbered following the same sequence of the original paper. All instructions previously mentioned for the preparation of article papers, case studies and technical notes also apply to the preparation of discussions.

Editorial Review

Each paper will be evaluated by reviewers selected by the editors according to the subject of the paper. The authors will be informed about the results of the review process. If the paper is accepted, the authors will be required to submit a version of the revised manuscript with the suggested modifications. If the manuscript is refused for publication, the authors will be informed about the reasons for rejection. In any situation comprising modification of the original text, classification of the manuscript in a category different from that proposed by the authors, or refusal for publication, the authors can reply presenting their reasons for disagreeing with the reviewers' comments

Submission

The author(s) must submit for review:

1. A hard copy of the manuscript to Editors - Soils and Rocks, Av. Prof. Almeida Prado, 532 – IPT, Prédio 54 – DEC/ABMS, 05508-901 - São Paulo, SP, Brazil. The first page of the manuscript should contain the identification of the author(s), or

2. The digital file of the manuscript, omitting the authors' name and any information that eventually could identify them, should be sent to **abms@ipt.br**. The following must be written in the subject of the e-mail message: "*Paper submitted to Soils and Rocks"*. The authors' names, academic degrees and affiliations should be mentioned in the e-mail message. The e-mail address from which the digital file of the paper was sent will be the only one used by the editors for communication with the corresponding author.

Follow Up

The ABMS Secretariat will provide a password to the corresponding author, which will enable him/her to follow the reviewing process of the submitted manuscript at the ABMS website, clicking in the item menu "Fluxo de Trabalhos."

Volume 31, N. 1, January-April 2008

Table of Contents